

POLITECNICO DI MILANO

Scuola di Ingegneria Industriale e dell'Informazione

Master Degree in Space Engineering



**DEVELOPMENT OF FIBER OPTIC BASED SMART
RETRACTOR FOR BRAIN SURGERY: EXPERIMENTAL
VALIDATION**

Thesis Supervisor: Prof. Paolo BETTINI

Author: Angel GARCÍA HERNÁNDEZ

Matr: 834566

Academic Year 2018-2019

Con todo mi amor para mi gran amada Familia!

Abstract

During surgery procedures, the lack of knowledge of the applied pressure in vital organs involves high risk of causing damage. The presented work follows the development of a brain retractor constituted with fiber optic sensors in order to obtain accurate measurements in real time of the applied pressure to the brain. This Thesis improves the measurement system that would allow the calibration of the retractor and the manufacturing process, followed by technological tests which ensure the correct embedment of the fiber sensors in the core material so to measure the thermomechanical loads and obtain the applied pressure in real time acting on the retractor.

Key Words: FBG, measurement of pressure and temperature, Micro Computed Tomography, flexure deformation, pull-out.

Contents

Abstract	i
List of Figures	x
List of Tables	xi
Nomenclature	xii
Introduction	xiii
1. State of the Art	1
1.1 Actual brain retractors	1
1.2 Selected Technology	5
1.3 Previous prototypes of Smart Retractors	11
1.4 Considerations of the Retractor SR03-03	13
1.5 Conclusion	19
2. Smart Retractor Model SR03-04	20
2.1 Introduction	20
2.2 Solutions: Smart Retractor modifications	20
2.3 Assembling method	25
2.3.1 Set-up	25
2.3.2 Defined procedure	29
2.4 Conclusion	39

3. Industrialization & Calibration Batch SR03-04-.....	40
3.1 Introduction	40
3.2 Industrialization and Observations	40
3.3 Calibration Test	45
3.3.1 Pressure	46
3.3.2 Temperature	53
3.4 Conclusion	59
4. Technological/Validation Tests	61
4.1 Introduction	61
4.2 Flexure deformation of the retractor	61
4.3 Tomography	70
4.4 Pull-Out prove	76
4.5 Conclusion	91
5. Conclusions and Future Analysis	92
Appendix A	95
Appendix B	96
Appendix C	100
References	103

List of Figures

Figure 1.1: Metallic ribbon hand-held	2
Figure 1.2: Self-retaining subcutaneous retractor	2
Figure 1.3: Brain Spatula: A) flat B) flat with rounded edges C) curved	3
Figure 1.4: Nicholson bran retractor	4
Figure 1.5: Ayad brain retractor	4
Figure 1.6: Smart Materials example; Macro fiber Composite actuator	5
Figure 1.7: Schematic of the basic structure of a Fiber Optic	6
Figure 1.8: Single Mode Vs Multimode Fiber Optic	6
Figure 1.9: Critical angle θ_c in different media.....	7
Figure 1.10: Fiber Bragg Grating sensor	9
Figure 1.11: FBG sensor subjected to strain	9
Figure 1.12: Commercial FBG with single centered in a two meter length FO	10
Figure 1.13: Smart Retractor 01 (SR01)	11
Figure 1.14: Smart Retractor 02 (SR02)	12
Figure 1.15: Smart Retractor 03 (SR03)	12
Figure 1.16: Sensor position in the smart retractor	13
Figure 1.17: Small Tip bonding area marked with color on the left	14
Figure 1.18: Laser verification of FO SR03-03	15
Figure 1.19: Pressure calibration test of batch SR03-03	16
Figure 1.20: Flexural test of batch SR03-03; Facing down central sensor	17
Figure 1.21: Flexural test of batch SR03-03; Facing up central sensor	17
Figure 1.22: Concave deformation of specimen SR03-03-03	18
Figure 2.1: CTE of Epotek before and after molding process	22
Figure 2.2: Left; big older support Right: new smaller support	22
Figure 2.3: Left; DSC test platform Polimi Right: adhesive sample of the test	23
Figure 2.4: UV exposure curing cycle to SR in Polimi laboratory	24
Figure 2.5: Left; FO with Bragg grating Right; close-up of the sensors (1, 2, 3)	25
Figure 2.6: Interrogation equipment in Fiber Optics Laboratory	26
Figure 2.7: Delicate position of the FO in the transducer	26
Figure 2.8: Splicer; FO junction tool Right; automatic positioning of the fiber	28
Figure 2.9: Correct alignment of the fiber	28
Figure 2.10: Geometry of the SR03-04	30
Figure 2.11: Tool with hot wire for FBG identification	31
Figure 2.12: Interrogation of FBG with box to seal from convection heating	31
Figure 2.13: Supports to hold the metal core with a ruler	32
Figure 2.14: Tool for bonding metal core with retractor in position	32
Figure 2.15: Mechanic removal of fiber coating	33

Figure 2.16: Correct positioning of fiber with metallic guides	33
Figure 2.17: Ensuring the FBG sensor inside of the V-groove by mechanical means ...	34
Figure 2.18: Adhesive deposition by a steady velocity flow rate through the V-groove	36
Figure 2.19: UV deposition of the fiber in the metal core	37
Figure 2.20: Final crosslinking of the adhesive in the oven	37
Figure 2.21: Last sensor verification after molding and stamping	38
Figure 3.1: Equipment: Laboratory of AMATECH Politecnico di Milano	41
Figure 3.2: Micron Optics, Computer, Pressure regulator; Galleria del Vento	46
Figure 3.3: Barometric aluminum chamber; AMATECH	47
Figure 3.4: Wavelength variation of external sensor in all runs	51
Figure 3.5 Standard wavelength deviation shift; external sensor, Retractor 14	52
Figure 3.6: Industrial Oven; AMATECH Politecnico di Milano	55
Figure 3.7: Three temperature measurements inside the oven	55
Figure 3.8: Temperature sensor response of specimens SR03-04	56
Figure 3.9: Temperature comparison between Naked optic fiber & Retractor	58
Figure 3.10: External sensor response of specimens SR03-04	58
Figure 4.1: Metallic set-up and signal interrogator Fiber Optic Laboratory	63
Figure 4.2: Exact weight masses	64
Figure 4.3: Transversal displacement of retractor as cantilever beam	64
Figure 4.4: Wavelength variation with increasing mass, SR03-04-10	65
Figure 4.5: Wavelength variation with increasing mass, SR03-04-11	65
Figure 4.6: Wavelength variation during flexural test, SR03-04-10	66
Figure 4.7: Wavelength variation during flexural test, SR03-04-11	66
Figure 4.8: Flexural test in cantilever retractor	67
Figure 4.9: Transversal displacement of retractor as simple supported	68
Figure 4.10: Wavelength variation with increasing mass, SR03-04-11	68
Figure 4.11: Wavelength variation with increasing mass, SR03-04-17	69
Figure 4.12: Flexural test in simple supported retractor	69
Figure 4.13: Schematic examples of examination	70
Figure 4.14: MicroComputed X-25 Scanner, NSI brochure	72
Figure 4.15: Positioned of retractor SR03-04-10 with foam in the scanner	73
Figure 4.16: Reconstruction image of the scanned tip of the retractor	74
Figure 4.17: Retractor reconstruction with different histograms	74
Figure 4.18: Solid imaging processing of the denser material	75
Figure 4.19: First photo: Glue solidification Second photo: FO intact	76
Figure 4.20: Pull-out free body diagram	77
Figure 4.21: Pull-out fix options	78
Figure 4.22: Specimens from retractor metal core	80
Figure 4.23: CAD designs of the adapter to Instron 4302	80

Figure 4.24: Aluminum adapter for FO pull-out prove	80
Figure 4.25: Production of pull-out samples	81
Figure 4.26: Composite base of FO attached	81
Figure 4.27: Pull-out samples	82
Figure 4.28: PO sample with mechanical adapter for tensile machine	82
Figure 4.29: PO Sample assembly on tensile machine Instron 4302	83
Figure 4.30: Force vs displacement curve PO-01	84
Figure 4.31: PO-01 Sample breakage	84
Figure 4.32: Force vs displacement curve PO-02	85
Figure 4.33: PO-2 Sample breakage	85
Figure 4.34: PO-3 Sample breakage	86
Figure 4.35: Force vs displacement curve PO-04	86
Figure 4.36: PO-4 Sample breakage	87
Figure 4.37: Force vs displacement curve PO-05	87
Figure 4.38: PO-5 Sample breakage	88
Figure 4.39: Force vs displacement curve PO-06	88
Figure 4.40: PO-6 Sample breakage	89
Figure 4.41: Dispersion of PO sample results	90
Figure A.1: Mono-modal and multi-modal FO	96
Figure A.2: Fiber Bragg Grating sensor	97
Figure A.3: Reflection of the fringes in Bragg grating	98
Figure A.4: Variation of the reflection spectrum of Bragg grating	98
Figure A.5: Variation of the reflection of a pattern subject to deformation	99
Figure B.1: Full retractor SR03-04 CAD design	100
Figure B.2: FO, reticulated adhesive and metal core	101
Figure B.3: Cantilever and SS model retractor	101
Figure B.4: Retractor self-construct mesh by ANSYS	102
Figure B.5: FO and reticulated adhesive meshing by ANSYS	102

List of Tables

Table 2.1: Materials CTE values	21
Table 2.2: Materials operative temperature	23
Table 2.3: New curing cycle for fiber embedment	24
Table 3.1: Smart Retractor Batch SR03-04	42
Table 3.2: Comparison of Retractor Batches in the tip bonding	43
Table 3.3: Comparison of Retractor Batches Liner Molding Process	44
Table 3.4: Comparison of Retractor Batches handle base	44
Table 3.5: Pressure calibration results in Run 1	48
Table 3.6: Run 1 and 2 of Retractor SR03-04-14	50
Table 3.7: Thermomechanical properties FO and metallic core	54
Table 3.8: Calibration Temperature Test	57
Table 4.1: Mean value of wavelength displacement; Flexural deformation test	70
Table 4.2: NSI Scanner Model X-25 characteristics	71
Table 4.3: Computed Tomography software	74
Table 4.4: Retractor's material density	75
Table 4.5: FO length in contact with metal core	79
Table 4.6: PO sample numeration	83
Table 4.7: Summary PO Test	89

Nomenclature

AMATECH	Aerospace Materials and Technology Lab
CAD	Computer Aided Design
CTE	Thermal Expansion Coefficient
DSC	Differential Scanning Calorimetry
E	Young's Modulus
EMI	Electromagnetic Impedance
Eng.	Engineer
FBG	Fiber Bragg Grating
FBGS	Fiber Bragg Grating Sensor
FEM	Fiber Element Method
FO	Fiber Optic
MC-T	MicroComputed Tomography
MEA	Mean Arterial Pressure
MEK	Methyl Ethyl Ketone
NA	Numerical Aperture
NDI	Non-Destructive Inspections
NSI	North Star Imaging
PO	Pull-out
RCBD	Regional Cerebral Blood Flow
SR01	Smart retractor Version 1
SR02	Smart retractor Version 2
SR03	Smart retractor Version 3
SR03-02	Smart retractor Version 3, Model 2
SR03-03	Smart retractor Version 3, Model 3
SR03-04	Smart retractor Version 3, Model 4
SSB	Simple Supported Beam
UV	Ultra Violet
λ_B	Bragg wavelength
Λ	Lattice period
η_{eff}	Effective refractive index
$\Delta\lambda$	Change of wavelength
ε	Strain
σ	Stress
J_x	Moment of Inertia
pm	Pico meters
ηm	Nano meters

Introduction

One of the main challenges during medical surgery is the knowledge of the maximum allowable applied pressure over any vital organs of the human body. The incorrect measurement or the overpassing of this value, might cause irreparable damage to the organ. Surgeons during neurosurgical operations have the need to employ retracting devices in order to separate the two sides of a surgical incision and then restrain the tissues to do not interfere with the operative process and to provide an adequate exposure to the lesion. In this process it is difficult for the surgeon to accurately estimate the amount of pressure applied to the brain during the placement of the retractors. Thus, injury in the brain can occur as a result of the retraction when either the force applied is excessive or when the pressure is not adequately distributed.

Politecnico di Milano addressed this problem with a smart retractor since the phase A of the design which compromised a full understanding of the problem through an engineering feasibility study of the project, defining the requirements and the architecture of the retractor which starts with the work done by Eng. Minerva describing the first design of the smart retractor and defining the properties of the former in order to enhance the neurosurgery procedures, which led to a first prototype. The continuation of this work was made by Eng. Cantarelli which designed the industrialization of the smart retractor from the criticalities underlined of the first the prototype. An improvement and a characterization of the design was done by Eng. Forero although leaving open points for enhancement of the design.

This Thesis work explains and justifies the enhances of the procedure, it is also analyzed the main difficulties of this technology, such as the identification of the sensor, and the damage interface with the host material by recovering numerical data coming from technological tests such as temperature and pressure calibration, pull-out and Ray-X tomography accompanied by a compilation of theoretical data subjected to calculations and FEM analysis of the smart retractor that led to technical solutions that brings the completion of the project.

Chapter 1

State of the Art

1.1 Actual brain retractors

The very firsts brain retractors for surgical operations were designed as flat blades in different materials such as stainless steel, copper, silver alloy, titanium, and later on plastic and acrylic.

With time, it was attached an articulate arm with a swivel joint articulation to the flat blade. This was attached to the skull. Several iterations of them causing an inferior effect to brain damage but reducing to a minimum time of pressure to the organ.

Damage caused from neurosurgical instruments:

In the early period, Cushing and Horsley [1] introduced the first brain retractor that presented a shape of metallic ribbon with different sizes and shapes. The rectangular ribbon was hand-held and can be modified according to its need.

This rectangular ribbon also was produced with one narrow end, and identified as a tapper. The initial materials used were stainless steel or copper and later on, silver alloy and titanium, while covered with silicone rubber.

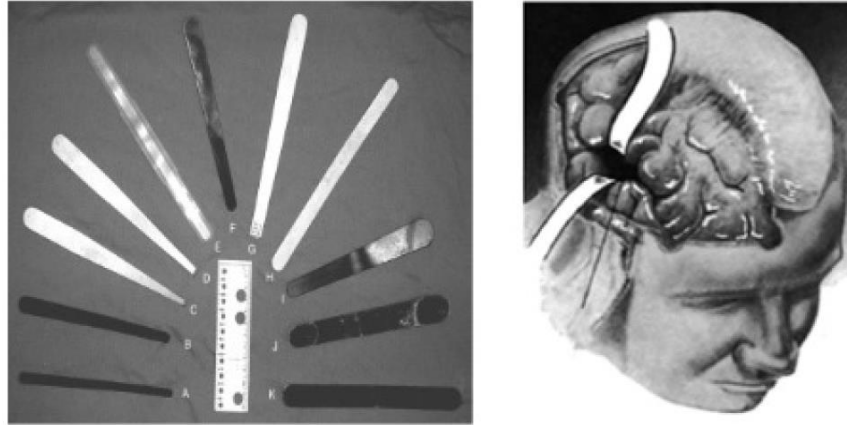


Figure 1.1: Metallic ribbon hand-held

Numerous microinstruments were introduced in the operative theater: the operating microscope, the irrigated bipolar coagulation, aneurismal clip, microsuction with dissecting tip, pneumatic drill, microsurgical sutures, microsurgical dissectors, and laser surgery.

The brain retractor improvement did not skip this major development. Although we did not see many changes on the blade or spatula, the significant change occurred at the level of the blade fixation. It was no longer accepted to have any movement of the brain retractor blade or the head of the patient occurring during surgical procedures.



Figure 1.2: Self-retaining subcutaneous retractor

However, Rosenorn [2] reported that there is no significant difference between the flat retractors and the retractors that have round edges or are curved. The regional cerebral blood flow values after being placed on the cortex were as follows: flat retractors (80 ml/100 g/ min), flat ones with round edges (90 ml/100 g/min), and curved retractors (75 ml/100 g/min). In other words, no difference in Regional Cerebral Blood Flow (rCBF) below the application area of the three different types of weights was observed. Thus no further risk of ischaemic nerve cell damage could be demonstrated by using the most easily handled retractors, the flat ones, instead of those more or less curved.



Figure 1.3: Brain Spatula: A) flat B) flat with rounded edges C) curved

In 1979, Laha [3] found that if the mean arterial pressure, normally between 70-105 mmHg, exceeds the brain retraction pressure by less than 70 mmHg, the cerebrum will be damaged. This means that the BRP should not exceed 40-45 mmHg. Furthermore, the maximum pressure should be limited to 15 minutes with a 5-minute recovery period between retractions.

By intra-operative brain retractor pressure monitoring in 37 patients, it was noticed that the average initial brain retractor pressure was 26.6 mmHg, when the brain was retracted safely and gently by experienced neurosurgeons.

The use of multiple retractors may be less harmful to the brain than retraction with a single retractor. An investigation of 120 retraction pressure recordings in 23 patients showed an initial steep and later a more gradual slope. The pressure at the tip was higher than at the center of the retractor.

Then Nicholson developed the first advanced electronic device for brain retractor. It was a pressure-responsive surgical tool assembly which included an inflatable enclosure and a pair of electrodes positioned therein. The electrodes are adapted to contact each other and operatively move away from each other under an increase of fluid pressure inside the enclosure until electrical contact is broken. An electrical lead is connected to each electrode for electrically

monitoring the condition of electrode contact. A flexible tubing is connected to the enclosure to provide fluid flow therein to increase the pressure inside. The surgical brain retractor overlies at least one of the electrodes and is adapted to transmit force applied from it to that associated electrode.

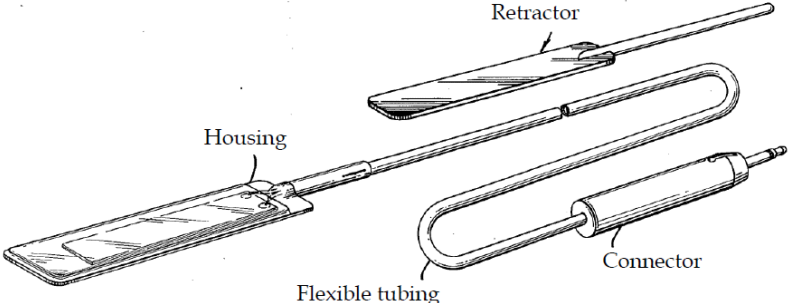


Figure 1.4: Nicholson brain retractor

Application of force by the tool initially causes the electrodes to contact other and to remain in contact until the pressure inside the enclosure substantially balances the applied pressure from the tool whereupon electrode contact is broken.

As the moment is work is written the last smartest retractor was made from Ayad (2007) that is an evolution of a device designed by Michaeli in 2001 which functionality is remained the same, however a measurement device and the brain retractor are integrated into a single tool.

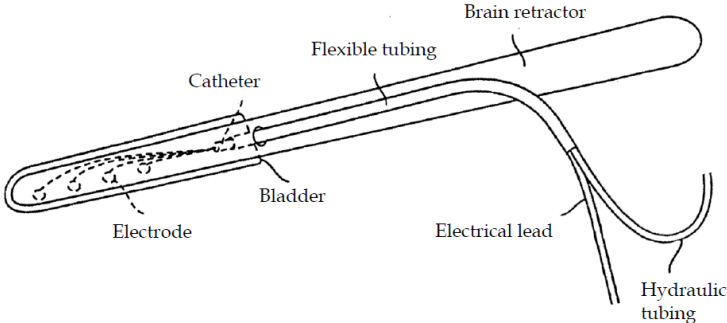


Figure 1.5: Ayad brain retractor

1.2 Selected Technology: Fiber Bragg Grating sensors

Fiber Optic Sensors:

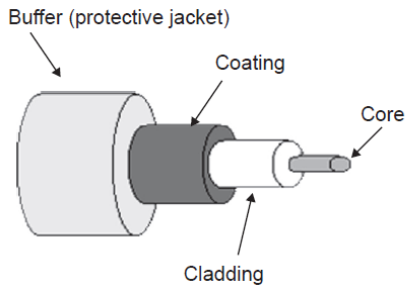
Fiber optics sensors are part of the SMART materials category [4] due to the response behavior that could mimic human sensory and nervous systems by employing embedded sensors and actuators with advance signal processing and control capabilities. Actual sensing techniques lacks of simplicity and accuracy and few technologies provides a non-costly and simple procedure techniques suited.



Figure 1.6: Smart Materials example; Macro fiber Composite actuator

The Fiber Optic (FO) or Optical Fiber is a kind of cable made from glass usually fused silica or polymeric materials that work with certain wavelengths of light, transmitting great amount of data over vast distances with low losses.

The FO Is composed by three main components, which are core, cladding and coating. The essential components are the core and the cladding, as they generate the effect of light transmission desired, the coating instead is added to provide extra mechanical resistance and external protection, in Figure 1.2 the three components are shown, with extra protection component used in the long transmission cables used in telecommunications mainly, in the present work only the three aforementioned components will be considered.



Sensor parameter	Single mode fiber (μm)	Multimode fiber (μm)	Material
Core	2–10	50–150	Silica-based
Cladding	80–120	100–250	Doped silica
Coating	250	250	Polymer
Buffer	900	900	Plastic

Figure 1.7: Schematic of the basic structure of an optical fiber

Fiber optics can be divided in two types, which is in function of the core and number of transversal propagation modes inside them. These are: Single mode and Multi-mode as shown in figure 1.3.

The single mode fibers have a small core (5 to 10 μm) and the propagation of the light inside is given by only one mode, this decreases the reflections of the light inside the fiber and thus, a lower loss of power (attenuation) which means a capability of traveling longer distances with the same amount of power, this is a heavy advantage for applications that require transmission of information through huge distances such as the sub oceanic cables and landlines of the telecommunications industry.

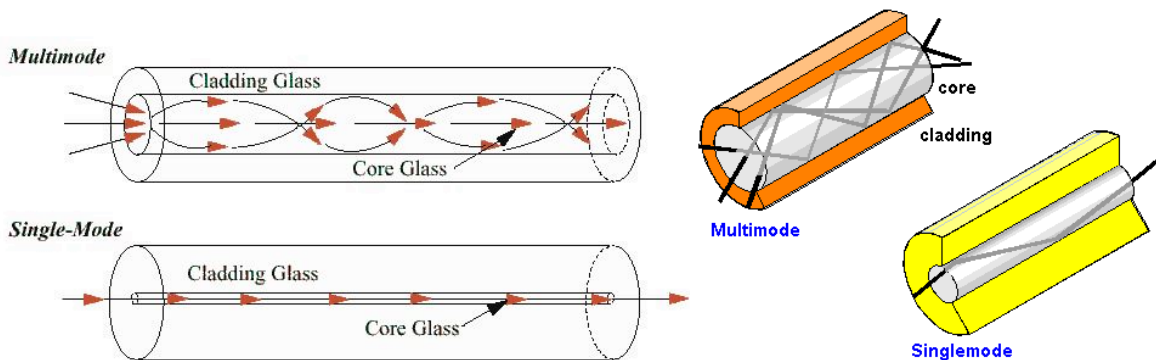


Figure 1.8: Single Mode Vs Multimode Fiber Optic

The multi-mode fiber, which has a thicker core (up to 100 μm) inside the same diameter of cable as the single core, this allow more modes of light to propagate through the core, and thus a higher power transmission in the same cable thickness, which translates in the ability also to transmit larger amounts of data,

at the expense of higher power attenuations over long distances, making it ideal for short length uses.[5]

The use of FO in industrial and medical application has increase this due to the low losses in high rate of data transmission, the non-generation of electromagnetic impedance (EMI) and immunity to it which makes it safe to use in explosive and flammable environments and easiness of installation in multiple applications e.g. embedding in composites and complex geometry parts as well as the sturdiness of the fibers with respect to other electronic devices that suffer from harshness environment.

The physical phenomena of the FO works by reflecting the light inside its body taking the advantage of the total reflection which is described by the *Snell's law* that correlates the refractive index n and the angle of incidence and refraction θ of a light ray in the interface between two mediums.

$$n_1 \sin \theta_1 = n_2 \sin \theta_2$$

The construction of the fiber optics is such that the core is made to have a higher refractive index than that of the cladding. Introducing the *critical angle* θ_c being the angle needed in order to obtain the total reflection angle and given the Snell's law relation, it can be obtained a total internal reflection when the incidence angle of the light passing through it is higher than the critical angle of the particular fiber.

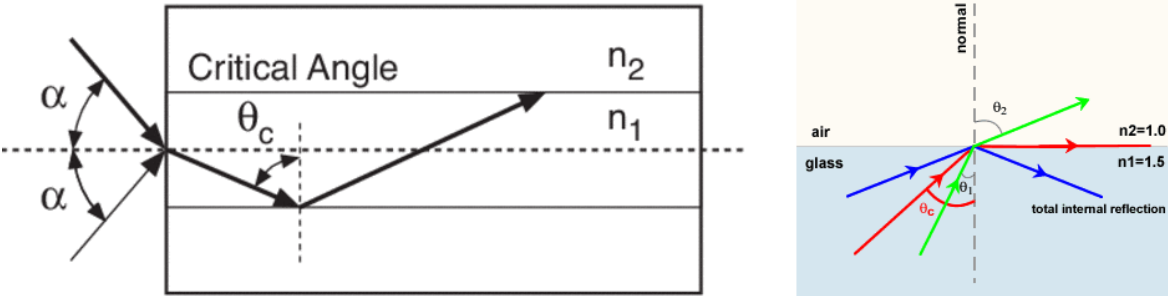


Figure 1.9: Critical angle θ_c in different media

Optical fiber is highly sensitive to stress, and due to its dimensions bending has a stronger effect, when optical fibers are subjected to bending stress, the light in the outer part of the core stops being guided by it and some of it is lost (attenuated) due to the incident beam exceeding the Numerical Aperture (NA) which is the space on which the light beam has to remain to obtain a total reflection and constant travel through the core, this lost light goes to the cladding and is dissipated.

This properties of the fiber means that curving the FO can generate attenuation, for single mode fibers, the light lost from the fundamental mode at bending consist of two components, a transition loss that arise from the coupling of light from the fundamental mode to leaky core modes when there is a change in curvature of the fiber, and the pure bend loss which consist of the continual loss of guidance at the outer portion of the evanescent field of the fundamental mode given by the phase velocity of the outer part of the evanescent field equaling the speed of light in the cladding, as the radius of the bend decreases the fraction of the evanescent field increases and more light is lost. [6]

Fiber Bragg Grating Sensors:

All existing fiber optic sensors base their operation on the sensitivity of the optical characteristics of the propagation medium, in this case the glass, to the variations of the state of mechanical effort or thermal, which will influence the transmitted light signal. After a suitable calibration, it is therefore possible to exploit this sensitivity of the propagation which means to reconstruct the state of effort in the piece in which the FO is incorporated.

Currently among all the existing techniques in FO sensors, the most used one employs the Bragg lattices or Fiber Bragg Gratings (FBG); these are sensors of spectral modulation obtained by photoengraving in the core of the fiber, able to measure different sizes, including mechanical deformation and temperature.

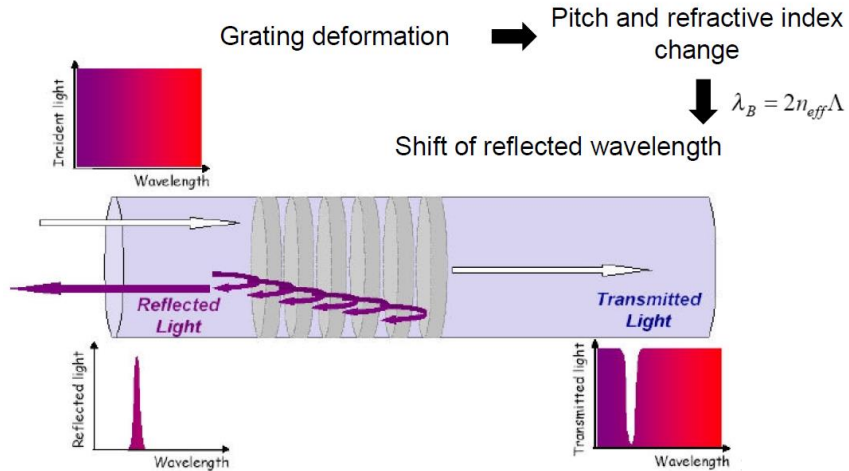


Figure 1.10: Fiber Bragg Grating sensor

The working principle is shown in figure above, is based on the capacity of the modified part to reflect a particular wavelength, which takes the *Bragg wavelength* or λ_B to be computable through the fundamental equation of Bragg, where Λ is the lattice period and n_{eff} the effective refractive index.

$$\lambda_B = 2n_{eff}\Lambda$$

Where:

$$n_{eff} = n \sin(\theta)$$

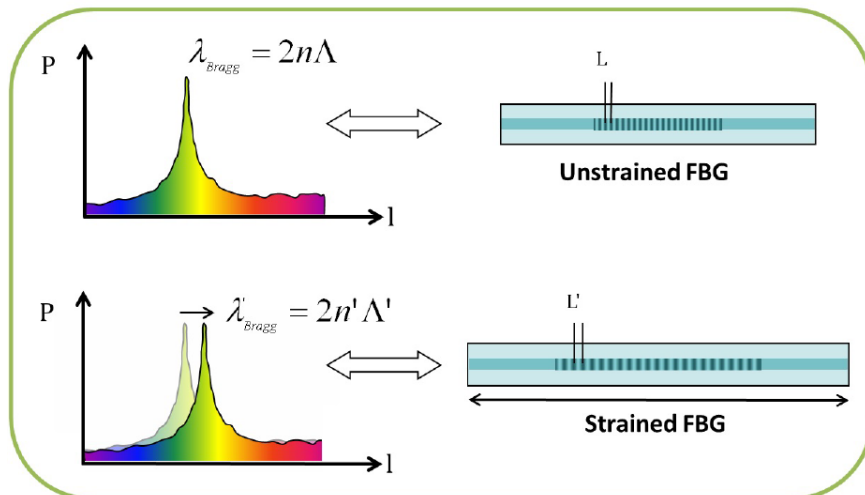


Figure 1.11: FBG sensor subjected to strain

If there is a mechanical tensile stress or an increase in temperature, there is a shift of the λ_B towards higher values, while in the opposite case the displacement will be towards shorter wavelengths.

Since each pair of lattice fringes or bars reflects only a small percentage of the light at the specific λ_B , only a large number allows to obtain a reflected spectrum characterized by a well-defined and little dispersed peak. The length of the lattice itself, usually is between 2 mm and 50 mm, therefore plays a fundamental role.



Figure 1.12: Commercial FBG with single centered in a two meter length FO

It is also possible, during production process of the FBG in the inscription phase of the lattice, to modulate the refractive index of the core, so as to obtain the maximum value in a gradual manner.

This procedure is called *Apodization* (mathematical operation made to correct the spectral distortion) and allows to obtain a cleaner reflected signal without side lobes.

There are different variants of the FBG sensors, but this type, being the easiest to query and interpret, as well as the least expensive, it is the most used in sensors. However, it only provides an average value of a very limited part of the fiber, which makes it suitable for specific area use.

1.3 Previous prototypes of Smart Retractors

First Designs

Politecnico di Milano took the work to enhance the brain retractor, project that started in the 2014 with all the ground work made by Eng. Minerva with the design of the first model proposed by Polimi with denomination of SR01 which set up the main requirements of the conceptual design of the retractor and the correspondence tools for the development of it, within the very first sensitivity test for the calibration procedures.

This first model was in fact sensitive to pressure and temperature providing fundamental information in real time for the neurosurgery. The signals, however, were affected by errors due to the calibration of the sensors and deformation of the spatula related to its use. [7]

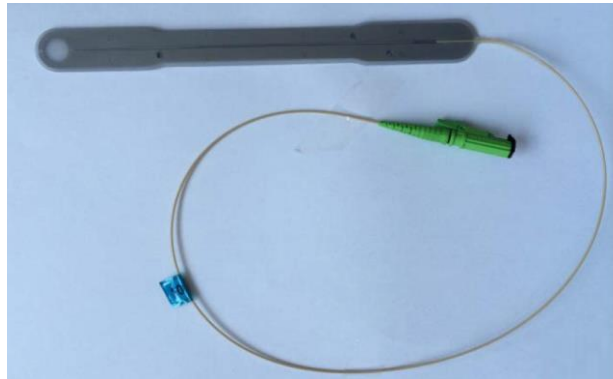


Figure 1.13: Smart Retractor 01 (SR01)

The continuation of the design was made by Eng. Cantarelli with the proposed model SR02 which was a big enhancement in the morphological shape and material wise. New specific requirements were identified that led to create the model SR03 with a reduction of the thickness of the metal core (from 1 mm to 0.8 mm) in order to reduce the stiffness of the instrument and thus allow the surgeon to obtain the desired shape when folding the retractor.

Also the spherical cap of the palpator was increased double the initial value up to a 0.4 mm, so the first contact between the brain tissue and the retractor is ensured to be with the palpator. This spherical cap became symmetric in both sides of the retractor that lead to the new final geometry.

This model dealt with the calibration of the sensor with respect of the non-linear sensitivity of the pressure. [8]

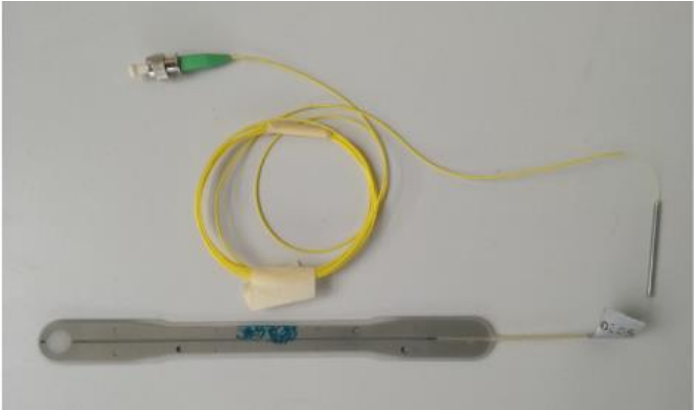


Figure 1.14: Smart Retractor 02 (SR02)

These very first models commented above were determinant in the geometry and functionality of the retractor which led to a more refined iteration that included the assembly procedure, dimension errors and surface wise design of the retractor.

The latest iterations were named SR03-02 and SR03-03 by Eng. Forero, that included considerations related to the error measurements while usage of the instrument being the predominant the flexural deformation and the temperature-pressure coupled effect, and their correspondent calibration test.[9]

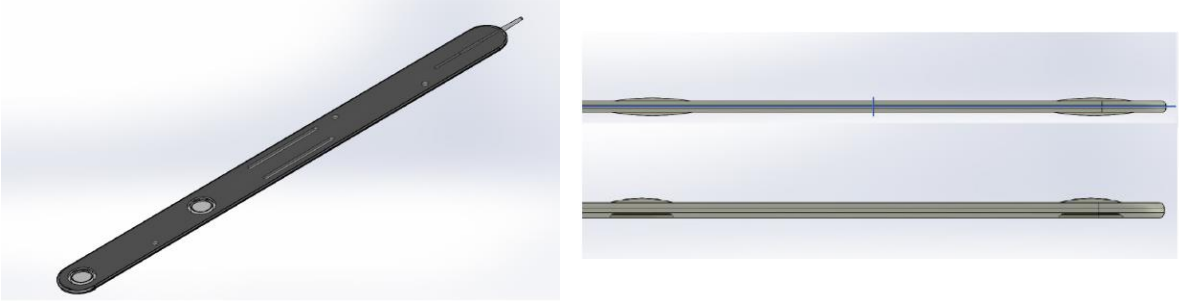


Figure 1.15: Smart Retractor design 03-03 (SR03-03)

The main design geometry of the retractor at this stage are the three FBG sensors in the FO with 55 mm separation between the pressure sensor 1 (Ext sensor) and pressure sensor 2 (Cent sensor). The temperature sensor (Temp sensor), is located exactly in the middle between the pressure sensors as shown in the next Figure.

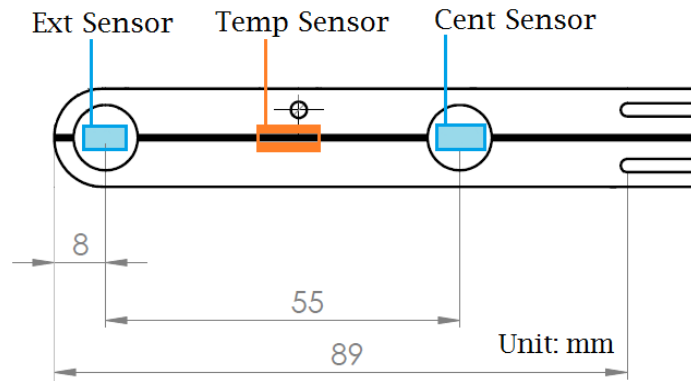


Figure 1.16: Sensors position in the smart retractor

For more information about the concept of the design, time line and changes of the smart retractor the reader is invited to address References 7, 8 and 9. Appendix A provides the nominal values used for the development of this Thesis work.

1.4 Considerations of the Retractor SR03-03

About the tip

The tip is the final end of the spatula that joins the FO with the metallic core and at the same time, due to its small geometry gets in contact with the lobes of the brain. Therefore, this part should ensure complete adhesion of the sensor, taking care that there is no error in the lecture and avoid damage to the brain from it.

In the middle of the tip there is a cavity with rectangular base and a semicircular side for a total contact area with the FO about 3.4 mm^2 , this pocket is filled first with the FO and the selected adhesive and at the end with the elastomeric membrane for the liner.

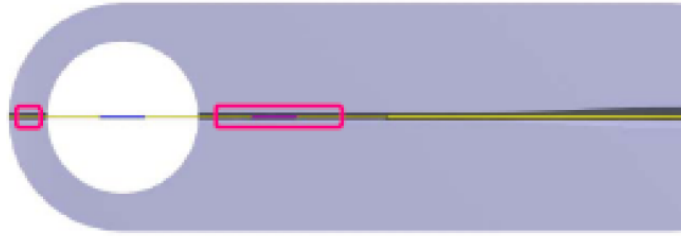


Figure 1.17: Small Tip bonding area marked with color on the left

Theoretically the elastomer has the function to transfer the contact pressure between the membrane and the cerebral lobes to the pressure sensor that is incorporated in the membrane itself. This sensor is, as already said, a FBG sensor inscribed in a standard optical fiber (with the polymeric coating and an outer diameter of 140 microns) which crosses the pocket longitudinally to a depth of 0.54 mm from the outer surface of the tip.

Although the geometrical consistence, this tip bonding point is not compliant with the requirement of holding the fiber, and as such it must be modified

About the bonding

The FO works better if fully naked, this means that all future iterations will be performed with a fully naked fiber.

Due to the tip few local area, the dimension ratio between the fiber diameter and the depth of the retractor and the difference of Thermal Expansion Coefficient (CTE) between metal and silicon fiber, the bonding of the FO is not guaranteed.

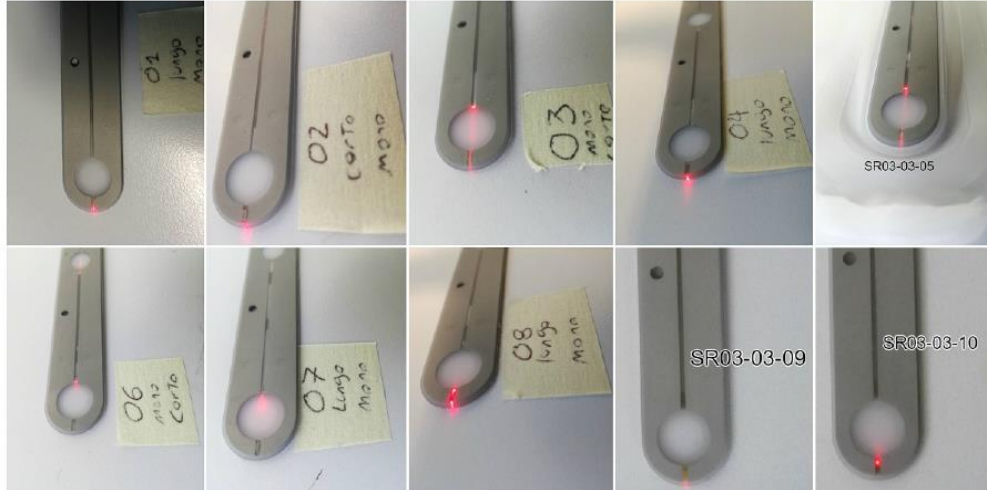


Figure 1.18: Laser verification of optical fiber S03-03

About the shape and geometry

In the design SR02 and SR03 was studied and tackled the problem of usage problem and maneuverability of the retractor.

The asymmetric configuration works in favor of both linearization of the response and heightening of the sensibility, so it will be maintained for the next iteration.

However, the position of the FO in the midplane of the metal core was not guaranteed. Also a small displacement of the fiber with respect to the vertical midplane was observed and during the fabrication procedure, some of the fibers were broken, sometimes the fibers were unglued so that, the assembly procedure must be revised in order to correct the issue.

The calibration testing made to the last retractor batch SR03-03 got inconsistencies in the pressure and temperature sensors coming from the damage made to the FBG during molding and during the test itself. Below are presented the pressure and flexural testing results.

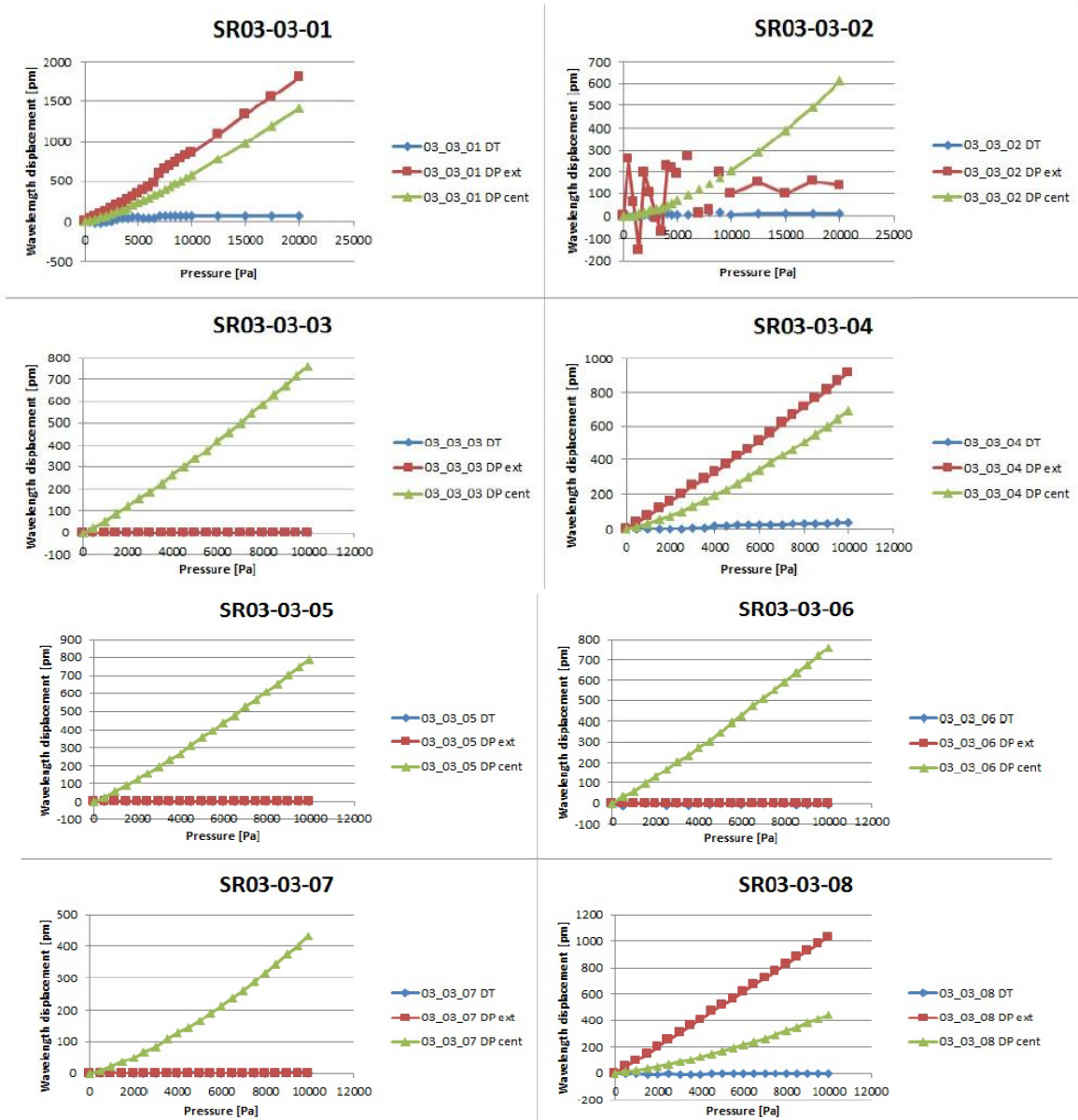


Figure 1.19: Pressure calibration test of batch SR03-03

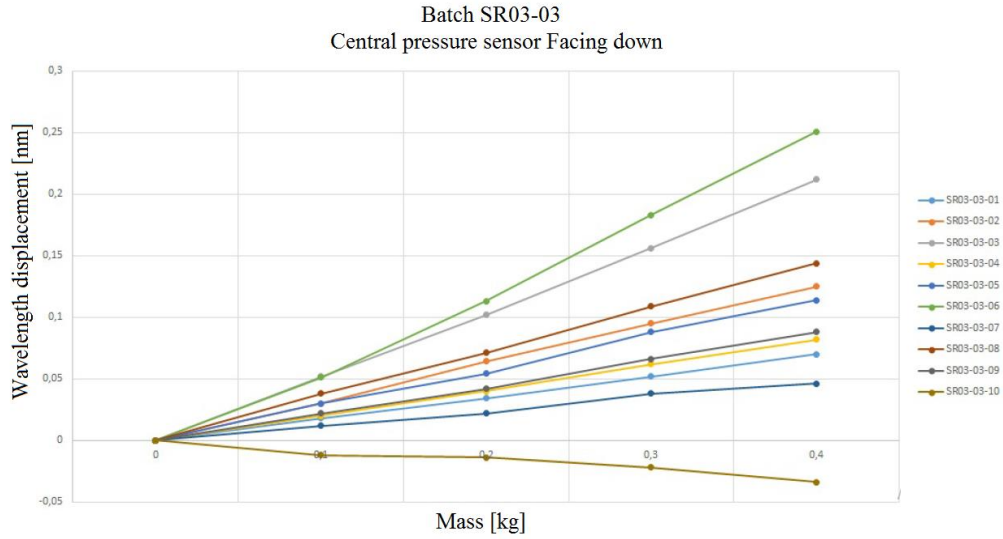


Figure 1.20: Flexural test of batch SR03-03; Facing down central sensor

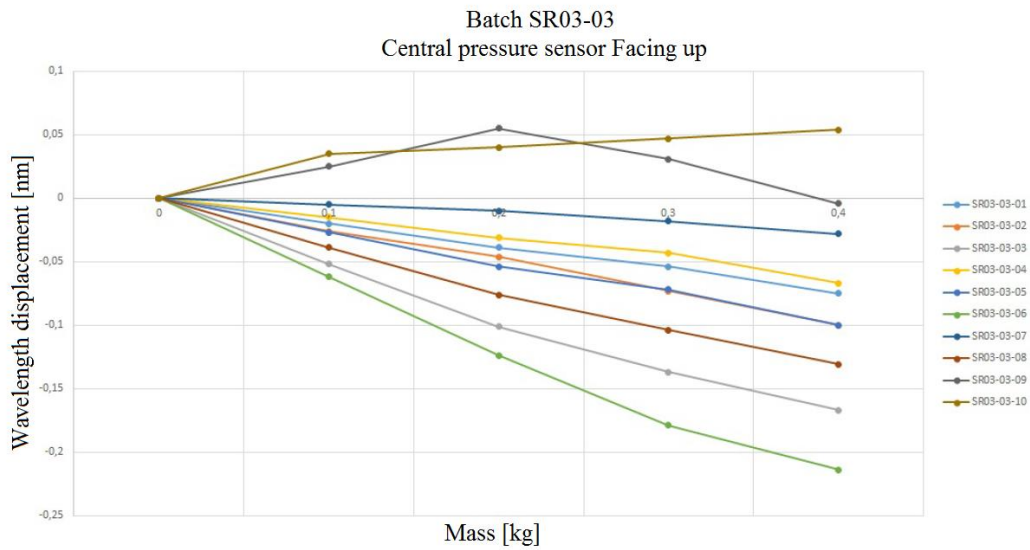


Figure 1.21: Flexural test of batch SR03-03; Facing up central sensor

The batch SR03-03 showed an improvement with respect to the SR03-02 batch, however they present a non-linear behavior of pressure measurement derived from the irregularities of the stamping and production method. [9]

About the stamping method

During the stamping method between the liner and the total FO and the metal core, the tip bonding point is not compliant with the requirement of holding fast the fiber this due to the biocomponent adhesive use to bond the FO and the metal core presents almost zero resistance to the chemical attack. This will lead to a change of the adhesive formula.

The last specimens fabricated, presented a deformation with respect to the horizontal axis that create a concave bend of the retractors coming after the molding process

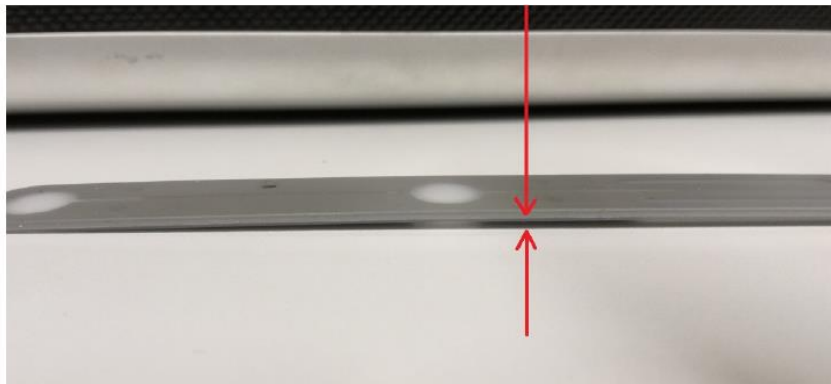


Figure 1.22: Concave deformation of specimen SR03-03-03

The last batch SR03-03, presents errors during measurements, so the temperature response would be corrected by properly calibrating the algorithm, and the next iteration design will be tested for temperature in order to evaluate the weakness of the tip bonding point has any correlation with the low temperature response of the external sensor.

1.5 Conclusion

From the first design of the smart retractor, the FBG technology proves to be suitable for the task in hand. Starting from the conceptualization design and research developed by the very first work of Eng. Veronica Minerva, the proof of concept and designs of Eng. Claudia Cantarelli, to the last retractor generalities modifications done by Eng. Andres Forero; a full study of the retractor design was identified and shown in representative form to mark the main differences and criticalities design.

The last retractor batch SR03-03 presented important enhancement in the geometric and material selection but lacking accuracy regarding the fabrication method and performance, where the tip end, the bonding between the material composition and stamping method were the main identified problematics.

Chapter 2

Smart Retractor Model SR03-04

2.1 Introduction

In the previous chapter, the main considerations of SR3-03 have been pointed out. The main criticalities are derived from the industrialization process that affects the functionality of the tool. In this chapter, the solutions to these issues are settled with the next version of the smart retractor SR03-04 together with the refinement of the production method, testing and calibration of the instrument.

2.2 Solutions: Smart Retractor modifications

The different iterations of the geometry and materials selected of the smart retractors have derived to the need of optimization and definition of the industrialization process. The last model developed by Eng. Forero, SR03-03, dealt with some adhesive complications during the manufacturing of the retractor and create an evaluation of the behavior of the retractor.

However, the considerations aforementioned in Chapter 1 are influential for the ideal industrialization process for manufacturing, correct final user experience and decrease reading errors of the retractor.

The next solutions presented is work done in the Aerospace Materials and Technologies laboratory (AMATECH) of the Dipartimento di Scienze e Tecnologie Aerospaziale (DAER) of Politecnico di Milano in order to solve the considerations stated before.

These solutions will create a batch of new retractors called SR03-04:

1. In order to correct the tip bonding point and correct adhesion of the fiber being an important pressure point, there are two possible solutions considered; to increase the amount of contact area up to a 4.5 mm^2 or to increase the efficiency of reticulation process during production ensuring the no contamination by the coating of the fiber and external dust during the production.

These specific part will be commented and discuss by a Pull-Out proof made into specimens similar to the retractor's tip in Chapter 4.

Table 2.1: Materials CTE values

Material	CTE ($\text{mm}/\text{m}/^\circ\text{C}$)
FO Glass	0.8×10^{-5}
AISI 316 Steel	0.0165

A reliable bonding means that:

- It must guarantee the appropriate mechanical characteristics by a uniform distribution of stresses during the operation of the retractor.
- The bonding method must feature chemical compatibility with all the other materials, by the means of *material properties* e.g. CTE in Table 2.1 of the retractor itself, in particular with the more abrasive one the Methyl Ethyl Ketone (MEK) used for picking the retractor before the application of the primer used to prepare the surface before all the moulding process. [8]

The final confirmation of the adhesive is that the CTE of the glued fiber should be equal or close to the one of the metal, this due to the physical phenomena that this expansion must follow the dilation of the metal core.

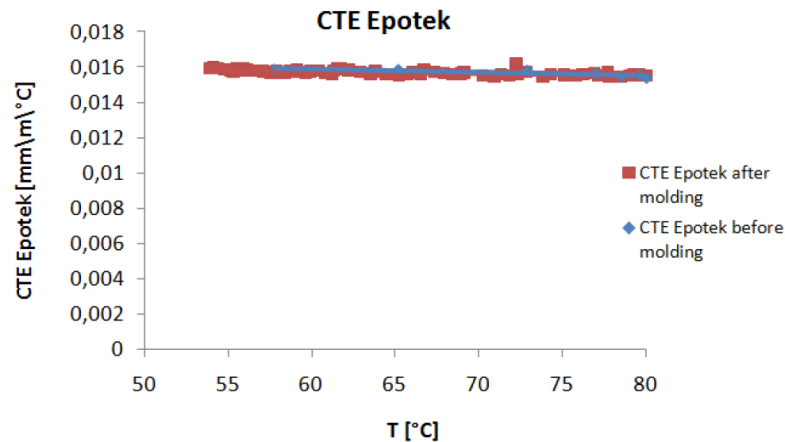


Figure 2.1: CTE of Epotek before and after molding process

A verification to this was achieved by computing the CTE of the glued fiber, based on general theory of FBG [Appendix B and 8] under thermal and mechanical solicitation. As presented in Figure 2.1 it is evident of the CTE is constant and similar to the one of the metal core.

2. The V-groove where the fiber lies on the metallic core becomes deeper up to a 0.54 mm in order to ensure the location of the FBG exactly in the midplane, so that the effect of bending stresses is minimized and possible measure errors will be eliminated.

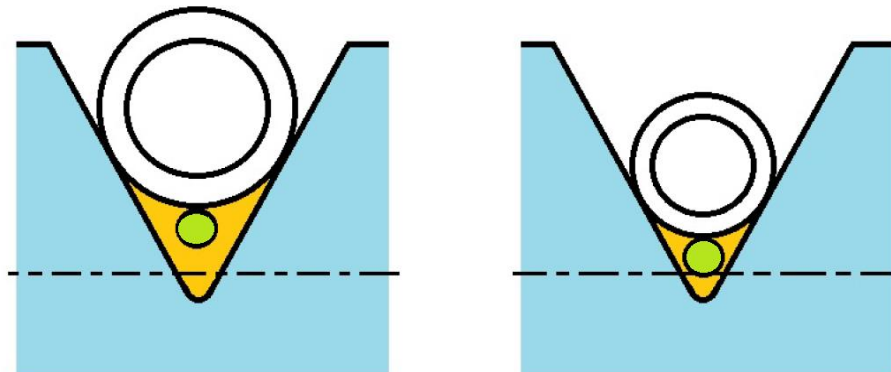


Figure 2.2: Left; big older supports Right: new smaller support
In green the FO and in white the supports

The new production process of the retractor leads to a change in the supports that holds the FO for a correct bonding of all the materials. With this, the FO is now closer to the bottom of the V-groove and for that closer to the midplane (Figure 2.2), also this will allow to the sensor to be in contact with the metallic soul in all their local area, so is not only conserved in the glue.

3. The monocomponent adhesive used to bond the fiber with the metal core presents higher resistance to the chemical attack rather than the biocomponent, these is seen during a Differential Scanning Calorimetry test (DSC) evaluating the reticulation level of the adhesive, which presents an identical performance response. It is decided to use it over the biocomponent adhesive. [9]



Figure 2.3: Left; DSC test platform Polimi Right: adhesive sample of the test

The adhesive selected feature thermal compatibility within temperature of curing cycle, the temperature of moulding process and ambient temperature that is for a noninvasive drying cycle and within the materials as presented below. [Appendix A]

Table 2.2: Materials operative temperature

Material	Operative Temperature
Epotek	From -50°C to 180° C
Polyacrylate coating FO	From -17°C to 120°C

4. It is guaranteed the adhesion of the FBG in the metallic core before the thermal cycle, this is achieved by a more accentuated exposition of UV rays of the retractor. The Epotek monocomponent adhesive will be used for the junction of the fiber, so that the correct angle of application of it ensures the correct bonding.

The suggested *curing cycle* of the Epotek monocomponent adhesive, consists in applying heat up to a temperature of 150°C for one hour, but the coating does not tolerate it. Investigations on the ideal cycle for the retractor has been suggested since the first iteration, however from analysis made in the DSC from model SR02 and SR03-03 from Eng. Cantarelli and Eng. Forero, respectively, leads to a final curing cycle of:

Table 2.3: New curing cycle for fiber embedment

Curing Cycle Adhesive	
Adhesive type	Epoxy monocomponent EPOTEK
UV Radiation	3 minutes
Electrical Oven Cycle	60 minutes at 150°C



Figure 2.4: UV exposure curing cycle to SR in Polimi laboratory

All these solutions, solve the considerations of the batch SR03-03 and leads to the new assembling method which is totally influential for the final production of the brain retractor.

2.3 Assembling method

New components, time frames, arrangement and materials involves the new design of the retractor which is the basis for the production of the new batch of retractors with name SR03-04.

2.3.1 Set-up

There are many considerations regarding the new assembling method that will ensure a proper production of the next iteration of the retractor. The ones presented next deals with the FBG itself, and the metal core which is practically the soul of the retractor.

Interrogation of the sensors

An interrogation of the exact position of the sensors must be done this due to the fact that the FBG sensor provider deliver the sensor with color red marked zones, so the integration of it, is easier. This position of the Bragg grating has a maximum tolerance of 3 mm.

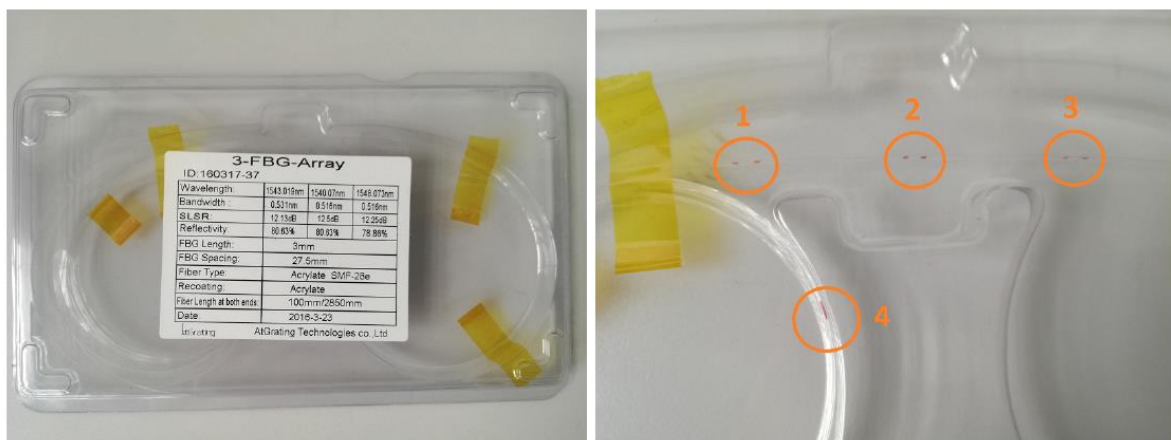


Figure 2.5: Left; Fiber optic with Bragg grating Right; close-up of the sensors (1, 2, 3) and marked zero (4)

Once arrived the FBG sensors, the correspondence coating must be stripped which the marks are lost. For that, an interrogation method has been developed by the Polimi laboratory. It consists of a hot wire with a distance transducer, the FBG is connected to the device and if this sensor passes, the electrically induce hot wire reflects a wavelength change so it can be located the exact position of the sensor with respect to the initial zero marked from the provider. (Figure 2.5)

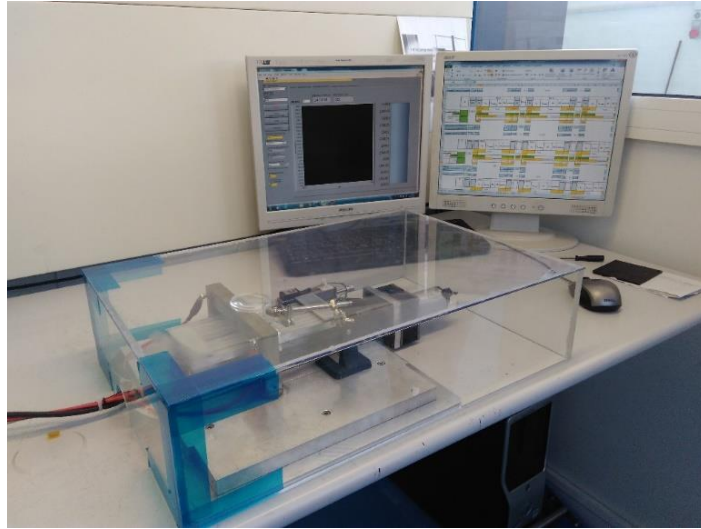


Figure 2.6: Interrogation equipment in Fiber Optics Laboratory

This interrogation procedure secures the first step of the total assembling method due to the risk of wrong positioning the FO is high due to the low tolerance. The distance verification of the sensors is shown in the figures below.

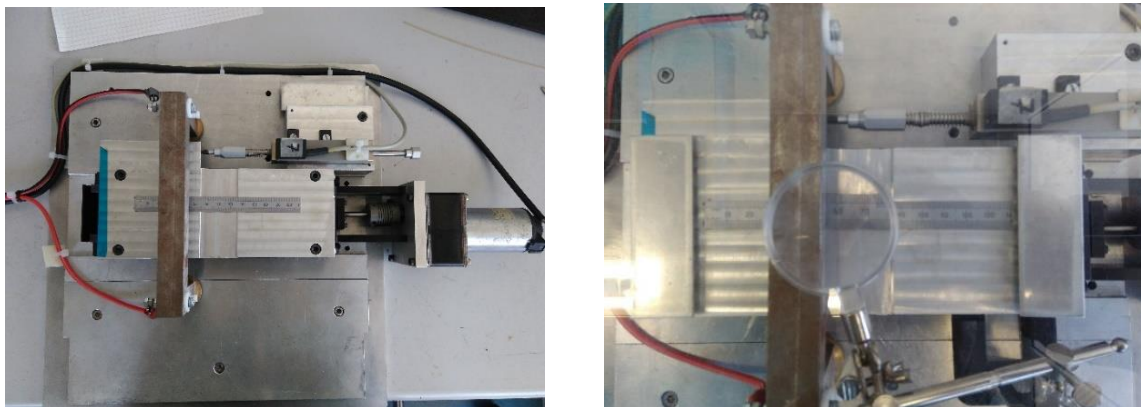


Figure 2.7: Delicate position of the FO in the transducer

The Splicing of the sensors

The need of FBG sensor to transmit signals, requires to be connected to a source, an exchanger and a receiver, where losses are a major point of concern. The junction between the FO is done by fusion of the silica of the fiber and is known as *splicing* which allows for disconnection and reconnection of the intended fibers.

Splicing by fusion is a process where are created sensitive losses. It can be measure the maximum tolerance of loss in each splice [10]. The signal loss is determined by:

$$K[dB] = -10 \log_{10} \left\{ \frac{P_0}{P_i} \right\}$$

Where $\{P_0/P_i\}$ is the ratio of output and input of the optical power between two fibers.

To avoid signal loss due to the splicing, the fibers to join must be adequately prepared at the ends, and the alignment between them should be precise and avoid an axial, transverse and an angular misalignment [11].

Fusion splicing, consist in the junction of two different fibers by heating their silica core and cladding with an electric arc. This process is done by an instrument called Splicer.

This advance instrument clamps the two ends of the fibers, already stripped of its core from the coating and cleaned, and align them with precision as shown in Figure 2.8. The electrical arc is generated which melt the parallel surfaces of both ends, allowing a fusion between them. After this process the fiber is tested in the splicer by a tension test and an estimated loss is reported.



Figure 2.8: Splicer; FO junction tool Right; automatic positioning of the fiber

This tension test indicates the possible loss of tensile strength in the fiber in the proximity of the splice, if a value of 10% is reached, the process must be done again. As a security measure to reinforce the junction, it is added in the same instrument a thermoretractable jacket with a metal bar that is placed over the join itself. After this it is heated until the thermoretractable jacket fix itself to the fiber, so that the bar can withstand the bending and some of the tensile stresses that the fiber might suffer during its use.



Figure 2.9: Correct alignment of the fiber

The interrogation and splicing of the fiber sensors are activities that requires regulation, tolerance and strict procedure since those involves the success of the next commented procedure which is the embedment of the total parts and materials of the brain retractor.

2.3.2 Defined procedure

As reported in the last Thesis works of the development of this instrument, there are inconsistencies and error measurements in both pressure and temperature sensors [7,8,9]. It can be seen these errors comes from a misdisplacement and breakage of the fiber in specific zones of the retractor.

Coming from a deep analysis of the production procedures designed for SR01 batch until SR03-03, and stated before in this work, the most delicate part of the total procedure is the proper and refine bonding of the FBG in the metal core of the retractor. The final procedure of this bonding is presented below, which will be critical to the performance of the batch SR03-04.

Bonding procedures of the sensorized fiber to the metal core in the smart retractors (SR03-04)

Terms Definition

- **Retractor:** is intended as the smart brain retractor.
- **Metal core:** the metallic body made of Steel 316, is the metal body on which all the work described in this document is carried out.
- **Fiber:** meaning as the optical fiber used as a "smart" element in the Smart Retractor.
- **Sensor:** the sensor is the sensor type FBG that are embedded in the optical fiber, there are by definition three fiber sensors for this particular process.
- **Temperature sensor:** means a sensor designed to measure temperature, one of the three sensors present in the total fiber.
- **Pressure sensor:** means a sensor designed to measure the pressure, two of the three sensors present in the optical fiber. The pressure sensors are positioned on the two sides of the temperature sensor.
- **Sheath:** means the sheath in PEEK that is arranged around the fiber optic is that it works as a cover of it.

- **Adhesive:** means the adhesive liquid product that allows to fix the fiber and the sheath in PEEK to the metal core, this particular adhesive is of the epoxy type, with cross-linking to UV radiation and high temperature cycle (150 ° C).
- **Hole:** these are intended as the perforations on the metal core to house the pressure sensors, they are two in number, have a diameter of 10 mm, are spaced 55 mm apart and are in the sensorized area of the retractor.
- **Quarry:** It means the channel localized in the metal core in which the fiber is housed and placed the adhesive.

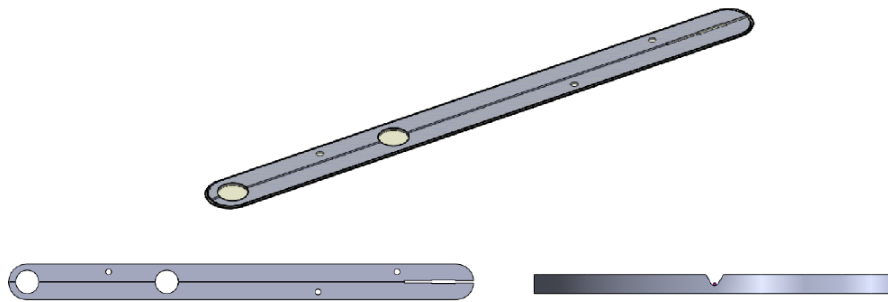


Figure 2.10: Geometry of the SR03-04

Identification of the sensors

- Connect the sensorized optical fiber to be identified.
- Connect the fiber to the interrogator to determine the wavelength of the peak reflected signal.
- Positioning and anchoring of the optical fiber in the hot wire equipment to identify the center of the FBG sensor.
- Scanning of the fiber by hot wire and monitoring by software of the variation of the sensor reading.
- Identification of the center of the FBG sensor (maximum signal variation) with respect to a visible reference (marker) outside the portion of fiber that will be incorporated in the adhesive.
- Registration of: fiber identifier, relative position of each sensor with respect to the visual reference.

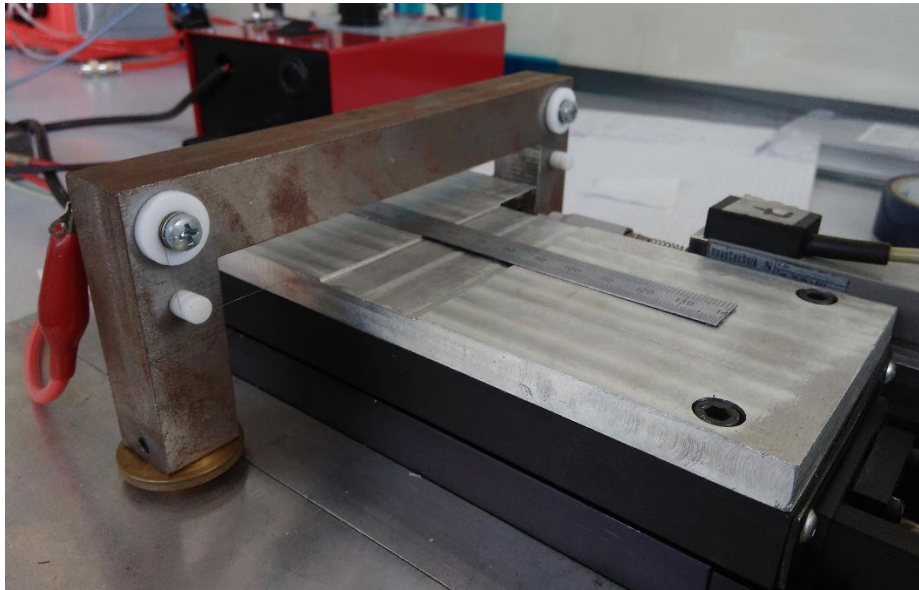


Figure 2.11: Tool with hot wire for FBG identification

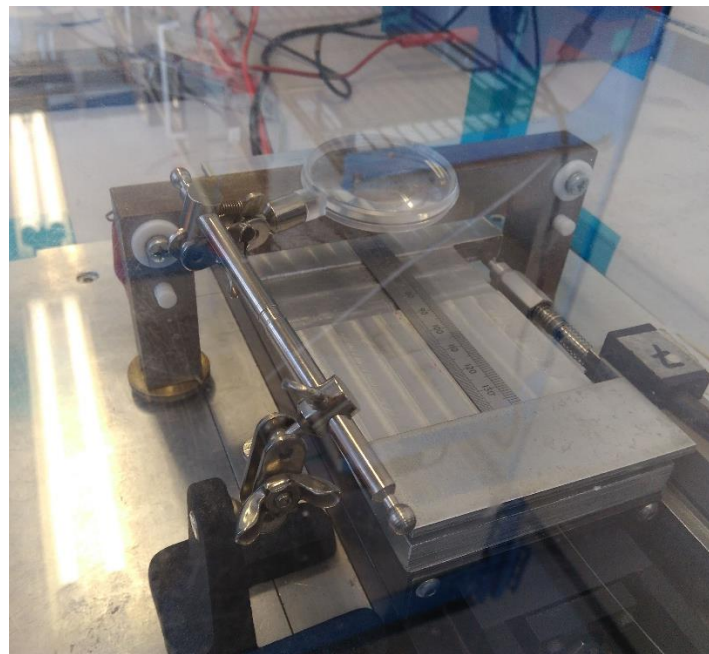


Figure 2.12: Interrogation of FBG with box to seal from convection heating

Preparation of the gluing equipment

- Mount the spatula support in the ferromagnetic material on a motorized slide.
- Place the fiber guides (metal core sections) and the thicker sheet to secure the fiber with adhesive tape.
- Place the metal core with the sensorized end on the side of the thick plate.



Figure 2.13: Supports to hold the metal core with a ruler

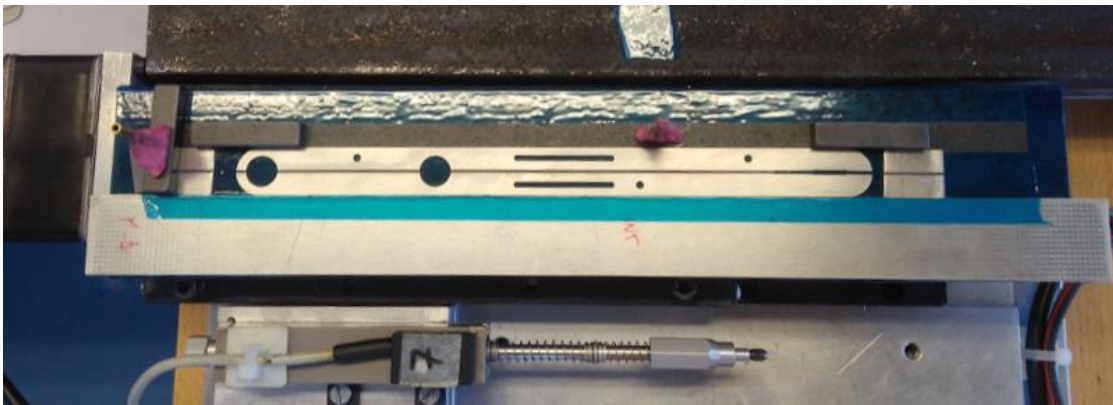


Figure 2.14: Tool for bonding metal core with retractor in position

Removal of the fiber coating

- Remove the fiber coating in the sensorized area, from the end up to 65 mm after the central sensor.
- The removal can be performed mechanically, using a stripper or chemically, by dipping the fiber in methyl ethyl ketone (MEK) and gently removing the coating.
- Clean the fiber from residues with a piece of cotton lightly soaked in isopropyl alcohol.
- Important to manage with the extreme care of naked fiber no longer protected by the covering.

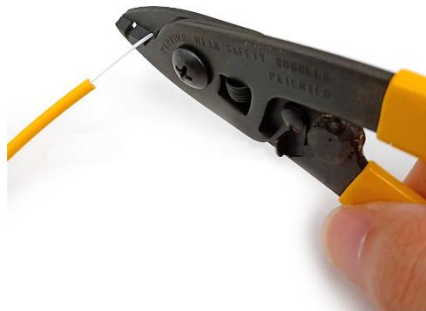


Figure 2.15: Mechanic removal of fiber coating

Positioning of the fiber on the metal core

- Place the nude fiber inside the special slot in the metal core.
- Place the visual reference, using the ruler, so that the center of the sensors is at the center of the designated holes to receive them.



Figure 2.16: Correct positioning of fiber with metallic guides in the end and beginning of the fiber in circles

Fixation and tension of the fiber

- Taking care to keep the sensors in place, fasten the short end of the fiber to the thicker film with appropriate adhesive tape.
- At the opposite end, place the fiber on a rounded edge with a radius of more than 20 mm.
- Apply weight to the fiber over the edge, using pre-stressed tweezers that interpose the elastomer, taking care not to damage the fiber.

Securing the fiber on the bottom of the quarry

- Prepare elastomer strips of the groove size.
- The elastomer strips will be held in place by small magnets that provide the force necessary to ensure that the fiber is placed at the bottom of the groove, such as small jaws.
- Place an elastomer ring on the metal guide near the fixing point.
- Place another jaw on the core in the center of the bending area, at a distance of about 20 mm from the beginning of the coating.



Figure 2.17: Ensuring the FBG sensor inside of the V-groove by mechanical means

UV deposition and cross-linking of the adhesive for bonding the fiber to the metal core

- The deposition and UV curing of the adhesive occurs in three phases: the first involves the sensorized part of the spatula up to the central jaw, the second goes from the central jaw up to a few millimeters before the end of the slot and the third is related to the fixing of the PEEK sheath in its seat.
- The continuous deposition of the adhesive must take place simultaneously with the relative displacement of the metal core with respect to the deposition nozzle, in order to guarantee a homogeneous distribution of the adhesive.
- The feeding speed and the adhesive flow must be such as to ensure complete filling of the groove without generating adhesive losses.
- In the first step it is important to avoid placing the adhesive on the fiber in the sensor area. To achieve this goal there are two options:
 - Cover the sensor with a screen that protects the sensor by lifting the nozzle of the syringe and collecting the excess resin, the screen must not come into contact with the fiber, especially if it has some adhesive parts;
 - By stopping the adhesive flow on the holes in the sensor housing and simultaneously lifting the syringe nozzle, this can be done manually or automatically by providing appropriate equipment.
- The deposition of the adhesive in the first phase ends with the deposition of the adhesive in the groove on the tip of the spatula. This gluing area is the most critical, as the available area is limited and many disconnections have occurred in the past. An effective solution, although it may be improved, is to use the excess resin present on the spout after the hole in the outer sensor housing to fill the apex cavity.
- Cross-linking can be carried out globally on the entire adhesive deposition area or locally in a limited area through a controlled-speed scan to guarantee the necessary exposure power over the entire bonding length. In the latter case, the reticulation must take place starting from the head of the fiber where it is constrained, to ensure that the tension produced by the weights acts in the gluing area.

- In the second phase, after removing the central jaw, the adhesive is placed in the quarry that is still free. Here the positioning on the bottom of the quarry is no longer fundamental for the operation of the retractor. However, as far as possible, discontinuities must be avoided that could cause interruptions in the transmission of the signal, in particular it is necessary to pay attention to the discontinuities represented by the fiber output from the already cross-linked resin and from the interruption point of the coating.
- The deposited adhesive is cross-linked following the same procedure as in the first phase.
- The third phase involves the insertion of the PEEK sheath on the fiber, which involves the removal of the weights for tensioning, at this point no longer necessary. This operation must be carried out carefully to avoid fiber breaks. The sheath must be positioned in the special housing on the metal core, leaving it spaced about 1mm from the end of the quarry, and locked, for example by means of a magnet.
- The adhesive is placed on the sides of the housing of the sheath in the appropriate side slits, filling them completely even at the cost of having excess resin. Crosslinking occurs following the same procedure as the first and second phase.

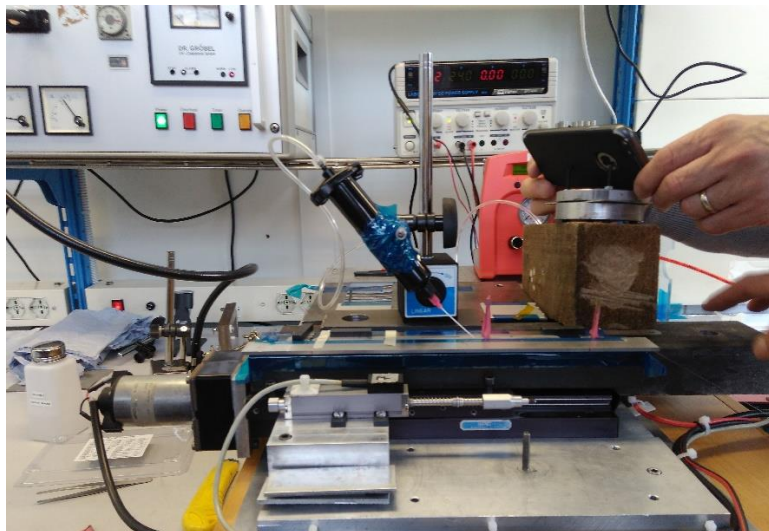


Figure 2.18: Adhesive deposition by a steady velocity flow rate through the V-groove

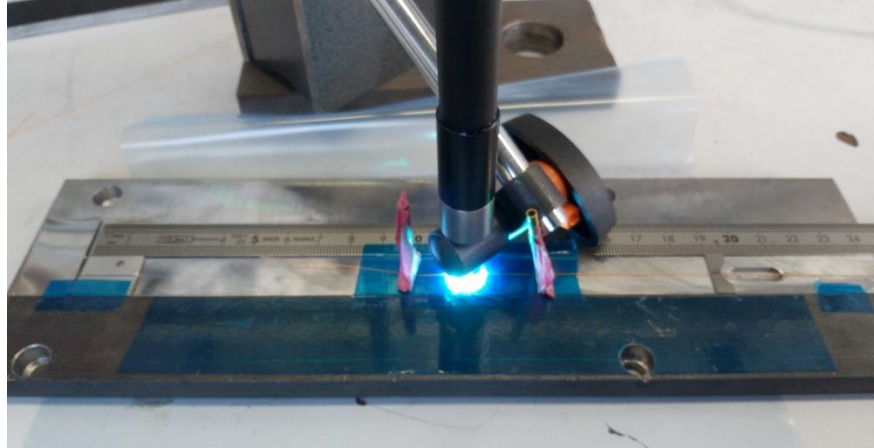


Figure 2.19: UV deposition of the fiber in the metal core

Crosslinking completion of the adhesive in the oven

- The adhesive used needs to be brought to a temperature of 150 ° C for 60 minutes to complete the cross-linking.
- The fiber coating (polyacrylate) suffers of stress deformation when it is at temperature. To avoid permanent deformation, the fiber must not be stressed during the passage in the oven.
- The passage in the oven can be done for several spatulas at the same time, in order to optimize production time.
- After 60 minutes, the spatulas should be left to cool at ambient temperature before being handled.



Figure 2.20: Final crosslinking of the adhesive in the oven

Positioning check

- This verification is done to validate the process and to correlate any deviations from the expected behavior of the retractor.
- The procedure is completely similar to the one of the sensor interrogation, with the difference that the fiber is no longer free but incorporated in the retractor, and the position of the sensors will no longer be checked with respect to the visible references on the fiber but with respect to the center of the dedicated holes.
- In production this step can take place as a sample within the scope of quality control.

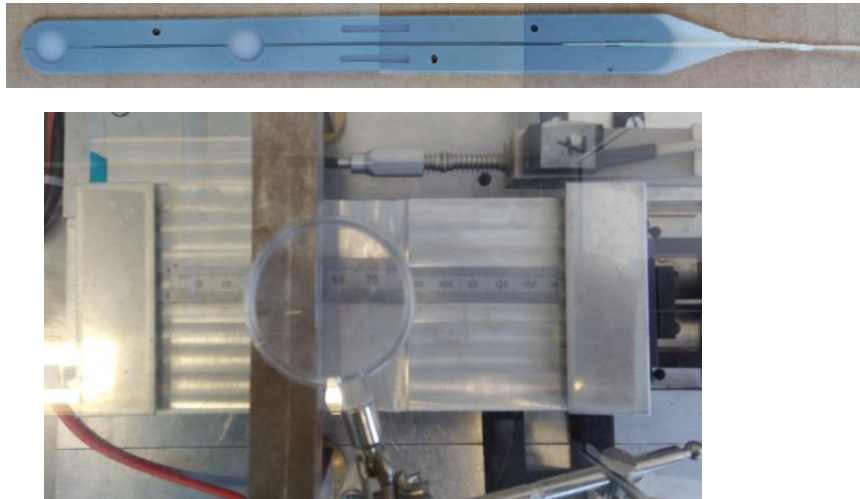


Figure 2.21: Last sensor verification after molding and stamping

2.4 Conclusion

This chapter summarize the new design modifications on the smart retractor that solve the requirements needed for an optimization of the batch SR03-03. This will marvel the bases for the specific technical requirements for the adequate equipment for the final phase of its design cycle.

The proposed solutions in the beginning of this Chapter came to realization of the newest batch SR03-04 with new adhesive selection to increase the efficiency of the reticulation process between the FBG sensor and the metal core to feature chemical compatibility by selecting the Epotek monocomponent adhesive which CTE remains similar during thermal solicitation.

The FO arrangement in the V-groove during UV exposure has been secure by ensuring to stay in the mid axis of the global retractor. Also, the assembling method was settle involving the interrogation method to ensure the readings and measurement tolerance of the Bragg grating of the FBG sensor. A correct splicing procedure was noted and correct bonding procedure was documented starting from the removal of the FO coating and its fixation, the UV deposition for 3 minutes in one run on the same fixation axis and the oven cross linking completion of 150° Celsius for 6 minutes.

All these iterations of the design and production led to the fabrication of eleven smart retractors with batch name SR03-04.

Chapter 3

Industrialization & Calibration Batch SR03-04

3.1 Introduction

Derived from the solutions defined in Chapter 2 the corresponding iteration of the retractor leads to the creation of new specimens with batch name SR03-04 which in return validates the procedure adopted above and give new values during the calibration of the smart retractor.

3.2 Industrialization and Observations

The final industrialization of the retractor is composed in its vast majority of the metallic core of AISI 316 steel, three-meter-long FBG sensor with 1540, 1543, 1548 ηm (nanometers) of characteristic wavelength, the epoxic monocomponent adhesive and the elastomeric liner applied during the molding process that serves as the soft interface with the brain tissue.[Appendix A]

The required equipment is the Micron Optics Instrument to read the wavelengths difference, the hot wire instrument for the identification, an industrial oven, an Ultra Violet (UV) laser with power regulation and the calibrated metal base with two-degrees of freedom in the z and y axis for proper fixation during the reticulation process.



Figure 3.1: Equipment acquired and developed from laboratory of AMATECH Politecnico di Milano

This new batch of retractors consists of 11 specimens with the exact technological procedure presented in Chapter 2 emphasizing in; the position verification of the sensor, production procedure of the host material and the embedment of the FBG to it, and the liner of the smart retractor.

The numeration of the retractors used in the calibration test are listed below:

Table 3.1: Smart Retractor Batch SR03-04

Numeration of the Retractor
SR03-04-05
SR03-04-06
SR03-04-07
SR03-04-10
SR03-04-11
SR03-04-13
SR03-04-14
SR03-04-15
SR03-04-17
SR03-04-18
SR03-04-82

Ideally, the retractor is fabricated with no production errors, the naked fiber is positioned exactly in the midplane of the metal core, so any mechanical deformation contribution as flexural deformation would not be major influential on the readings.[13]




This fully naked fiber over the metal core will give the reference configuration of the three sensors and avoid potential mechanical deformation during strapping the fiber from its coating. This also increases the sensitivity of the retractor since pure flexural contribution is influencing the sensor. More about this deformation is treated in Chapter 4.

This material difference will stand out the mechanical and diameter variation, but as analytical and experimental results convey to similar values as presented further in this chapter, the midplane assumption on this laminar composite retractor is valid.

Production Visual Analysis

As any laboratory production and experimentation the batch might be subjected to imperfections. To minimized the obvious damage of the production, a visual external evaluation is executed and a comparison with the past retractors batch.

Table 3.2: Comparison of Retractor Batches in the tip bonding

Batch SR03-02	
Batch SR03-03	
Batch SR03-04	

The Table above gives a comparison of the different production of the retractors exposing the main difference in the tip bonding, which showcase the enhancement of the procedure stated in Chapter 2. In the third photo of the table above, it is seen the laser beam verification for continuity of the fiber get exactly at the end of the FBG sensor tip.



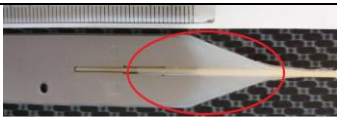
Other past production errors have been dealt as the liner molding in the retractor, which verifies the new adapted geometry and metal core production with sand refinement.

Table 3.3: Comparison of Retractor Batches Liner Molding Process

Batch SR01	
Batch SR02-05	
Batch SR03-03	
Batch SR03-04	

By the visual inspection of the new batch, it is validated that the surface errors of the metal core have been overcome. At the same time the liner molding procedure has been enhanced in the retractor. Table 3.3 shows the uniformity of the liner appliance and how is merged successfully with the new methodology and glue procedure.

Table 3.4: Comparison of Retractor Batches handle base

Batch SR01	
Batch SR02	
Batch SR03-04	

The liner designed in the new batch has an extra geometric elastomer appliance in the handle base where the final user interacts with the retractor to have a safer and secure grip to the retractor, minimizing the risk of detachment and break down of the FBG sensor during usage. The 11 specimens produced has the same response in the verification, integrity and geometry consistence by the simple visual analysis. This represents a successful production procedure that ensures the quality and the performance of the retractor.

However, the considerations aforementioned in Chapter 1 are influential for the ideal industrialization process for manufacturing and correct final user experience to decrease reading errors of the retractor.

3.3 Calibration Test

A calibration test is executed to validate the geometrical, design and material considerations and as well to quantify the readings accuracy. It is necessary to measure the pressure and temperature dependence of the retractor in order to analyze the response of the embedment sensor at different thermomechanical values. In order to measure this accuracy of the retractor readings, the calibration procedure is applied in the same methodology developed from batch SR03-01 for pressure and temperature with small modifications.[8]

Having these contributions will allow to settle a sensibility value of either the properties.

The next technological test presented below, cover the analysis during application of pressure and temperature in the entire new batch of retractors.

3.3.1 Pressure

The processing of the next results allows to determine if the new production modification provides a quality retractor with repeatable performance in:

- Appropriate mechanical characterization for a uniform stress distribution and proper overall stiffness to tolerate curvatures while using the retractor without breakage.
- To prove chemical compatibility of the monocomponent EPOTEK and optimal adhesion during curing cycle.

Set-up considerations

The test consists of air pressure applied to the sensors in an isostatic aluminum barometric chamber developed in the AMATECH.[8]

Calibration is achieved by the comparison of measurements values delivered by the retractor with those of a standard known accuracy seen in the air pressure injector, which deals with the overall sensibility.

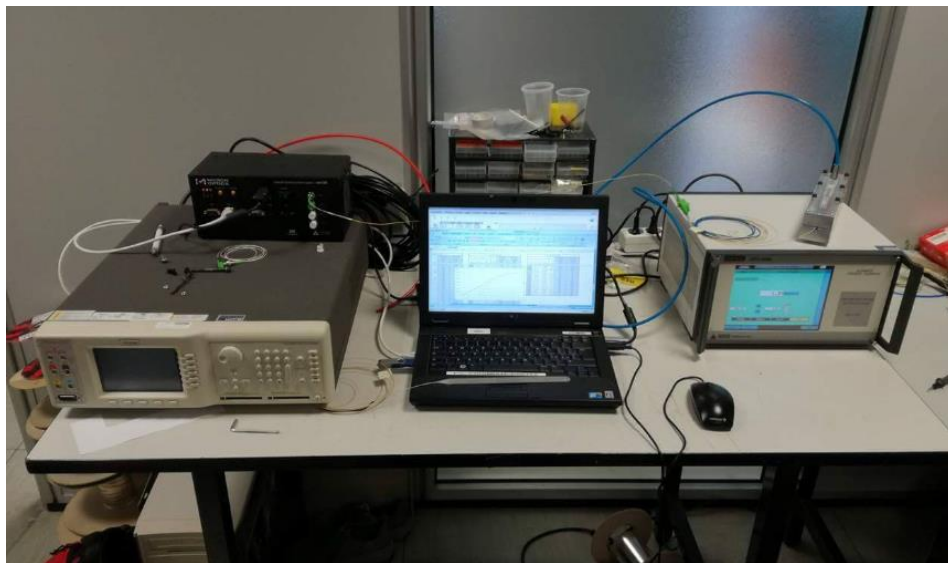


Figure 3.2: Micron Optics, Computer data collector, Pressure regulator;
Galleria del Vento Politecnico di Milano

Air pressure is used to calibrate the sensors by relating the pneumatic pressure applied to the displacement of the wavelength peak of the FBG pressure sensor, the sealing inside the instrument is made by the elastomeric material the liner is fabricated from.[9]

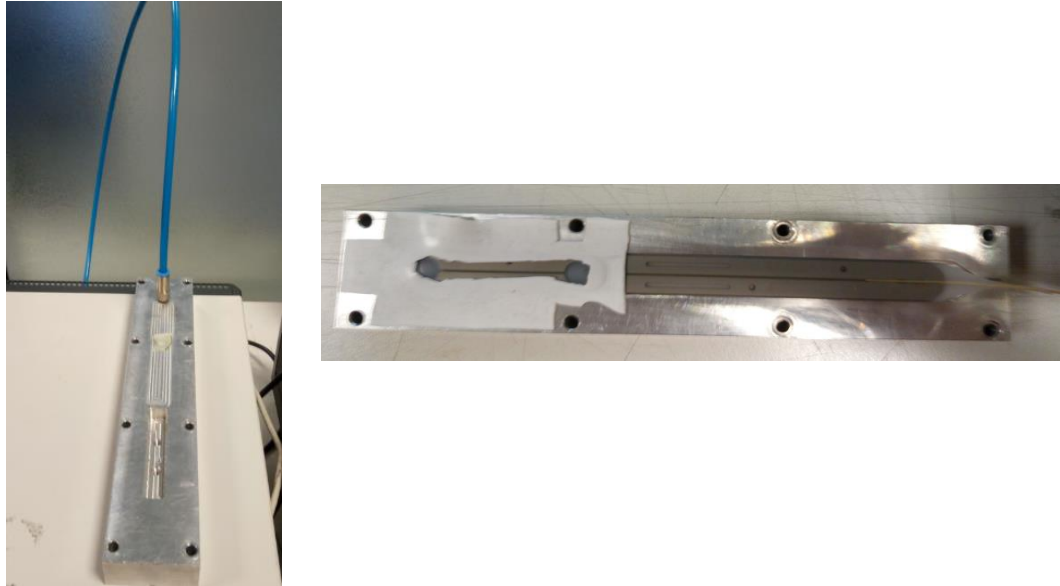


Figure 3.3: Barometric aluminum chamber; AMATECH Politecnico di Milano

The procedure

The isostatic pressure test is done by similar means and procedure of the SR03-03 specimens considering the geometry change that suits for the new model SR03-04.

Starts with the positioning of the retractor in the equipment composed of two blocks of aluminum as in Figure 3.2 that are placed together by eight bolts, inside these blocks the imprint of the retractor is replicate and in the position of the sensors airflow at certain pressure is exerted.

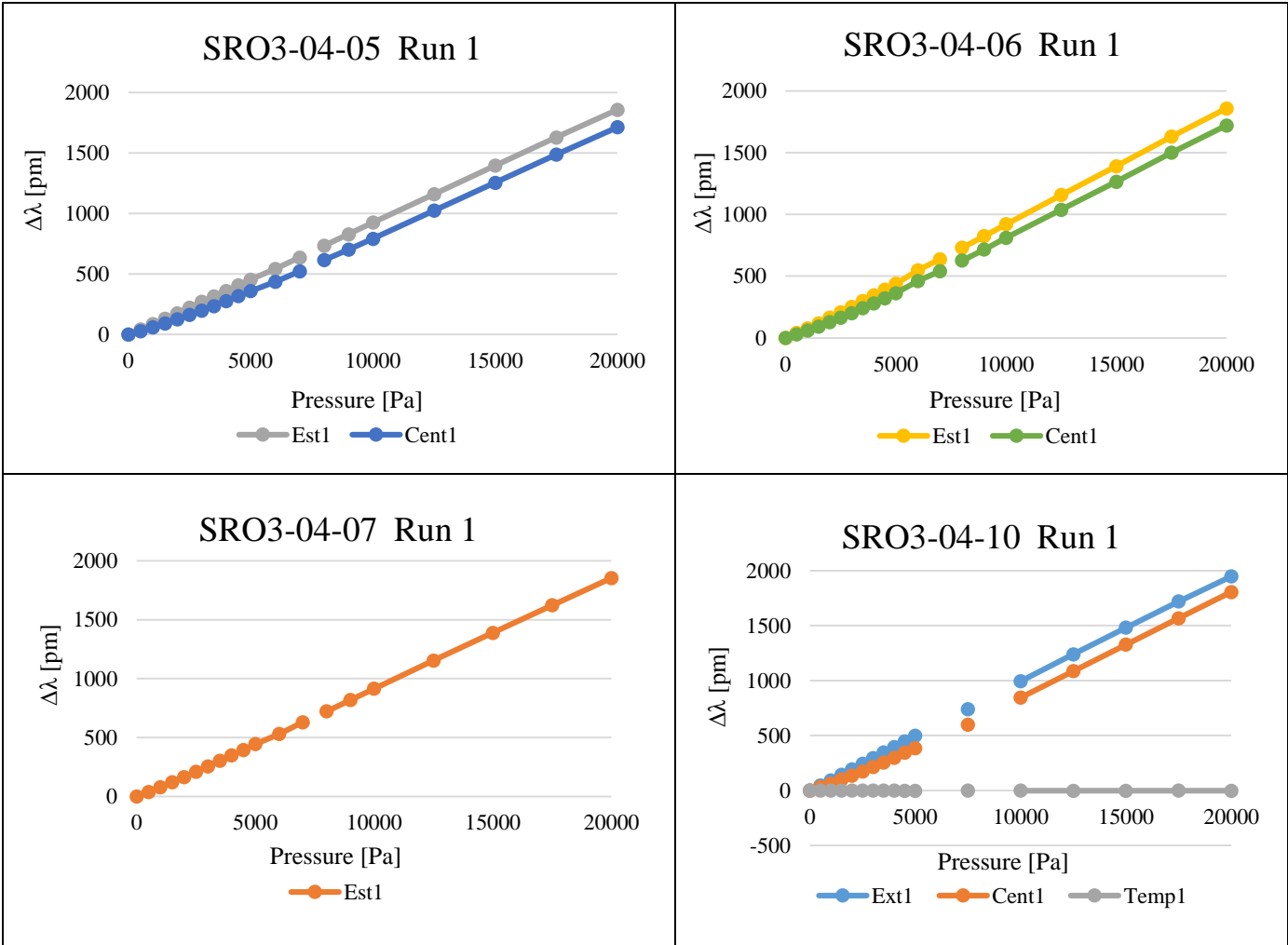
The chamber has a pneumatic exit that is connected to an accurate air pressure dispenser, this air pressure is used to calibrate the sensors by associating the pneumatic pressure and the displacement of the FBG sensors wavelength peak.

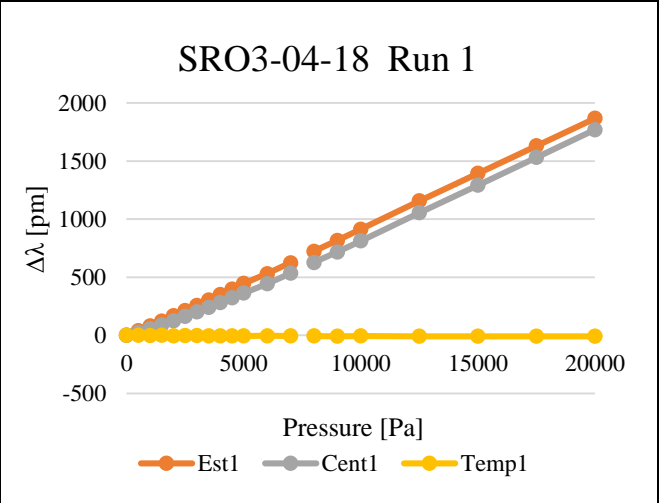
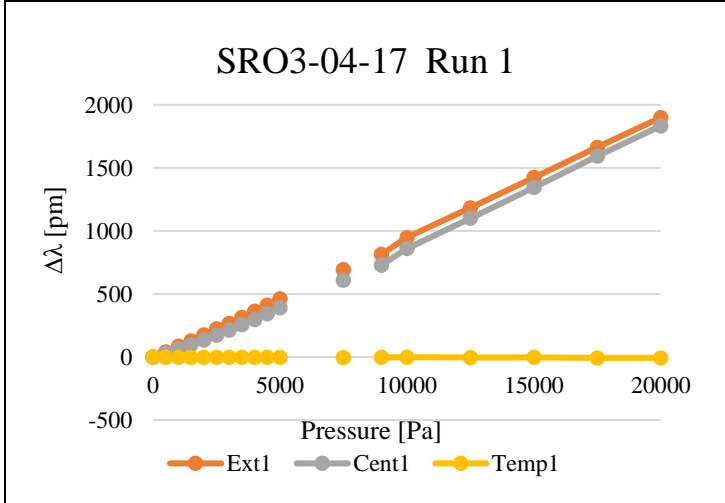
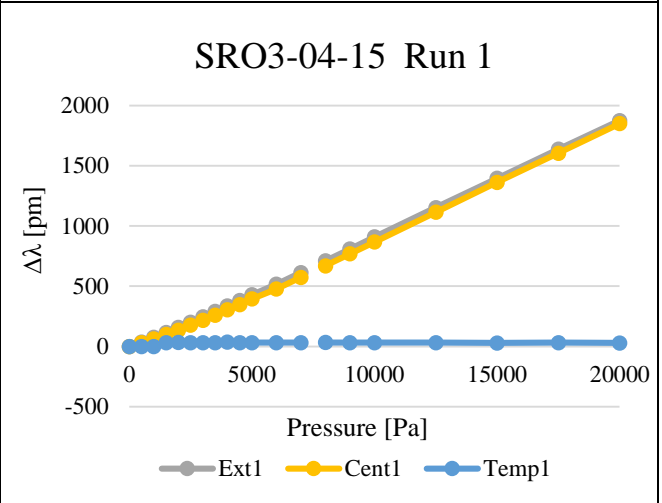
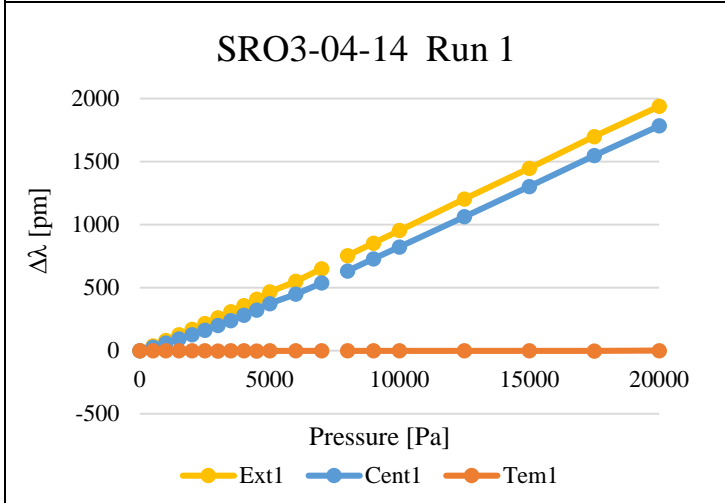
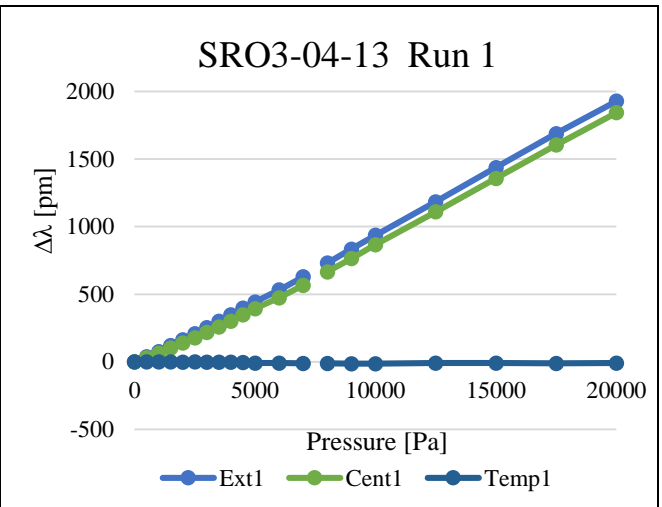
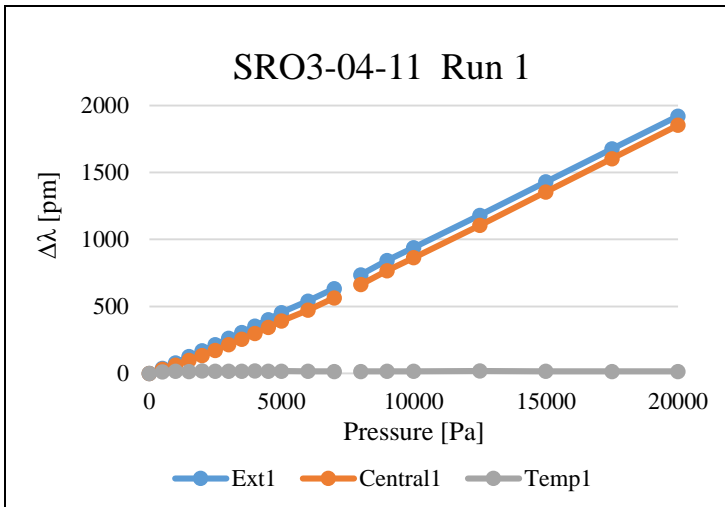
The pressure applied in the test starts from ambient pressure value and then increase it with a 500 Pa step, until 5000 Pa. A second step of 1000 Pa is applied until 10000 Pa. The last step is of 2500 Pa until 20000 Pa.

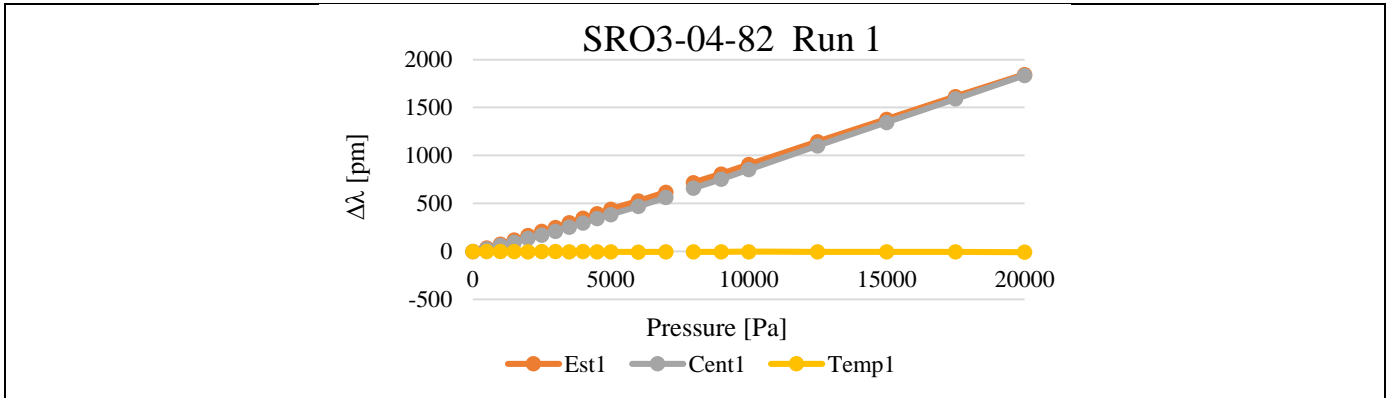
The results

The complete analysis has been done 10 times in each retractor to prove repeatability and accuracy. Table 3.5 shows the Run 1 out of 10 runs that substantially validates the optimal adhesion of the FBG sensor to the metallic core.

Table 3.5: Pressure calibration results in Run 1







As a general observation from the data acquired reflects that the new batch has been produced correctly and all the sensors of the 11 specimens are fully functional. Retractors 05, 06 and 07 are fabricated only with two and one sensors respectively, this only to produce more specimens to test the reliability of the new production method.

Table 3.6: Run 1 and 2 of Retractor SR03-04-14

Retractor SR03-04-14						
Pressure	$\Delta\lambda_{Est}$	$\Delta\lambda_{Cent}$	$\Delta\lambda_{Temp}$	$\Delta\lambda_{Est}$	$\Delta\lambda_{Cent}$	$\Delta\lambda_{Temp}$
KPascals	Run 1 [pm]			Run 2 [pm]		
0.0	0	0	0	0	0	0
0.5	38	28	0			
1.0	81	59	0	80	59	1
1.5	125	93	-1			
2.0	169	125	-1	163	127	2
2.5	215	163	-2			
3.0	261	199	-3	258	201	-1
3.5	310	238	-1			
4.0	358	282	-1	346	280	-1
4.5	408	322	-4			
5.0	466	373	-2	442	362	1
6.0	550	448	-2			
7.0	650	537	-2			
7.5				676	578	3
8.0	754	632	-1			
9.0	853	729	-2			
10.0	953	822	-1	927	818	1
12.5	1203	1062	-2			
15.0	1447	1302	-2	1415	1294	0
17.5	1699	1548	-3			
20.0	1938	1784	0	1884	1761	1

Run 1 is made with three step functions in order to provide displacement data on the first usage of the retractor by the final user. The second run of the test (Run 2) is measured starting from ambient pressure and increase with a step of 1000 Pa reaching up to 5000 Pa and the final measurements reach up to 20000 Pa as shown in Table 3.6 for retractor with termination number 14.

Indeed, from Run 2 to Run 10 is made to prove repeatability and to get a standard deviation of the wavelength variation for each value of pressure. Due to the problematics in the past productions, the most important part to inquire is in the area of the tip bonding of the fiber where the external sensor (Est) is positioned.

In retractor 14, the evaluation of all the runs are shown below.

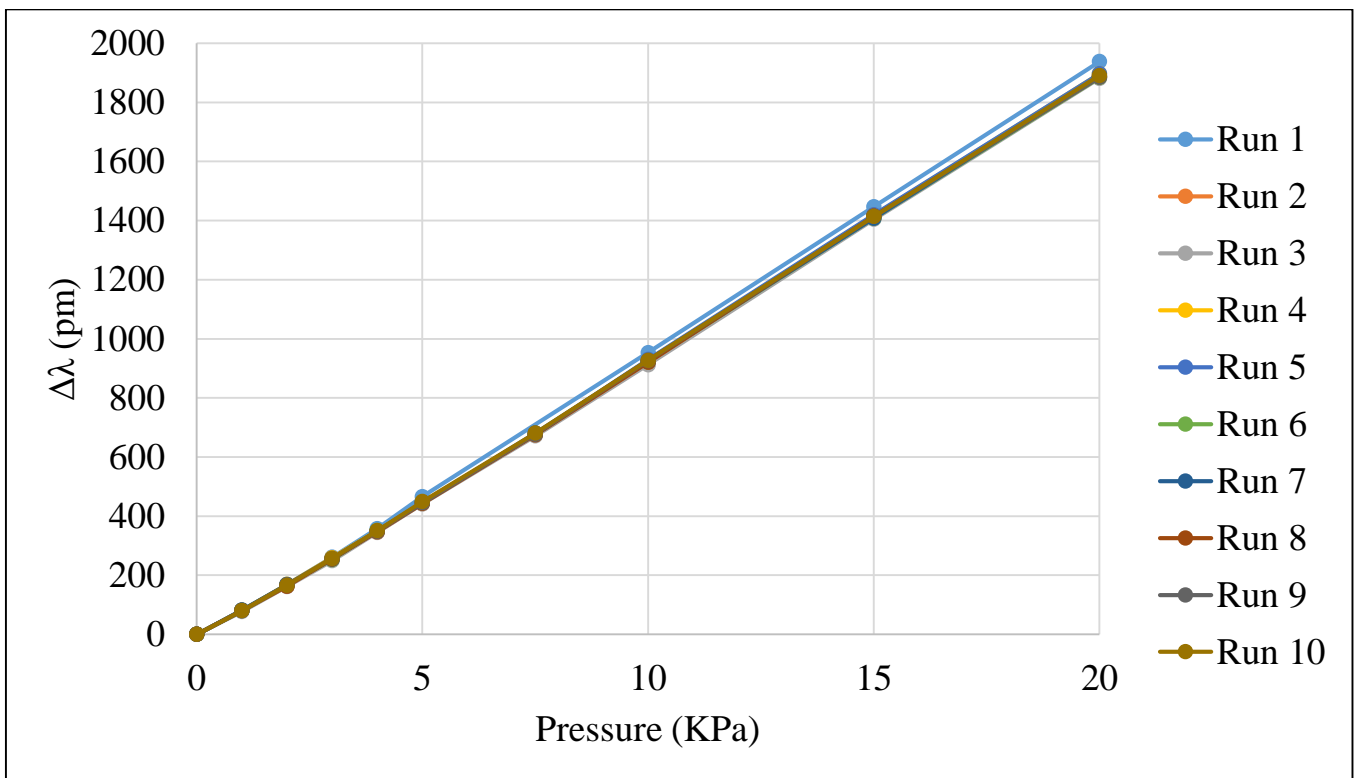


Figure 3.4: Wavelength variation of external sensor in all runs

As seen in Figure 3.4 the condition of linearity is achieved from different pressure values in the external sensor being the most critical one out of the three due is in contact with the brain, as mentioned in Chapter 1.

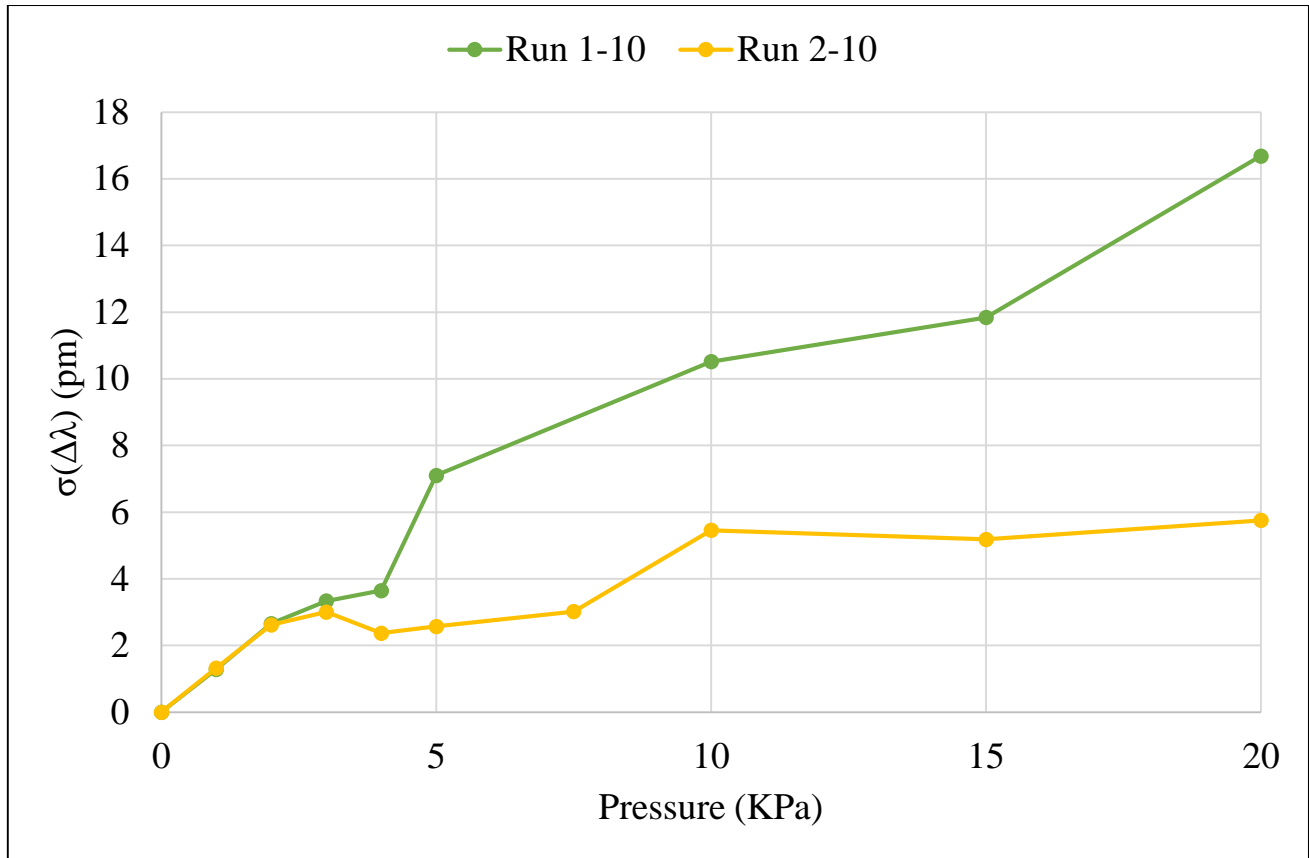


Figure 3.5 Standard wavelength deviation shift in the external sensor, Retractor 14

The measure of the amount of dispersion of the set of values is called standard variation σ_{sv} , and this is obtained to set a nominal calibration constant which express the variability of the margin of error during usage of the retractor. Values are shown in Figure 3.5.

3.3.2 Temperature

The usage of the retractor during brain surgery should not exceed the natural temperature of the brain itself, to avoid outwards effects in the arteries, especially in the Mean Arterial Pressure (MAP). This means that the retractor must be in ambient temperature before usage and during usage due to the time in contact with the brain, temperature must not be higher than 38°C. [5,7]

The temperature that acts on the retractor is only by means of conduction if the applied pressure is low enough. The central wavelength of the spectrum of the light reflected λ_B in the FBG that make the differentiation of the characterization of the sensors, is influenced at the same time by mechanical and temperature deformation acting in the optical fiber. (see Appendix B)

The variation is described as follow:

$$\Delta\lambda_B = 2 \left(\Lambda \frac{\partial n}{\partial l} + n \frac{\partial \Lambda}{\partial l} \right) \Delta l + 2 \left(\Lambda \frac{\partial n}{\partial T} + n \frac{\partial \Lambda}{\partial T} \right) \Delta T$$

Or simply

$$\Delta\lambda_B = K_\varepsilon \Delta\varepsilon + K_T \Delta T$$

$K_\varepsilon \Delta\varepsilon$ represents the effects of the deformation variation of the central wavelength. The deformation causes variation of the spacing of the grating which in turn change the refractive index through opto-elastic relation. $K_T \Delta T$ represents the temperature dependence responsible of the thermal expansion of the FO ($\alpha_{CTE_{FO}}$) and the variation of the spacing of the grating and the refractive index change.

The next verifications are needed to observe the behavior of the global CTE of the retractor under thermal increasing loads. The thermo-optic coefficient ζ of the FBG is calculated with:

$$K_T = \lambda_B (\zeta + \alpha_{CTE_{FO}})$$

When calculating thermal expansion, it is necessary to consider whether the body is free to expand or is constrained. If the body is free to expand, the expansion or strain resulting from an increase in temperature can be simply calculated by using the applicable coefficient of thermal expansion.

If the body is constrained so that it cannot expand, then internal stress will be caused (or changed) by a change in temperature. This stress can be calculated by considering the strain that would occur if the body were free to expand and the stress required to reduce that strain to zero, through a stress-strain relationship characterized by Young's modulus.

Table 3.7: Thermomechanical properties FO and metallic core

Material	CTE ($mm/m/^\circ C$)	Young Modulus (GPa) @ nominal $23^\circ C$
FO Glass	0.8×10^{-5}	2.079
AISI 316 Steel	0.0165	193

The mechanical properties of the materials are presented above, however applying mid plane theory for composites materials and being the total retractor thickness nine times bigger than the FO diameter, it can be assumed that the dominant CTE is the driver of the temperature deformation. (see Appendix A) Hence:

$$\alpha_{CTE_{FO}} \approx \alpha_{AISI-316\ steel}$$

The processing of the next results allows to determine if the new production modification provides a quality retractor with repeatable performance in:

- Appropriate performance of the adhesive under temperature.
- Verify the same thermo-optic coefficient for the three FBG sensors.

Set-up considerations

The temperature test is executed with an industrial oven to three different retractors 05, 10 and 15 in a separate experiment.



Figure 3.6: Industrial Oven; AMATECH Politecnico di Milano

To have a better overview of the process and temperature response inside the oven, a thermocouple and an external fully naked with cladding FBG sensor is placed to compare the behavior. The thermocouple serves to measure the temperature in the air surroundings of the retractor, and the naked fiber provides an external value from the FO in the retractor as presented below.



Figure 3.7: Three temperature measurements inside the oven

The procedure

Each experiment starts from an ambient temperature 19°C then increase to 25°C which is the average temperature the retractor is going to be working in operation conditions. A step of 5°C is applied up to a 50°C to validate the repeatability and non-damage of the retractor itself.

The results

The expected result is to have a small linearized variation of the delta wavelength in the sensors.

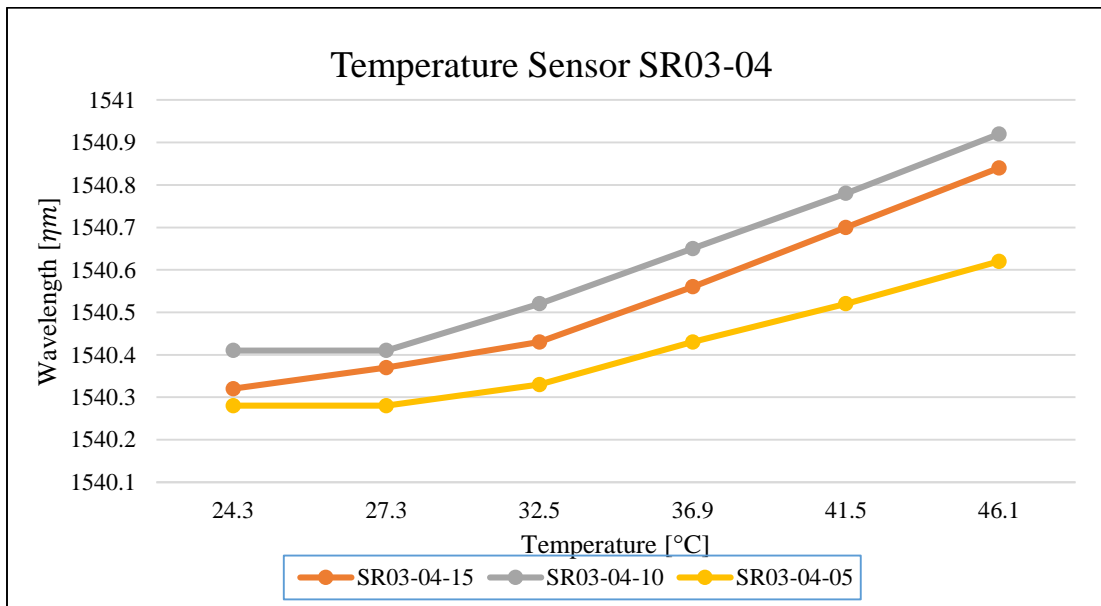


Figure 3.8: Temperature sensor response of specimens SR03-04

Results shown in Figure 3.8 gives a similar behavior in the temperature sensor for all three tested retractors with wavelength difference of 0.2 nanometers in each 5°C step. Which represent around 200% production enhancement from the batch with numeration SR03-02.[9]

The temperature value shown in Figure 3.8 is the measured from the thermocouple positioned close to the retractor and naked fiber in the oven as explained in the set-up.

Table 3.8: Calibration Temperature Test

Retractor SR03-04-10							
Oven Temperature [°C]	Thermocouple [°C]	FBG Nude [ηm]			Retractor SR03-04-10 [ηm]		
		Temp	Ext	Cent	Temp	Ext	Cent
22	19.81	1540.33	1543.27	1548.20	1540.38	1543.33	1548.51
28	27.72	1540.38	1543.30	1548.23	1540.41	1543.37	1548.55
30	28.00	1540.38	1543.31	1548.23	1540.41	1543.37	1548.55
36	33.13	1540.42	1543.35	1548.27	1540.52	1543.45	1548.62
41	36.62	1540.47	1543.39	1548.31	1540.65	1543.52	1548.71
46	41.53	1540.51	1543.44	1548.36	1540.78	1543.6	1548.81
50	46.00	1540.56	1543.48	1548.40	1540.92	1543.68	1548.92

In the Table above, the nominal temperature value is retrieved from the nominal oven sensor which is attached in the walls. This quantity does not take into account the heat transfer by convection in the oven, as a result the value of thermocouple instrument is lower than the nominal than the oven.

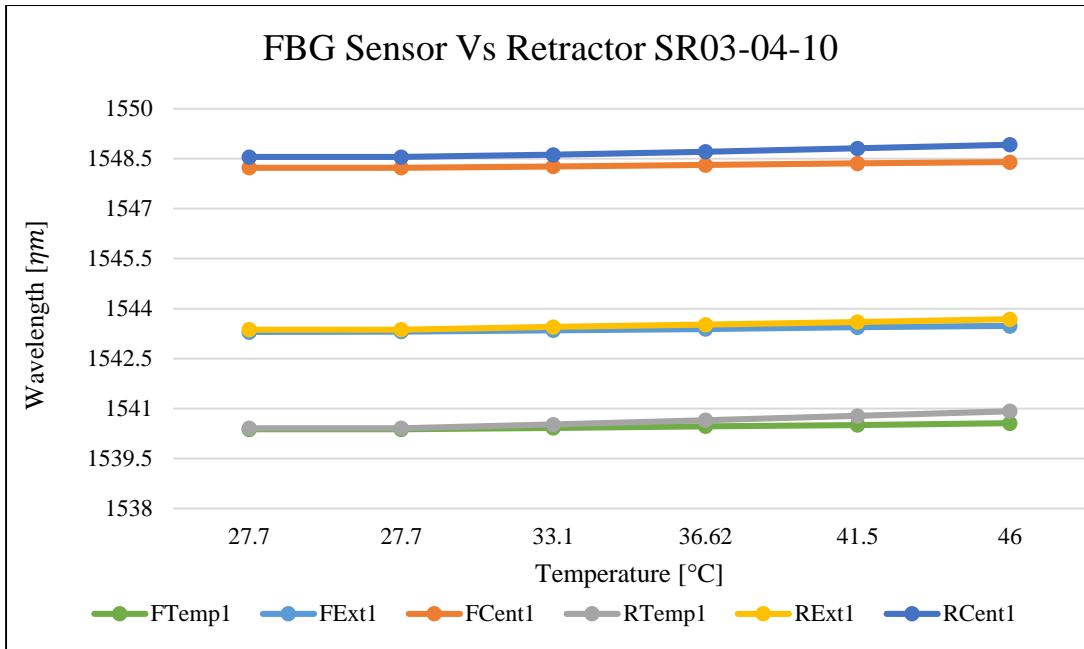


Figure 3.9: Temperature comparison between Naked optic fiber & Retractor

Temperature sensor of the retractor SR03-04-10 is compared with the FBG nude sensor to observe the thermo-optical change in the reading, which the average difference between the readings is 0.1371 nanometers and this value increases with respect to temperature.

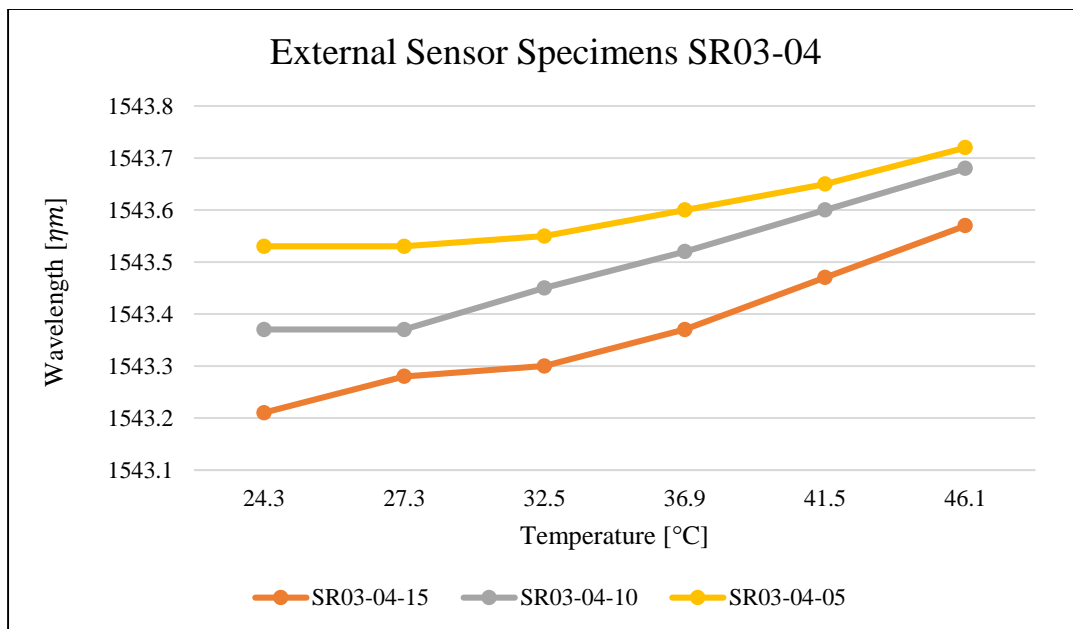


Figure 3.10: External sensor response of specimens in SR03-04 batch

Figure 3.10 gives the wavelength displacement in function of the temperature of the external sensor which during usage of the retractor has more contact area in the brain. The figure above shows that the temperature sensor shown in Figure 3.8 is more sensible for temperature variation than the external pressure sensor as design. This is an enhancement on the production due to optimal adhesion of the temperature sensor in the metal core.

3.4 Conclusion

The improvement on the industrialization procedure and the enhancements of the design led to the fabrication of 11 new retractors and a visual analysis was performed displaying a remarkable upgrade with respect of the past designs.

The calibration test of the retractor is executed in function of pressure and temperature parameters. The test gave as a result the appropriate displacement measurement of the FBG characteristic reference wavelength of the three retractor's sensors in function of pressure. The maximum considered pressure was of 20,000 Pa, being the double of the usual exercised during neurosurgery and applied 10 times on each of the retractors exhibiting repeatability and linearized behavior during readings. It also displays an expected behavior on the temperature sensor, which during this pressure test proved to be less sensible with wavelength displacement average of 19.2 picometers, being lower than the other two pressure sensors, as designed.

During the temperature test, the retractors under study reflected the design linearized variation on the temperature sensor subjected up to 50° Celsius, 30% more of the retractor usage temperature, and compared it during the test with a FBG nude sensor displaying a similar variation. This means that the temperature dominance during usage would not influence the final reading in the other pressure sensors.

Stating that due to the transmission of temperature from the retractor to the FO, the stresses increased by temperature sollicitation are not influential enough for the final gauge values of the retractor.

And at the same time, this validates the assumption of the CTE dominance of the material in the retractor and as well healthy and operational certainty of the embed FBG sensor.

Chapter 4

Technological/Validation Test

4.1 Introduction

It is necessary to provide validation to the latest design and production procedure that has been upgraded for the batch SR03-04 in order to quantify and justify all the geometrical, design and material considerations.

The next technological tests presented below, cover the analysis of the flexural response during two different cases, the effective glued area on the tip of the retractor and verification of the position of the FO in the globalize retractor.

4.2 Flexural deformation of the retractor

In order to prove the strength of the fiber, the adhesion and the correct molding of the whole retractor, a flexural deformation test is done to 10 of the new retractors.

The procedure is similar to the one applied in the batch SR03-03, in order to analyze the effect of the total response and arrive to a correction factor for bending to minimize error readings.

It is necessary to evaluate the results coming from wavelength displacement into strain and displacement of the FO itself, so it can be measure the distance between the FO with respect to the retractor mid axis.

The equation of strain ε on the optical fiber is:

$$\varepsilon = 1.27 \left(\frac{\Delta\lambda}{\lambda} \right)$$

Where λ is the unload reference wavelength and $\Delta\lambda$ is the change of the wavelength with the applied load. As the whole retractor is modeled as a slender beam, the constitutive law which relates stress and strain is:

$$\sigma = E\varepsilon$$

Where E is the Young Modulus's and σ stress, hence:

$$\sigma = \frac{M_x}{J_x} * y$$

Which y gives the distance of the fiber to the mid plane and J_x and M_x as the moment of inertia and moment in x axis respectively. J_x can be calculated with:

$$J_x = \frac{b * h^3}{12}$$

Where h is the thickness of the cross sectional area and b the width of the retractor. And M_x is calculated with:

$$M_x = F * d$$

Where F is the force applied in the beam and d the distance from the load to the desired measurement point, in this case where the sensors are.(see Figure 1.16). From the last analysis it is seen that it's possible to determine y , the displacement of the fiber to the mid plane.[9]. However, production modification has led to a minor displacement of the fiber and also achieved to be fully constrain between the metal core and the reticulated glue.

So for this analysis we are interested to study the $\Delta\lambda$ of the FO and a linearization of the wavelength displacement value during flexure deformation. The process of the experimentation results will provide data of:

- Wavelength displacement response of an applied force in two different conditions before breakage of the retractor.
- Error lectures in the sensors and analyze the uniform stress distribution, fiber displacement and overall stiffness.

Set-up considerations

The tests consist in the application of masses in the retractor in two different set-ups configurations simulating the usage during the brain operation. In Chapter 1 gives an overview of these retractors are used so is decided to modeled as a cantilever beam and simple supported beam for the test.

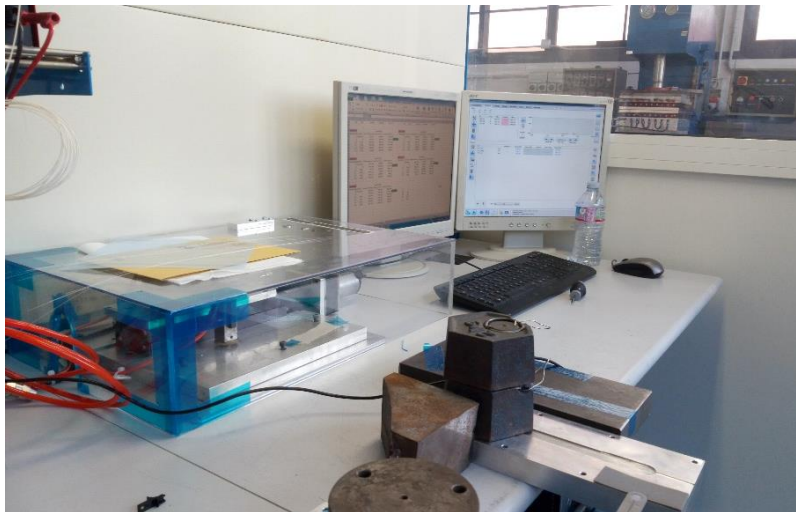


Figure 4.1: Metallic set-up and signal interrogator
Fiber Optic Laboratory Politecnico di Milano

The procedure

As a first approximation it can be model as a beam subjected only to flexural deformation with no axial nor torsional deformation of it.

This simple assumption comes from the fact of how the final user of the retractor use and hold the tool during the brain surgery. [5]

Using a combination of exact weight masses in the laboratory, the total values applied in the retractor to evaluate the forces are 100 gr, 200 gr, 300 gr and 400 gr exerted as a punctual force right in the middle in the case of a simple supported beam and in the tip of the retractor close to the external sensor for the case of a cantilever beam.



Figure 4.2: Exact weight masses

The results

Cantilever Retractor

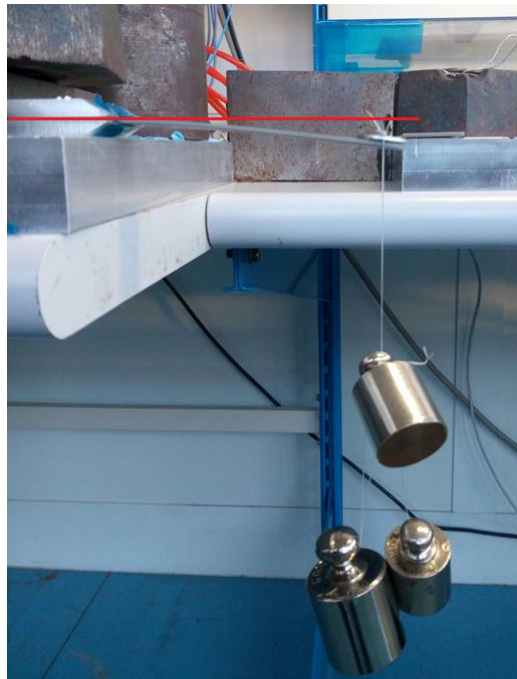


Figure 4.3: Transversal displacement of retractor as cantilever beam

The values obtained from the analysis of a cantilever beam modeling in retractors with numeration SR03-04-10 and SR03-04-11 are:

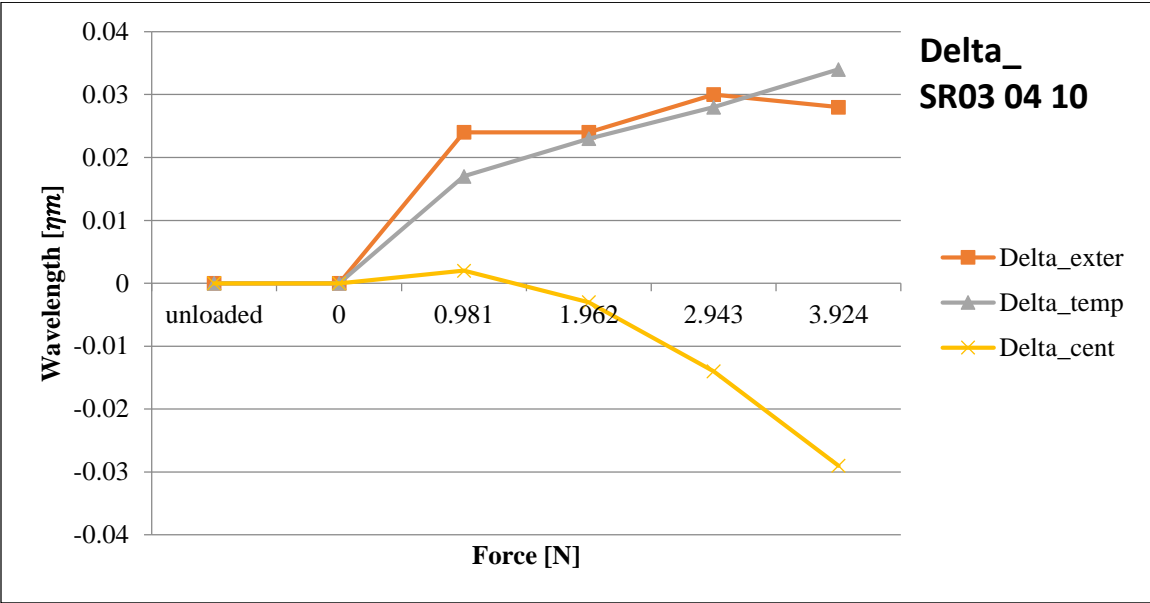


Figure 4.4: Wavelength variation with increasing mass, SR03-04-10

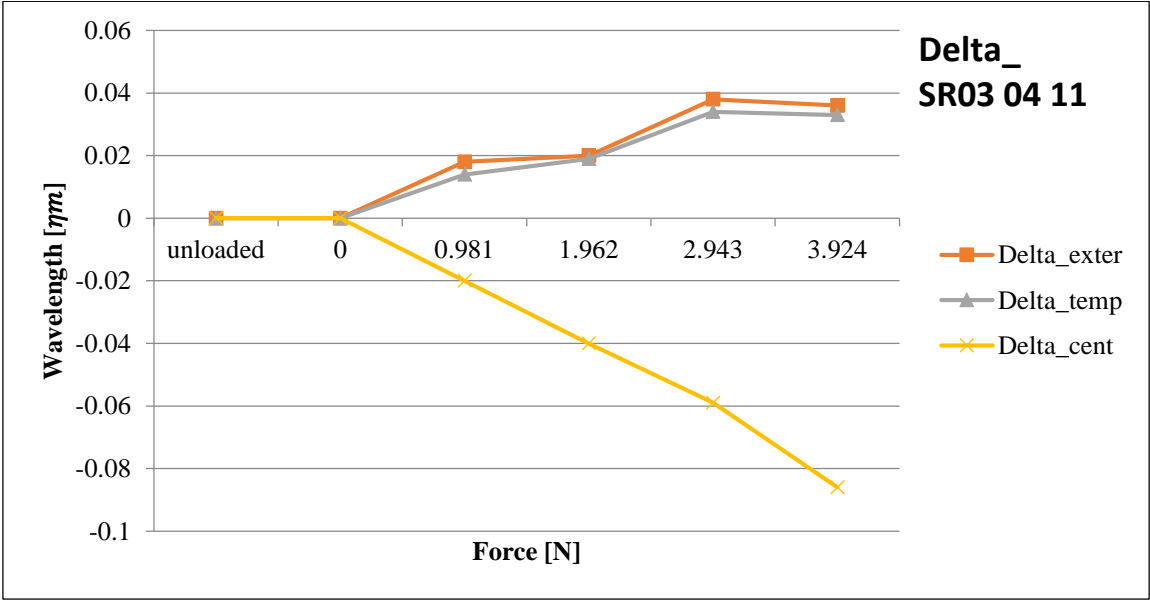


Figure 4.5: Wavelength variation with increasing mass, SR03-04-11

Figure 4.4 and Figure 4.5 gives the variation on the wavelength during the increasing mass in the cantilever analysis.

As seen in the Figures above a tiny variation is achieved by the procedure enhancement and gives a maximum delta variation in retractor 10 and 11 of -0.029 nanometers and 0.089 nanometers respectively.

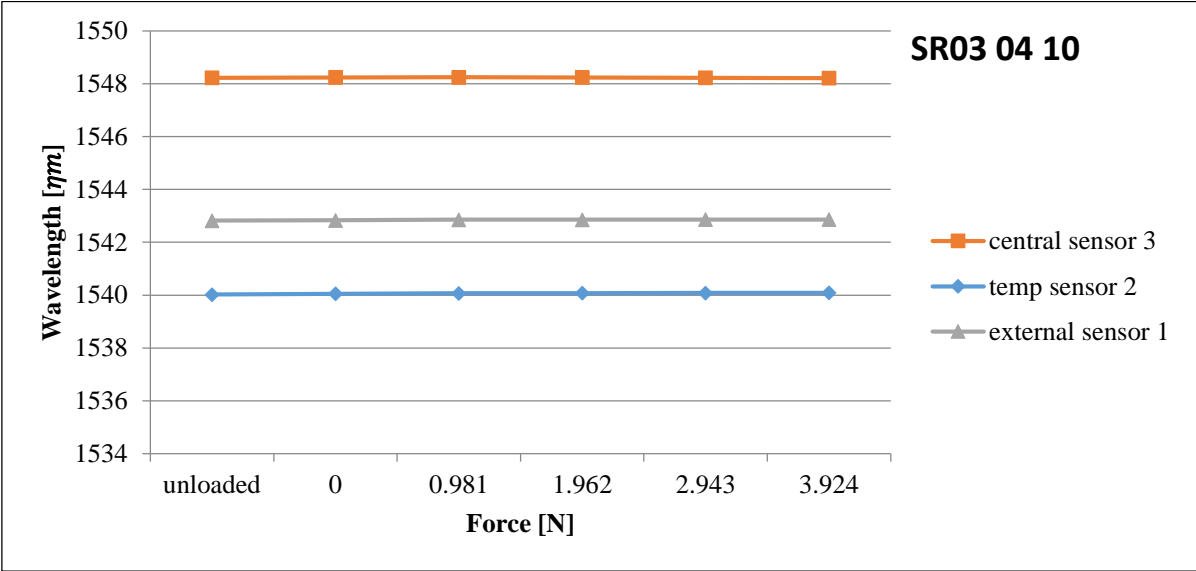


Figure 4.6: Wavelength variation during flexural test, SR03-04-10

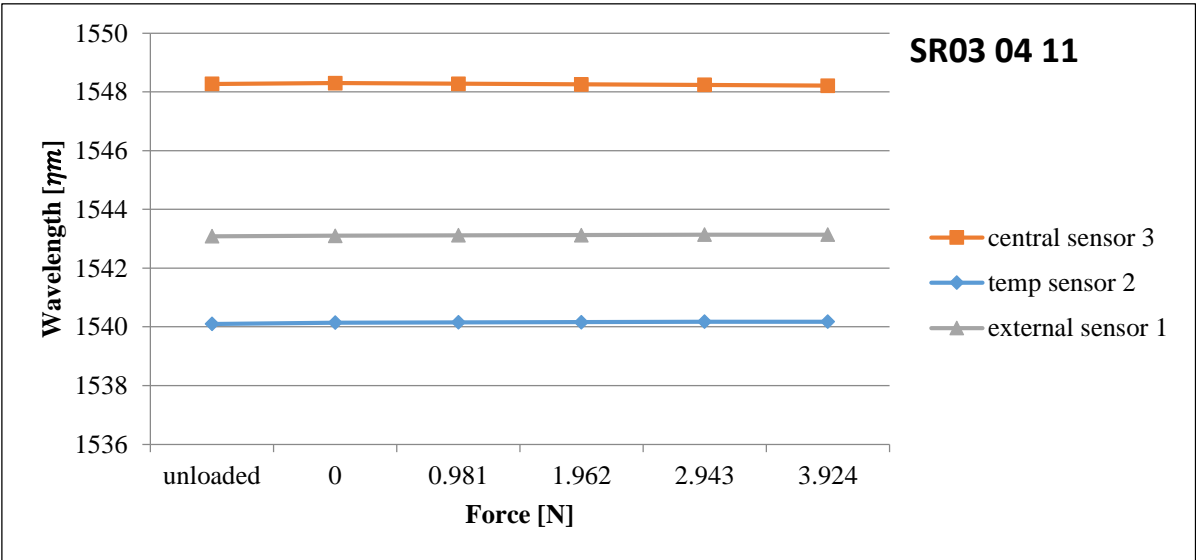


Figure 4.7: Wavelength variation during flexural test, SR03-04-11

The contribution of flexural deformation gives, as stated before, an approximate displacement value of the fiber from the mid axis of the whole composite retractor.

As seen in Figure 4.3, the displacement from the mid axis of the retractor can be computed with the suitable theory of cantilever beams. Even this variation is small, gives data of the transverse response and hence the stress-strain state of the retractor can be compute. The analysis must be done as a composite material, with the mechanical properties involved from the complete retractor (liner, metal core, reticulated adhesive and the FO). A suggested FEM analysis is present in Appendix C which can bring data of the health of the fiber, reliability and accuracy of the readings during flexural deformation.

The variation of the retractor FBG wavelength is almost null for the apply force during usage and proves an enhancement production with the bonding process and positioning of the fiber in the metal core with respect to the past batch SR03-03.[9]

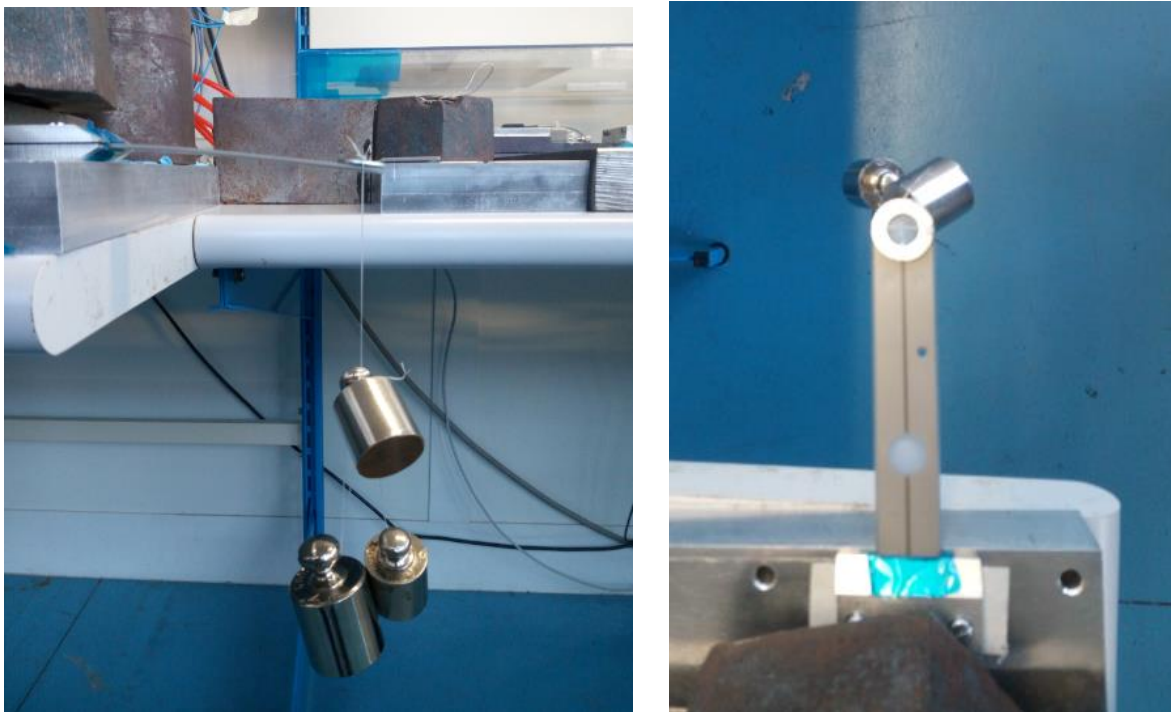


Figure 4.8: Flexural test in cantilever retractor

Simply supported Retractor

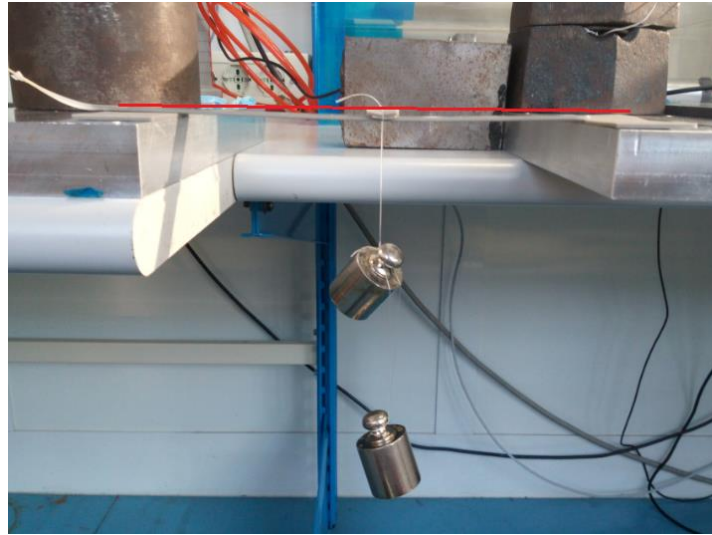


Figure 4.9: Transversal displacement of retractor as simple supported

The values obtained from the analysis of a simple supported beam modeling in retractors with numeration SR03-04-11 and SR03-04-17 are:

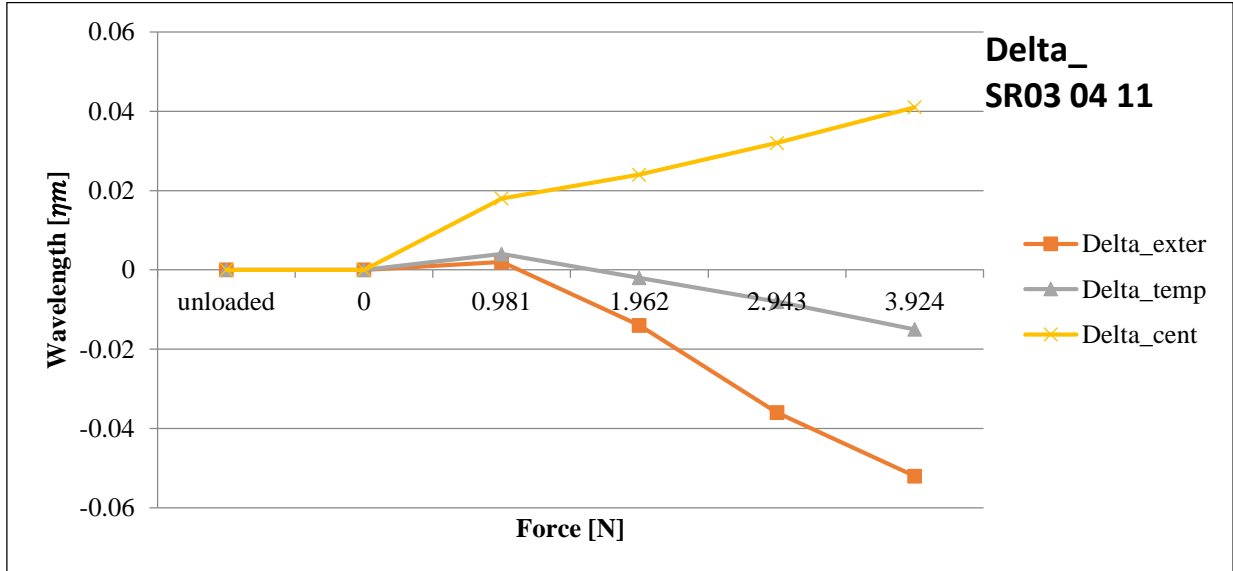


Figure 4.10: Wavelength variation with increasing mass, SR03-04-11

As seen in the Figures 4.10 and 4.11 the response delta difference between the intrinsic wavelength of the FBG with respect to the maximum mass applied, is repeated in the retractors.

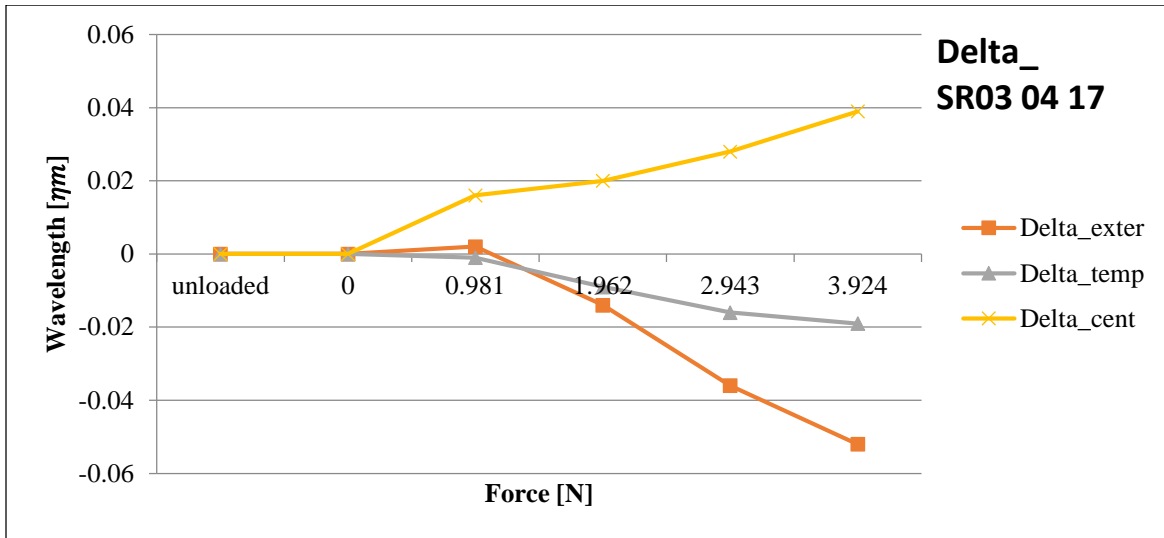


Figure 4.11: Wavelength variation with increasing mass, SR03-04-17

This means that the production of them and specially the embedment of the fiber to the metal core, achieved a more optimal level from the past production batch SR03-03.

The most notable observation is that the bending response for the external sensor is higher than the other two, in the retractors above. For this kind of beam modeling, the force applied is in the center of the retractor, left side of the central pressure sensor, which displacement must be higher. Although observing the rest of the specimens, this variation of the wavelength is so low with respect to the central sensor, in fact up to 200 gr applied the displacement in the central sensor is indeed higher than the other two sensors.



Figure 4.12: Flexural test in simple supported retractor

The data obtained for the 10 retractors gives a uniformity during the molding process and the mid plane theory is valid for the composite retractor. The delta displacement of the reference wavelength with respect of the force applied is still present.

Table 4.1: Mean value of wavelength displacement in the flexural deformation test

Retractor Batch	SR03-02	SR03-03	SR03-04
Wavelength displacement [ηm]	136.4	95.6	43.1

However, giving a comparison between the results of the SR03-02 and SR03-03 batches where the same flexural deformation test was performed in the case of a simply supported model, the new batch SR03-04 provides a better performance in terms of average displacement wavelength for the three sensors of the all the retractors (Table 4.1).

4.3 Tomography

The embedment quality of FO sensors in carbon fiber reinforced polymers and other materials plays an important role in the resultant properties of the composite, as well as for the correct monitoring of the structure. Therefore, the availability of a tool able to check the FBG sensor and composite interaction becomes essential.

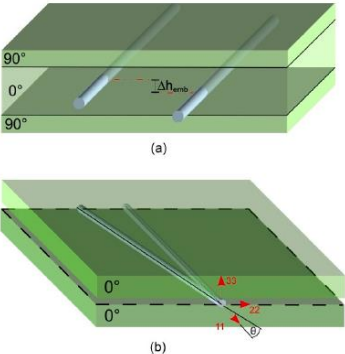


Figure 4.13: Schematic examples of examination a) mal-positioning through thickness during embedment b) misalignment between sensor and materials

Among the non-destructive inspections (NDI) techniques of FO internal condition monitoring, such as thermography, ultrasounds or radiography, tomography or X-ray MicroComputed are able to detect any defects or material inclusion of smaller size in a composite one. If strongly focused, this technique allows detecting cracks of a few hundreds of microns and therefore, the name of MicroComputed tomography. The result is a scan in a 3D reconstruction of the inspected volume. [15]

The process of the experimentation results will provide data to:

- Adhesion verification of the FO sensor in the quarry interface of the metallic core in localized tip area.
- Damage inspection on the fiber while embedment in the metallic core and liner application.

Set-up considerations

The test is performed in the non-destructive tests laboratory of Politecnico di Milano. It is executed with a X-25 North Star Imaging X-ray scanner which characteristics are presented in the next Table.

Table 4.2: NSI Scanner Model X-25 characteristics

System/manipulator Capabilities	
Geometric magnification	3000x
Manipulator travel dimensions	81 cm diameter / 121 cm tall
Rotation of sample	360°
Tilt	± 20°
Maximum sample weight	227 kg
X-ray Source	
Voltage range	10 kVolts – 450 kVolts
X-ray Tubes types	Nano-focus, Micro-focus
Overall maximum resolution	500 η m
X-ray Detector	
Digital X-ray type	Flat panel (DDA), Linear Diode Array
Detector size	40 cm x 40 cm



Figure 4.14: MicroComputed X-25 Scanner, NSI brochure

The procedure

High-resolution 3D X-ray MicroComputed Tomography, or Micro-CT, is a relatively new non-destructive inspection technique which enables investigations of the internal structure of a sample without actually compromising its integrity. In this work the feasibility of inspecting the position, the orientation and, more generally, the quality of the embedment of the FO sensor in the retractor is present.

The test is performed with aid of the personal in the laboratory with the safe conditions related to X-ray possible damage. It makes use of an X-ray beam which is sent through the retractor to measure the local linear attenuation coefficient for X-ray in the object, yielding morphological information.

This MC-T set-up consists of the X-ray source directing its rays towards the sample, which is usually mounted on a manipulator, and an X-ray detector positioned behind the sample. The transmitted X-rays hitting the detector yield a 2D projection or radiograph of the sample.

The detector system is the energy dispersive detector. Each pixel of the scintillator panel captures X-rays and converts them into light image. The equipment transfers the image to a charge-couple device (CCD) sensor, where the light is transformed into an electric signal. The latter is further sent to an analogue to digital converter and stored on a hard drive, as a radiograph.

In order to recover the 3D distribution of the local attenuation of the retractor sample, multiple radiographs are taken from different viewing angles, covering 360°.

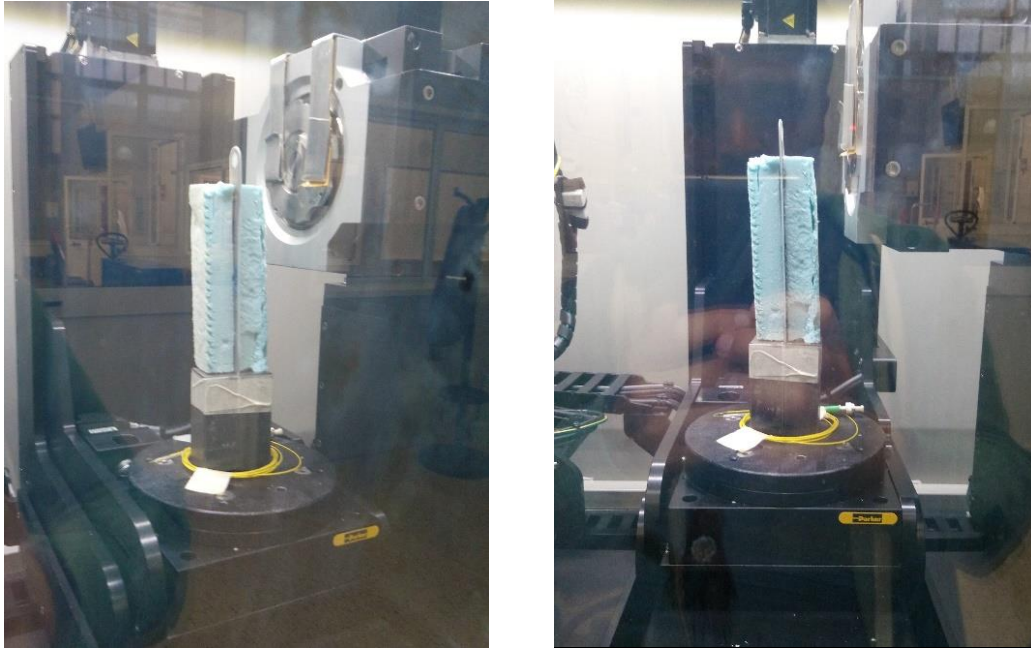


Figure 4.15: Positioned of retractor SR03-04-10 with foam in the scanner

The core of this test is to verify the tip bonding of the FO in the meta core, hence a 360° tomography is applied in the interested area. The specimen selected for this test is the SR03-04-10.

The results

The sample is fixed on a high precision piezo-positioning manipulator and rotates, allowing to obtain projections at different orientations. After collecting all projection data, a reconstruction algorithm calculates cross-sections of the scanned object, which can be further rendered as a 3D volume using suitable visualization software. This allows virtual inspection into the micro-structure.

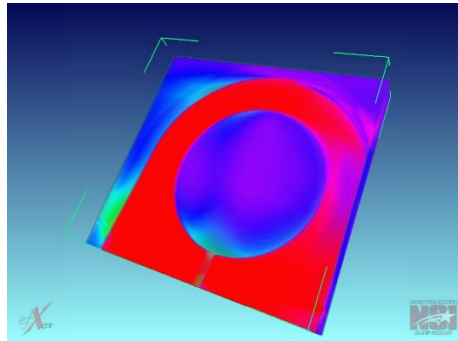


Figure 4.16: Reconstruction image of the scanned tip of the retractor

The micro-structural investigation in this work is used with maximum resolution of $500\eta\text{m}$ due to the intrinsic size of the retractor and the fiber. Imaginary reconstruction has the next characteristics:

Table 4.3: Computed Tomography software

Orientation & Resolution	
Number of radiographs	1500
Rotation of sample	360°
Angle CT reconstruction radiograph	$\pm 16^\circ$
Geometric magnification	120x
Resolution	$500\eta\text{m}$

As commented, the 3D rendering is made by the NSI product. The tip of the retractor is evaluated with effective volume area of the sample of 491mm^3 , and the next histograms are retrieved.

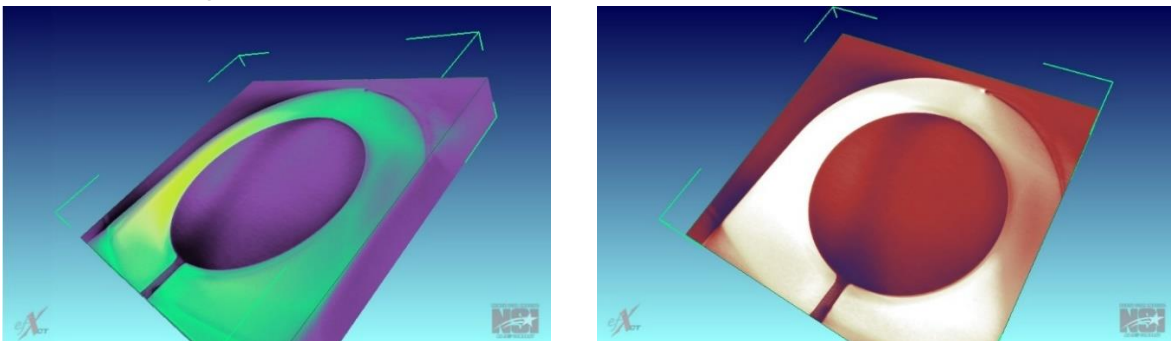


Figure 4.17: Retractor reconstruction with different histograms

By the theory of the MicroComputed Tomography, it is known that the resolution of the radiographies is increased by placing the sample closer to the X-ray source until the focal spot size becomes a limiting factor.[15]

Due to the sample composition and size volume, it is selected to use the high voltage X-ray source operated up to 120 kVolts with 25 μ A tube current. As the X-ray hits the surface of the retractor and then to the detector, the success of retrieving and processing the data from the tomography comes from the material properties difference and composition i.e. effective atomic number.

Table 4.4: Retractor’s material density

Material composition	
Retractor component	Material density [gr/cm³]
Metallic core	7.99
FBG sensor	1.22
EPOXY Glue	1.05
Liner	1.12

The density of them are presented in Table 4.5 which is the reason the evidence in Figure 4.17 few attenuation of the fiber is given.

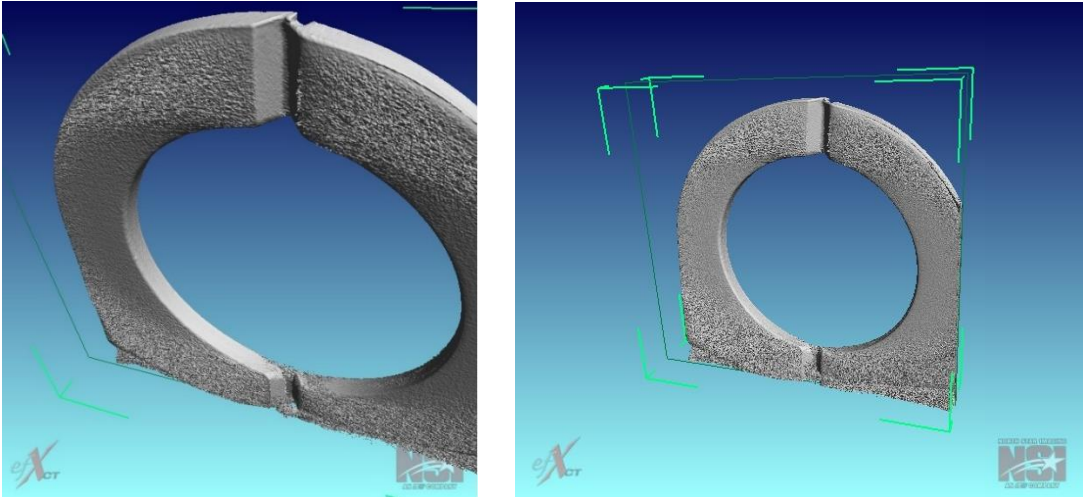


Figure 4.18: Solid imaging processing of the denser material

Nevertheless, the data retrieves a quasiexact model of the quarry in the metallic core as shown in Figure 4.18. At the same time, it proves the health, the position of the FO in the retractor and integrity of the composite retractor after liner application.

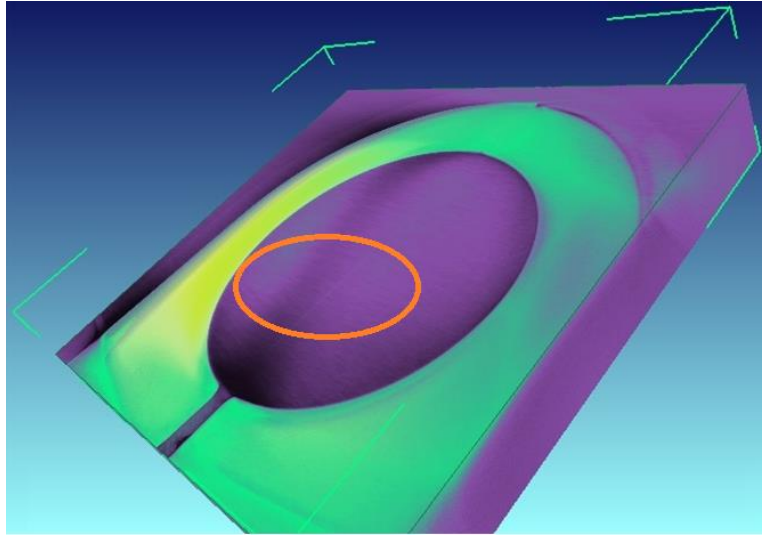
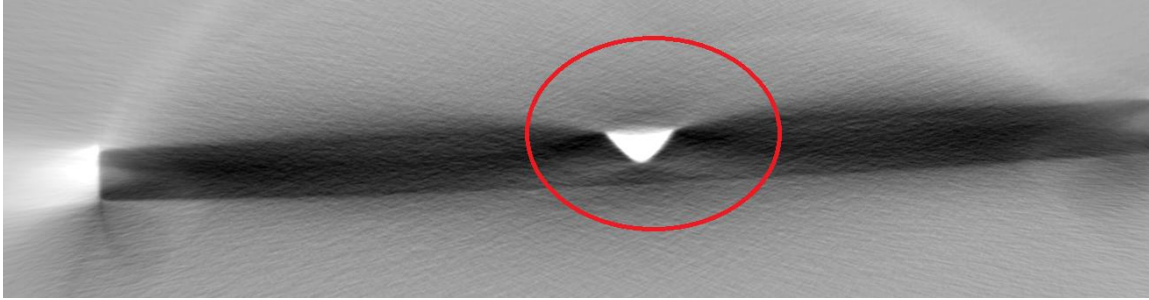


Figure 4.19: First photo: Glue solidification in the metal core quarry
Second photo: FO intact by the liner procedure

The MC-T allows to easily define the position of the embedded fiber, but as presented before depends of the scanning time and reconstruction algorithm that are high consuming time operations.[15]

4.4 Pull-Out prove

The optimum adhesion between the FBG sensor and the host material, it's a guaranty for low invasiveness in the retractor. This part of the project involves a survey of the adhesion between the FO and metal core.

Pull-out it's a destructive inspection technique that its principle consists to lead the interface until rupture and through the measurement of force and displacement, it is possible to analyze the failure modes and the transmitted loads.

A sample for a pull-out test is composed by a single fiber fully covered by a cube of the host material. The procedure consists to apply a traction force opposite to the hinged cube in order to remove the fiber from the cube.[16]. It is possible to evaluate the interface forces by imposing equilibrium from the applied force in the opposite direction from the interface that is hinged.

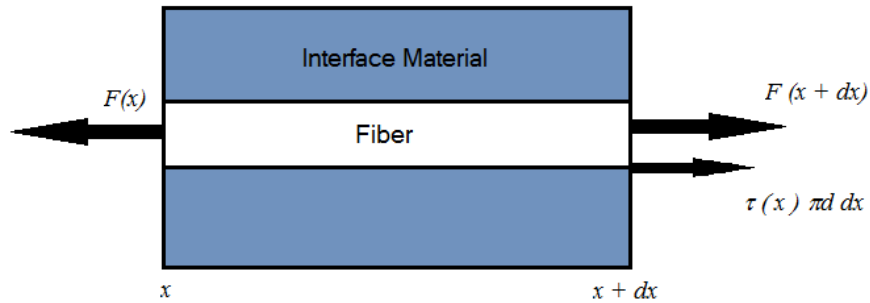


Figure 4.20: Pull-out free body diagram

Hence, the force equilibrium in the sample is written as:

$$F(x + dx) - F(x) + \tau(x)\pi d dx = 0$$

If we know the geometry of the sample and having the record of the force and displacement, we can get the values of the shear force at x . So that;

$$\tau(x) = \frac{-1}{\pi d} \frac{dF(x)}{dx}$$

Considering a limit value of F_{MAX} and for simplicity sake assume that the shear is uniform in the total cover length l . The most commonly calculated end point of these tests is the ultimate shear strength of the interface $\tau_{Interface}$. Which is the value calculated by dividing the maximum pullout force F_{max} by the nominal interface area A .

$$\tau_{Interface} = \frac{F_{max}}{A}$$

Considering cylindrical shape of the FO.

$$A = \pi D l_e$$

Where D is the outer diameter of the cylindrical material and l_e is the *embedment length* of the FO in contact with the interface. There are two different methods to fix the pull-out sample to apply the opposite force, as presented in Figure 4.21. They differ in how is set-up the system in order to have optimum conditions in the section of interest.

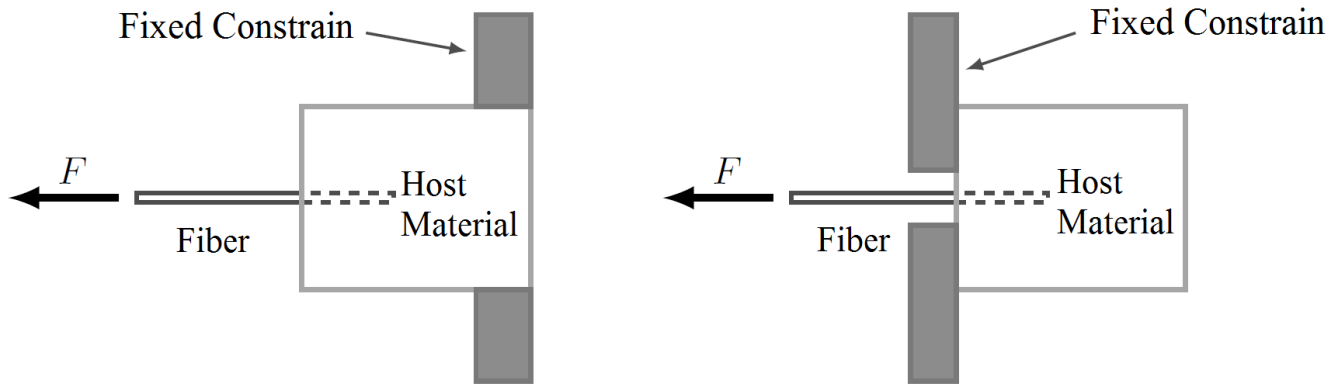


Figure 4.21: Pull-out fix options

First method consists on the compression of the embedment material which could influence the magnitude of the extraction force. The applied method for this project is the Restrained Top Constrain that only introduce the force directed to the fiber and is able to guarantee the vertical direction of the applied load.

It is important to state that there are not direct references regarding the interface study between FO and specific embedment materials, therefore, from the different possible tests it is consider the one which refers to a single fiber for the observation of the shear stress in the interface.

The process of the pull-out experimentation results will provide data to:

- Obtain the maximum load that can be transferred without interface degradation of the FO in the Epoxy monocomponent glue on the metal core.

- Evaluate possible failures during the manipulation and industrialization of the retractor.

Set-up considerations

In order to stage a pull-out prove for this project, an adapter was designed and manufactured for three special specimens that were taken into account. The design and the industrialization had many iterations with the porpoise to adapt it to the specimens shown below.

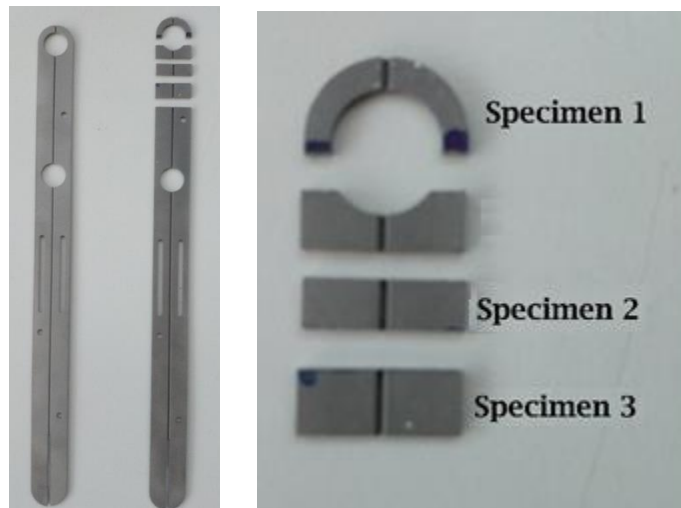


Figure 4.22: Specimens from retractor metal core

The three types of specimens have different dimensions in the longitudinal axis 3mm, 4mm and 5 mm respectively, each one designed for specific examination porpoises, regarding the section of the retractor and special attention is paid in the smallest specimen which is obtain from the up tip of the retractor.

Table 4.5: FO length in contact with metal core

Metal core longitude quarry distance	
Specimen 1	3 mm
Specimen 2	4 mm
Specimen 3	5 mm

The adapter and the specimens suffered many modifications in order to be as modular as possible for the three different sample configurations.

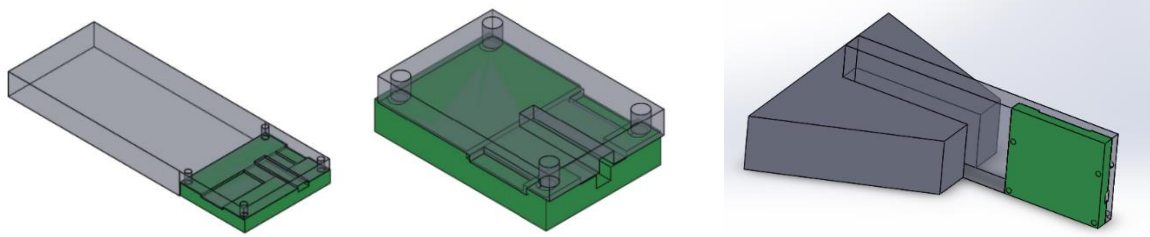


Figure 4.23: CAD designs of the adapter to Instron 4302

Fabricated in AMATECH of Politecnico di Milano, the main requirements for the adapter are to be the most symmetric as possible and to have the center axis aligned with the Tensile testing machine (Instron 4302).

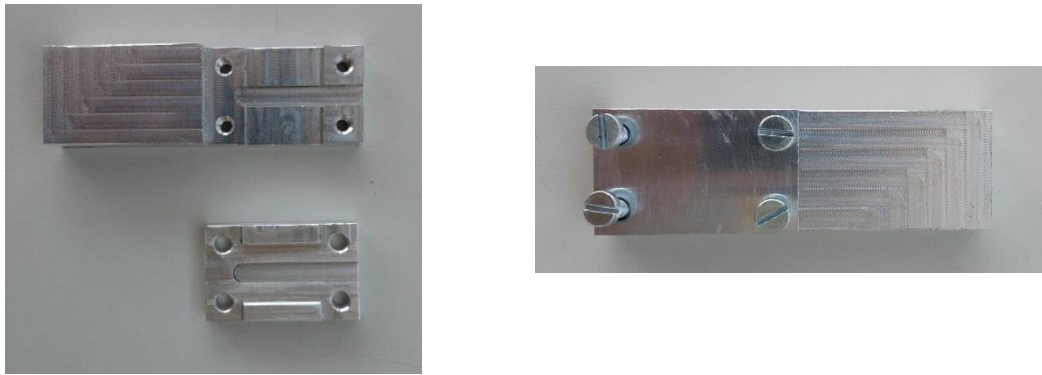
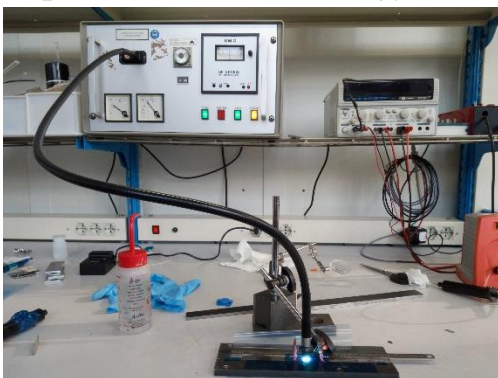


Figure 4.24 Aluminum adapter for fiber optic pull-out prove

To execute the pull-out prove, the fabrication of the samples is done with the same material FO of the retractor sensor, and at the same time made with the same production methodology of the Batch 03-04. (see Chapter 2)



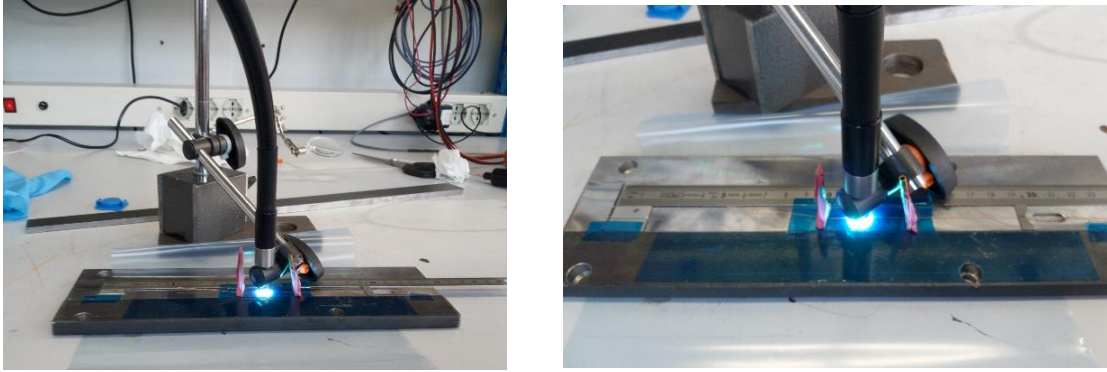


Figure 4.25: Production of pull-out samples

The FO is attached in one end by the specimen to be tested and the other it has in the base a composite material that hold the fiber to execute the pull.

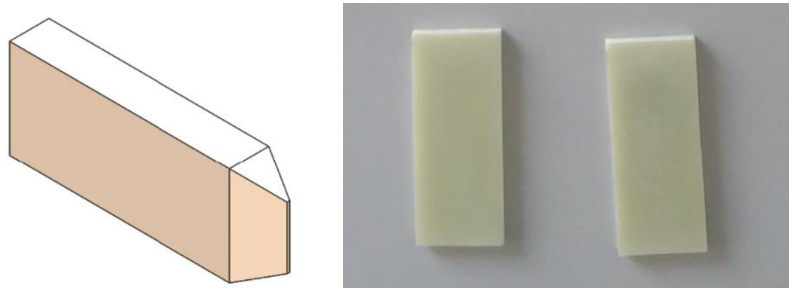


Figure 4.26: Composite base of FO attached

In order to fabricate the composite base, the naked FO with only coating from the lower end to the specimen is positioned in the mid axis of the composite base and let in a pressurized and thermal machine for 90 minutes from 26°C to 127° C at 8 Pascals. The result are 6 samples to be tested.



Figure 4.27: Pull-out samples

The procedure

In order to guarantee optimum conditions of the test, It's necessary to satisfy some requirements.

Reduction of the applied forces in the fiber:

It is necessary to prevent FO rupture during the test, to have a clear understanding of the possible outcomes. To achieve this conditions, it is necessary to have the minimum damage and no change of mechanical properties in the fiber, so that is use the cold bonding technique for the composite elements attach in the FO, so less thermomechanical deformation during this process is achieved.

Homogeneity and regularity in the host material.

The material that covers the fiber shall be as regular as possible, complying orthogonality in the matrix and guarantee no creation of bubbles in the embedment process specially in the interface area of the fiber.

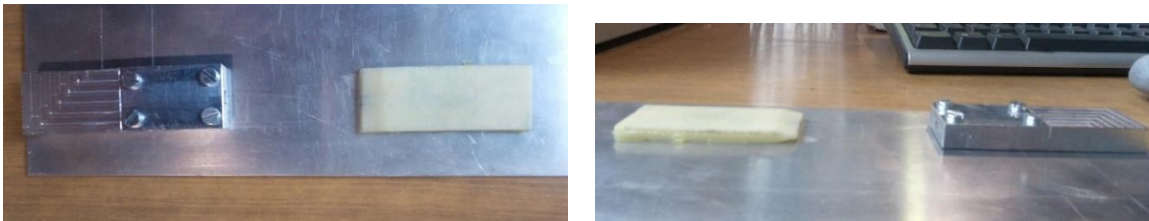


Figure 4.28: PO sample with mechanical adapter for tensile machine

For this test, the next considerations shall be considered:

- FO mid axis should be centered in the middle of the complete system of the prove; meaning the test machine, the fastening instrument and the specimen.
- The production process of the specimen should be the same as the one designed for the complete retractor.

The results

The first 6 samples tested were produce with the next characteristics:

Table 4.6: PO sample numeration

Pull-out samples	
Sample number	Specimen size
PO-01	5 mm
PO-02	3 mm
PO-03	4 mm
PO-04	3 mm
PO-05	5 mm
PO-06	4 mm

In the pull-out test a load is applied to the sample via the Instron 4302 Tensile machine with the adapter device connected to the crosshead of the machine and a force-displacement curve is recorded.

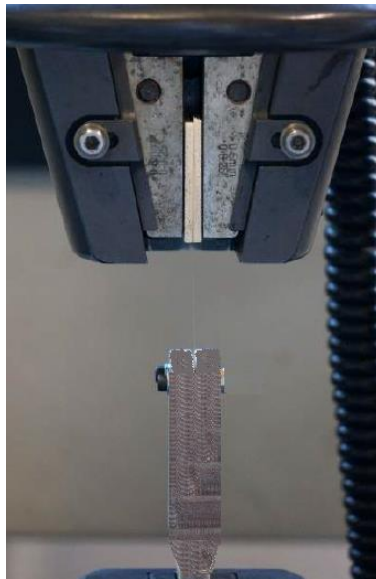


Figure 4.29: PO Sample assembly on tensile machine Instron 4302

This curve typically shows the force along the vertical axis and the position of the crosshead along the horizontal axis. The test is run until the FO in the sample fails, easily recognized as a sudden displacement of the fiber in the implant.

The test is performed having control of the displacement with a predetermined speed of $0.5\text{mm}/\text{min}$, during which the displacement and the force is acquired. So that, the curve can be obtain. The results of the test are presented below.

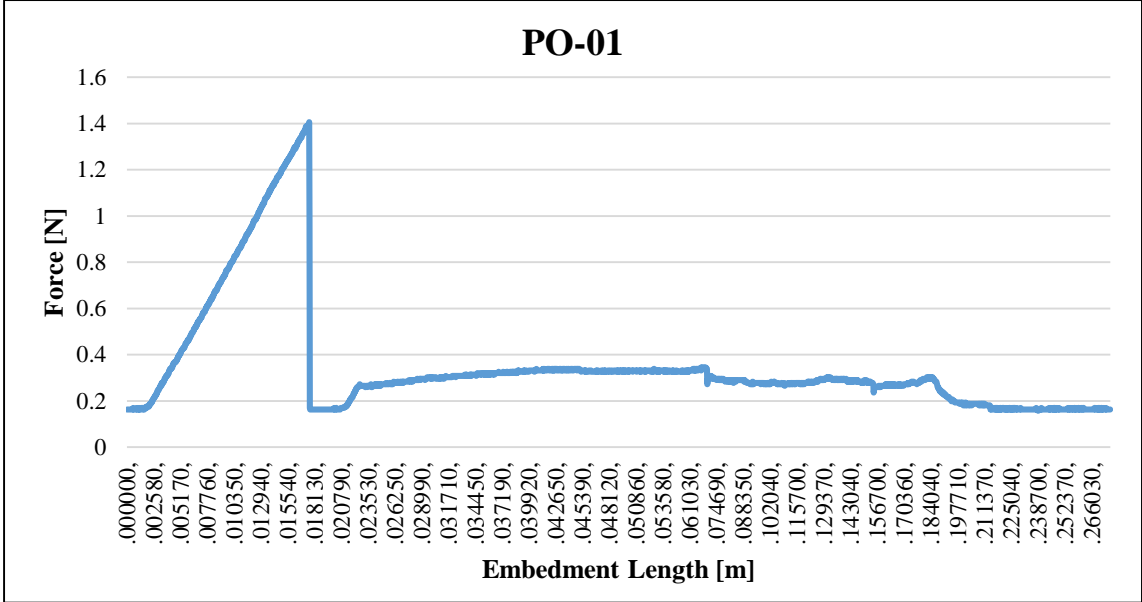


Figure 4.30: Force vs displacement curve PO-01

PO-01 had the expected behavior of the retractor design and the rupture happened without doing any damage to the specimen in study due to the longitude long enough to withstand the force on the mayor area attachment.

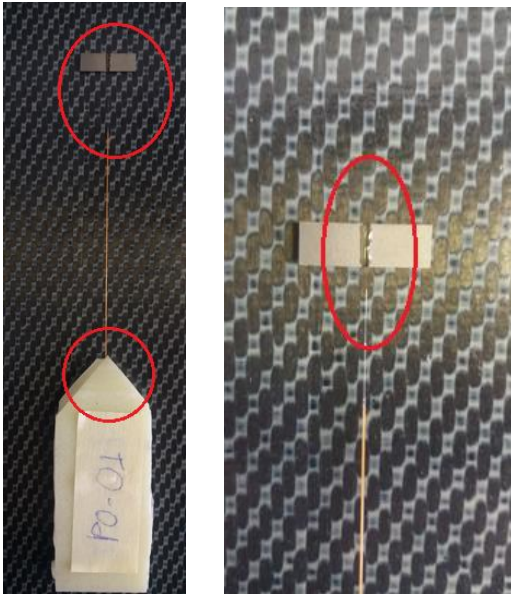


Figure 4.31: PO-01 Sample breakage

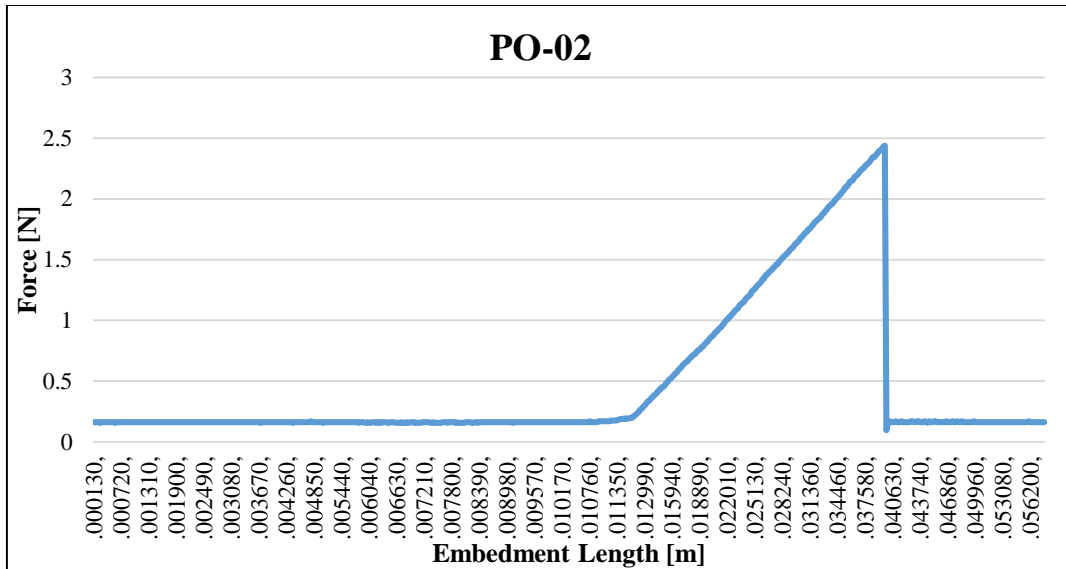


Figure 4.32: Force vs displacement curve PO-02

PO-02 instead, being one of the specimen more adapted to the retractor due to the geometry has a response where the FO retracting force is fortified due to the glue wrapping.

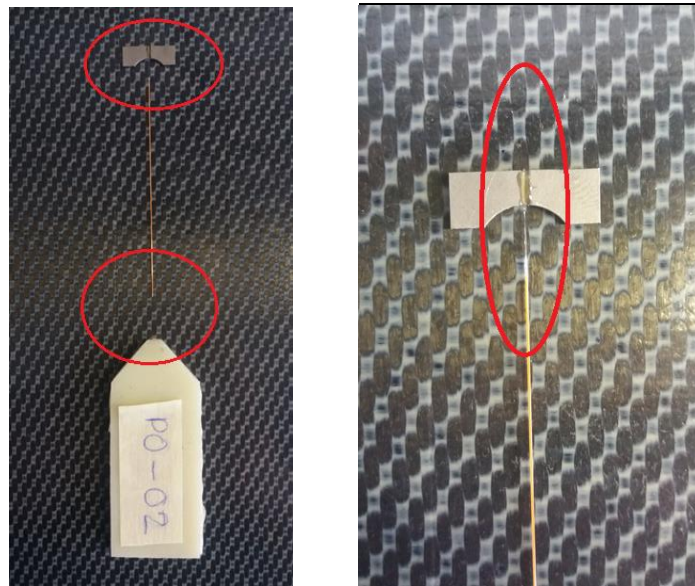


Figure 4.33: PO-02 Sample breakage

Specimen PO-03 had a rupture of the fiber while adapting the sample to the tensile machine, this could have happened due to torsion in the FO influencing during suiting the test in the Instron 4302 or a production error in the specimen due to the location of the rupture (Figure 4.34).

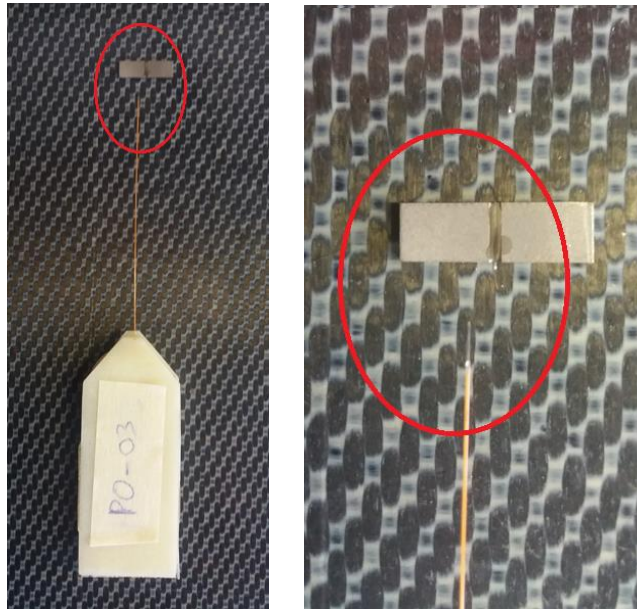


Figure 4.34: PO-3 Sample breakage

PO-04 is the specimen with exact geometrical characteristics of the retractor, being the tip bonding end of the FBG sensor in the metal core.

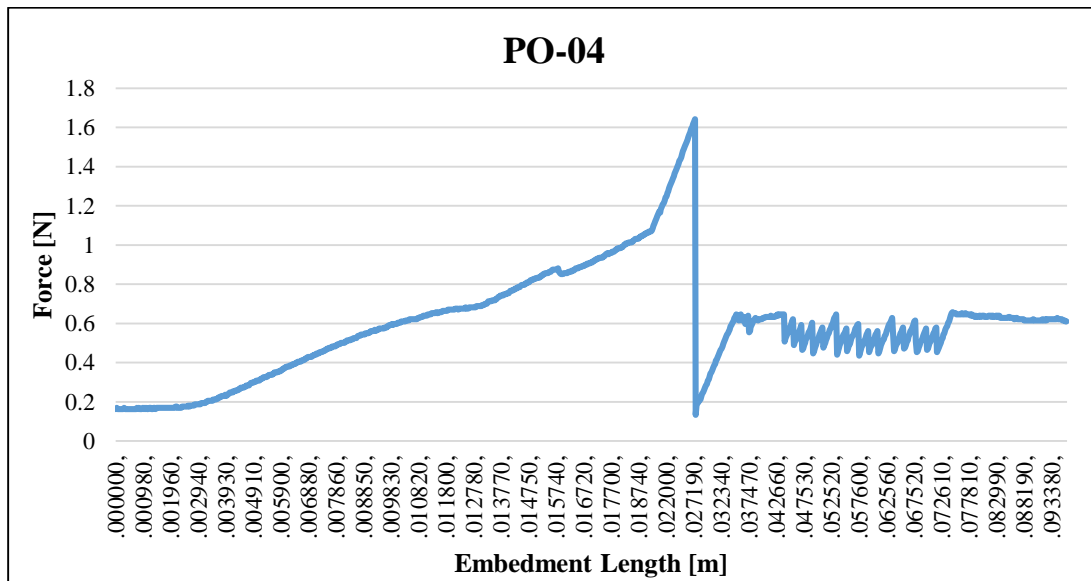


Figure 4.35: Force vs displacement curve PO-04

As expected the pull-out rupture happened at a displacement of 27.35 mm, which in deed reflects to withstand force of 1.64 Newtons applied in the horizontal axis of the retractor.

The rupture location is in the lower part of the sample where stresses are distributed due to the base composite constrain and not due to the glue bonding of the specimen as shown in Figures 4.35 and 4.36.

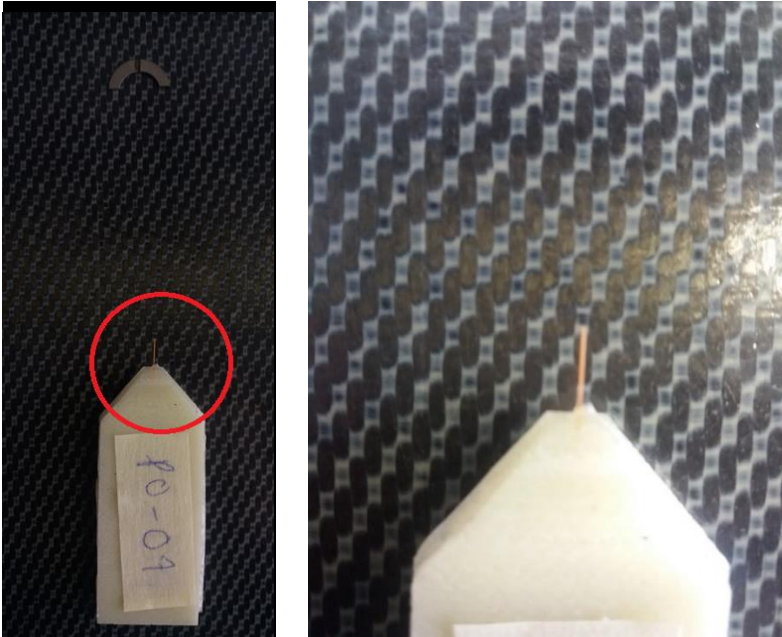


Figure 4.36: PO-4 Sample breakage

For sample PO-05, the behavior shown was slightly different. In the cases where the extraction force is lower, there is no instantaneous removal of the FO and is possible to appreciate the effect of friction which causes the pick increases and variation visible in Figure 4.37.

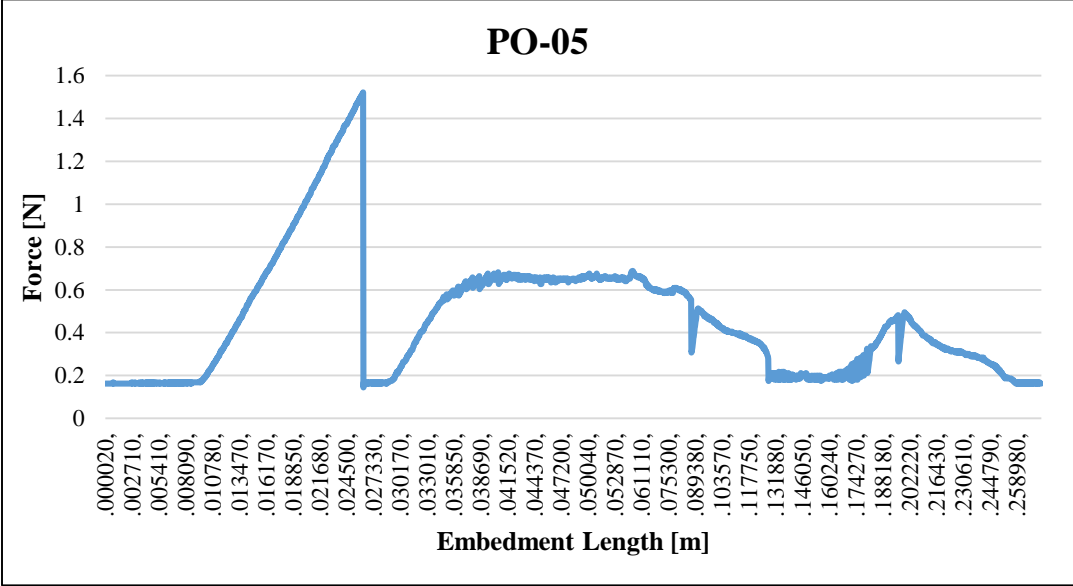


Figure 4.37: Force vs displacement curve PO-05



Figure 4.38: PO-5 Sample breakage

Shown in Figure 4.38, PO-06 sample had breakage in the composite base in a tensile force of 1.48 Newtons, at the same the specimen was able to withstand the stresses in the 4 mm specimen just pulling out the cladding of the fiber and not the complete FO out of the metal core.

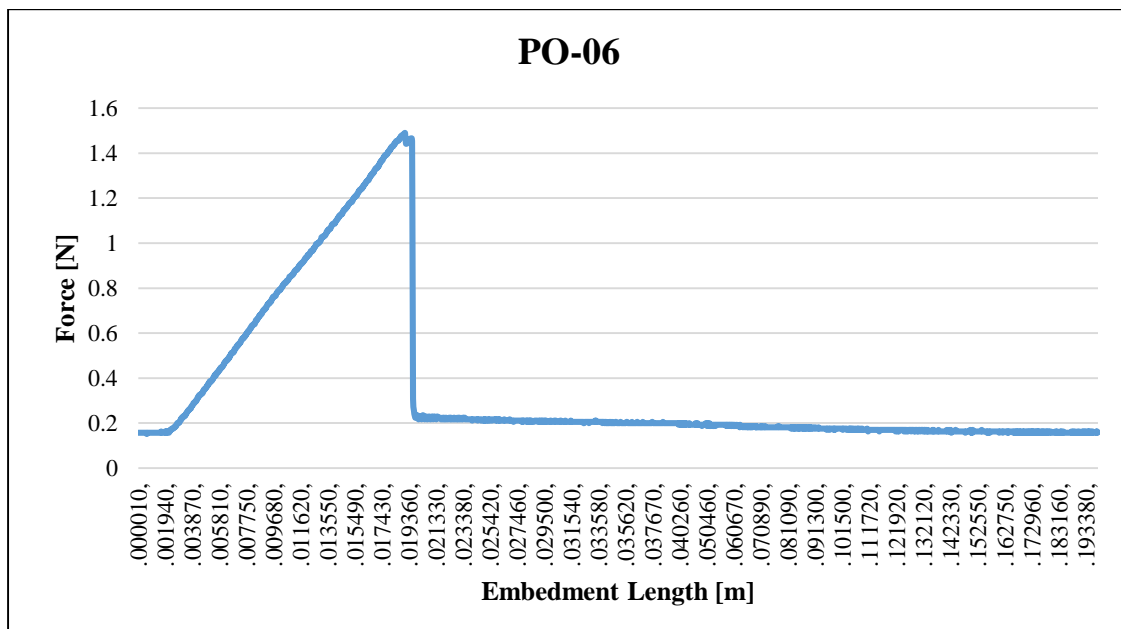


Figure 4.39: Force vs displacement curve PO-06

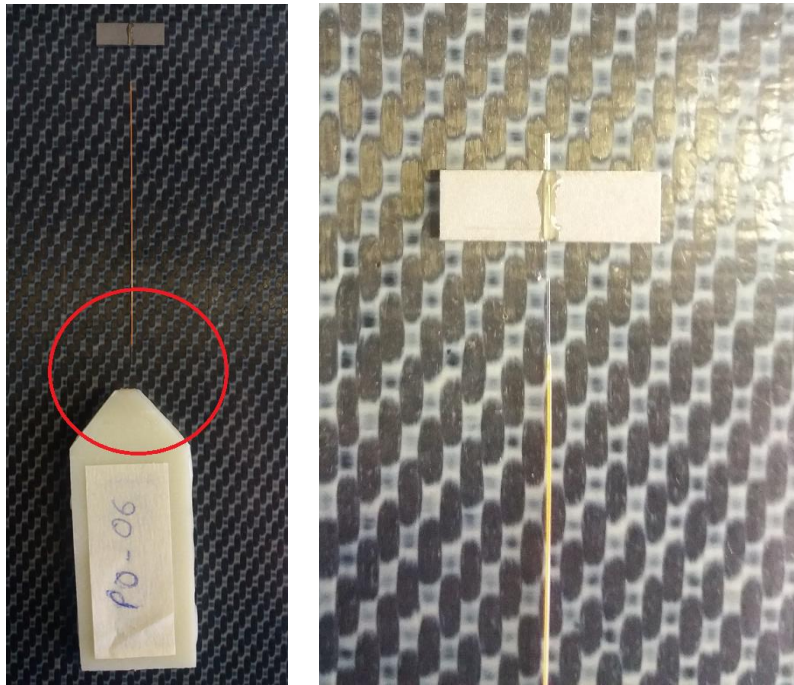


Figure 4.40: PO-6 Sample breakage

The Table below presents a summary of the influential data of the six samples pull-out test.

Table 4.7: Summary PO Test

Pull-out prove board Results				
Sample No.	Specimen Length [mm]	Breakage Max Force [N]	Displacement Length [mm]	Breakage Closer Location
PO-01	5	1.4062	17.61	At Specimen
PO-02	3	2.4383	39.84	At Base
PO-03	4	N/A	N/A	During Set-up
PO-04	3	1.6416	27.35	At Specimen
PO-05	5	1.5209	26.24	At Specimen
PO-06	4	1.4545	19.56	At Base

As seen in the summary results of the pull-out test, two of the samples failed closer to the region where the FO is attached in the composite base which means that the concentration of stresses is higher due to damage of the fiber during the bonding and miss symmetric of the base as seen in the respective Figures.

The sample PO-03 failed during the set-up of the test due to the intrinsic manageability of the sample and the Instron 4302.

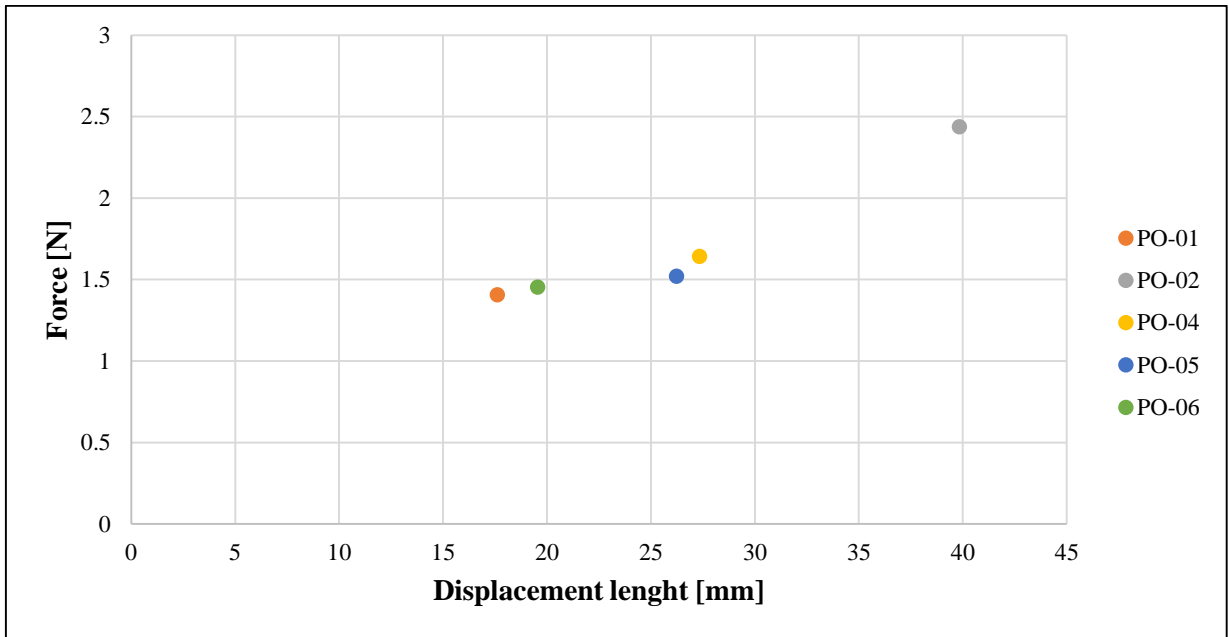


Figure 4.41: Dispersion of PO sample results

This means that the remaining three samples PO-01, 04 and 05, can be considered as reliable data as shown in the dispersion Figure above considering the maximum force and displacement of the working samples.

4.5 Conclusion

Three validation test were executed, during the flexural test important data is retrieved giving as a result a preliminary displacement of the fiber with respect to the mid axis, in cantilever and simple supported mode assumptions of usage, with a maximum applied mass of 400 grams. Analyzing the past flexural data of Batches SR03-02 and SR03-03, this new batch presents a big enhancement of the positioning of the fiber by having an overall 3.1 times less wavelength displacement of the FBG as desired. The Tomography test was executed to validate the displacement of the fiber at an observable level and measurement. During the non-destructive test, some images where retrieved that shows the health of the FBG sensor in the bottom the retractor and a characterization of the metal core is reached.

The pull-out test executed with 6 samples gave an analysis of the contact area of the FO to the metal core and adhesive with 3, 4 and 5 mm specimens that studied the tip end bonding of the retractor. Whit this test it was achieved a study method with ground assumptions for the test itself, an adapter of specimens for the testing machine and 3 working samples for the retractor, stating that the 3 mm length quarry of the tip bonding of the retractor are sufficient to withstand a force up to a 1.64 Newtons force in the horizontal axis.

Chapter 5

Conclusions and Future Analysis

The presented work reflects the efforts of Politecnico di Milano to design, fabricate and test a smart retractor for neurosurgery and this Thesis was aimed to improve the industrialization process and validate the performance of the last design enhancement that led to the fabrication of the smart retractor batch SR03-04.

The industrialization of the new retractor batch SR03-04 is executed successfully in accordance of the procedure established in Chapter 2. A visual analysis was executed to compare the overall behavior of the retractor with respect to the other batches and for the first time, complies with the expected results stated in the procedure.

A proper calibration test was performed not only to prove the functionality of the retractor but to state the sensibility and measurements errors during usage. In the pressure test the retractor shows performance enhancement with respect to the executed in batch SR03-03. This confirms and gives the first gauge values for error measurements.

The temperature test is applied in three of the retractors and validates the assumptions of the materials design. The gauge error measurement during usage do to temperature can be determined now.

A validation of the retractor functionality has been carried out through the flexural, tomography and pull-out test. The procedure of the flexural test gives the deformation of the wavelength in function of the force applied and the strength of the bonding has been confirmed to support higher forces than the subjected during usage of the retractor in two different scenarios and the confirmation of the low fiber displacement from mid axis has been proved, shown in Chapter 4.

The tomography gives the first non-destructive visualization inside the complete retractor confirming the non-damage of the FBG sensors during liner application in this new retractor batch. In the other hand, to inquire the optimization of the design in terms of geometry, the pull-out test presented gives a very first analysis and methodology for next research of the tip optimal area of the retractor. In the overall, the batch SR03-04 has been proved to be more efficient and better produced.

Certainly, it can be stated that many goals have been achieved. Nevertheless, an optimization of the smart retractor study can be done by the next few considerations:

About the Calibration: The gauge must be defined with the delta reference Bragg wavelength data acquired from the pressure, temperature and flexural tests. Now the proportionality coefficients and correction constants can be calculated and define a value of the overall gauge measure.

Numerical Analysis: The retrieve data from last experiments must encounter a deepest numerical campaign, not only considering the deformation on the FO, but increasing the analysis as a composite element to measure the total stress variation during pressure, temperature and flexural test. A dynamic analysis is recommended to have a mode variation of the photomechanical properties of the FBG sensor and have a secure structural design of the retractor. A FEM analysis would bring out information in the sensitivity of the FBG sensor wrapped in the elastomer liner due to the distribution of stresses. It would be interesting to model the complete retractor as suggested in Appendix C.

Validation enhancement: The flexural deformation test can be held till the point of breaking to know the maximum force before breakage with other specimens dedicated for this test but with the same mechanical properties of the retractor. Tomography quality is influence on the density of each material, hence the displacement of the fiber can be measure by having a clear image of it with a specimen having similar density properties not only to prove the FO embedment in the metal core but to reply the production procedure. For an improvement of the pull-out prove, the sample fabrication involves the success and the reliability of the test. If the need of optimization of the tip bonding area of the retractor, specimens between 2.5 mm and 3.5 mm can retrieve more clean data.

These last suggestions can bring a fully optimization of the retractor, however the presented experiments and analysis in this Thesis work indicates that once the calibration gauges have been defined, the batch SR03-04 is ready for experimental procedures with an optimal rate of success, and as soon as all certifications are accomplished, the smart retractor can be introduced into the market.

Appendix A

Smart Retractor SR03-04 Generalities

The smart retractor is composed by the next list of components which material nominal generalities considered in this Thesis are presented below.

- **FO sensor**

Fiber Bragg Grating sensor	
Density [kg/m^3]	1220
Young Modulus (Pa)	2.079×10^9
CTE ($\text{mm/m/}^\circ\text{C}$)	0.8×10^{-5}
Poisson's ratio	0.37
Characteristic FBG wavelength Temperature, external, central	1540 1543 1548 nanometers

- **Adhesive**

EPO-TEK Epoxic monocomponet	
Density [kg/m^3]	1050
Young Modulus (Pa)	3.0987×10^9
CTE ($\text{mm/m/}^\circ\text{C}$)	0.0159
Poisson's ratio	0.325

- **Metal core**

Steel AISI 316	
Density [kg/m^3]	7990
Young Modulus (Pa)	1.93×10^{11}
CTE ($\text{mm/m/}^\circ\text{C}$)	0.0165
Poisson's ratio	0.31

- **Liner**

Dow Corning - Elastomer	
Density [kg/m^3]	1130
Young Modulus (Pa)	7.7×10^6
Poisson's ratio	0.45

Appendix B

Fiber Optic Characterization

The optical fiber base is constituted by a glassy or polymeric filament with a circular section formed by two coaxial layers said core and cladding. The core represents the central part and has a typical diameter of $9\mu\text{m}$ in mono-modal fiber and $50\sim 62.5\mu\text{m}$ for those multi-modal. The cladding coaxially surrounds the core and together with it form the waveguide itself. Core and cladding are made with materials having a refractive index slightly different, to be precise the cladding has a lower refractive index (typically $\eta_{cladding} = 1.475$) compared to the core (typically $\eta_{core} = 1.5$).

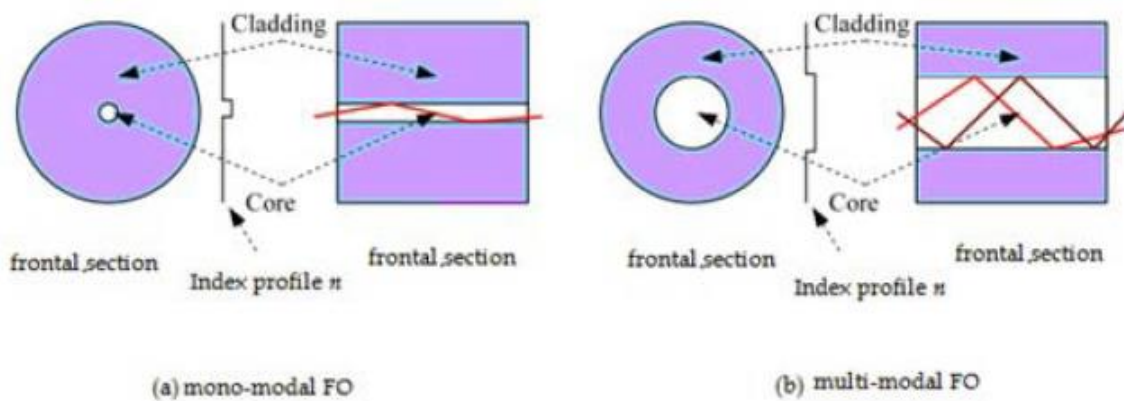


Figure A.1: Mono-modal and multi-modal FO

To provide more strength and protection to the fiber, in implementation phase a buffer is added to a layer or coating, of variable diameter depending on the material used, from 150 μm coatings for poly-imide, to 250 μm for those in poly-acrylate, in larger diameters for metallic coatings. In case it is required increased mechanical protection of the fiber you can add an additional layer coating called jacket, whose diameter and material are chosen in function of the final use of the fiber.

Fiber Bragg Grating Sensors:

The Bragg grating sensors are particular sensors formed within a suitably doped optical fiber to make it light sensitive. The peculiarity of this fiber is the capacity to be able to modify the local value of the refractive index of the core through the exposure of the same to a suitable energy source, such as may be a laser light beam. Modulating the laser source in an appropriate manner it is possible to inscribe in a core pattern consisting of a series of fringes having a different refractive index.

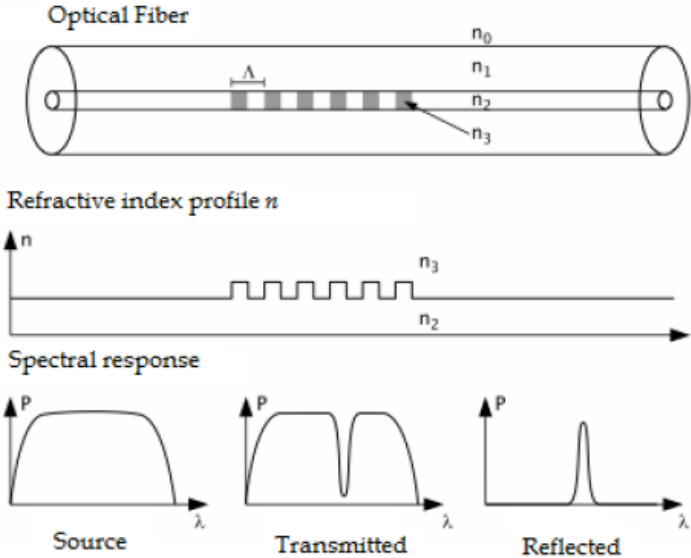


Figure A.2: Fiber Bragg Grating sensor

In Figure A.3, each jump in refractive index, represented from single fringe, reflects part of the light that hits it and has an additive combination of these contributions only for those wavelengths λ_B related to the lattice step Λ .

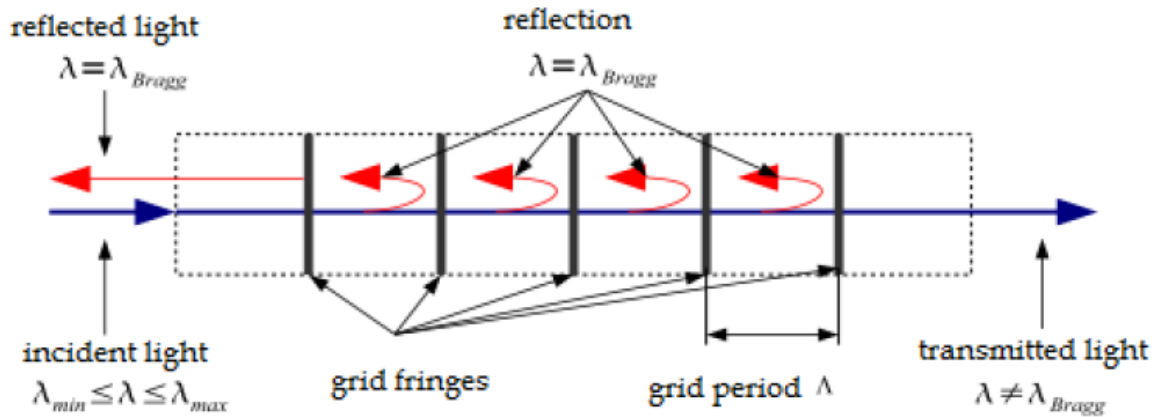


Figure A.3: Reflection of the fringes in Bragg gratings

Each effect which causes a variation of the length L , the period Λ or the refractive index η_{eff} of the pattern determines a change of the Bragg wavelength λ_B , and therefore can be measured as in the next figure.

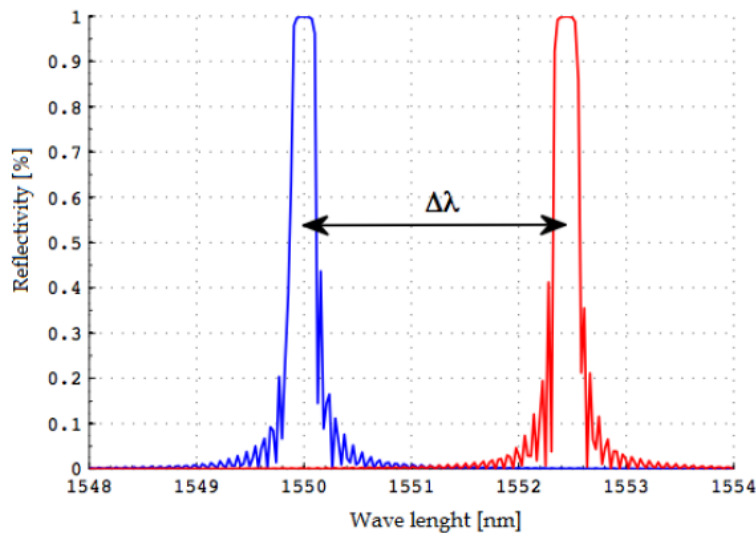


Figure A.4: Variation of the reflection spectrum of a Bragg grating subjected to a uniform stress

In the case in which the stress is uniform throughout the grating, it could be observed that the reflection spectrum exhibits a rigid translation along the axis of the lengths waveform, as shown in Fig. A.6 (a). In the case of measurement

of mechanical deformations there is a shift towards higher wavelengths in the case of traction stress and vice versa to the lower wavelengths in the case of compression. Similarly, it is for the temperature measurements.

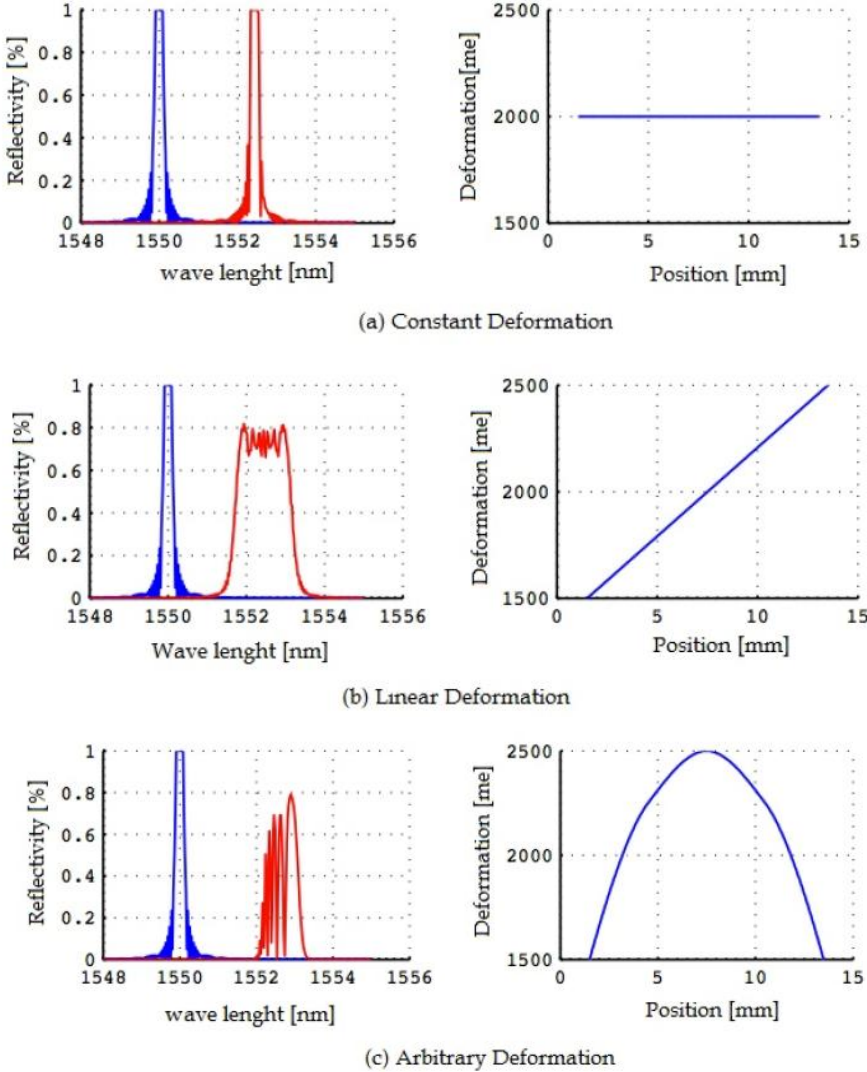


Figure A.5: Variation of the reflection spectrum of a pattern subject to deformations that have different trends, but equal value average strain, equal to $200\mu\epsilon$

If the stress exhibits a linear pattern along the grating, we observe an increase in the width of the spectrum and a reduction of its peak value, as shown in Fig. A.5 (b). The measurement of only $\Delta\lambda_B$ then provides an assessment of the average value of the magnitude in question along the sensor.

Appendix C

Suggested FEM Analysis

The shape and response of the FBG reflected spectrum depends on the way that the grating is deformed, being the stress and strain field an important value quantity to measure along the FO and specially in the grating the measure signal response.[17]. The smart retractor in consideration is composed by several materials that can be studied as a composite tool, hence the properties that influence its deformation upon stress are not the same along the forces applied.

A preliminary FEM analysis with ANSYS software of the smart retractor has been pre-designed and suggested to continue for a deeper numerical analysis of the retractor.

The fully smart retractor (being the FO, reticulated adhesive, metal core and liner) has been design in CAD model and settle with the respective mechanical properties.

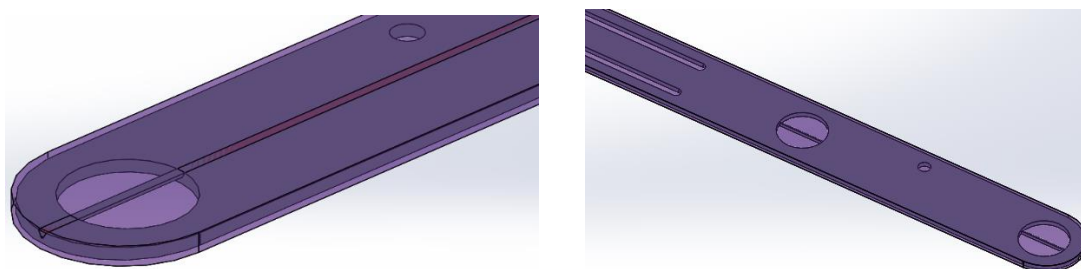


Figure B.1: Full retractor SR03-04 CAD design

Problematics on the material homogeneity and production error might occur, especially in the bottom of the retractor, where the pressure sensors are located. As seen in Figure B.2 the FO is the slender component in the retractor and critically attractive for them FEM analysis.

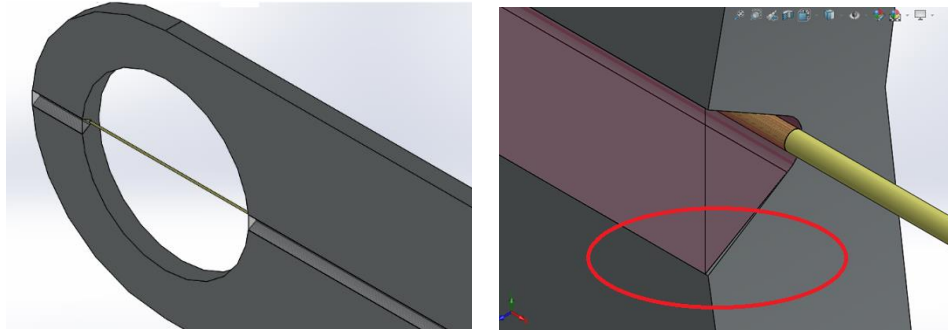


Figure B.2: FO, reticulated adhesive and metal core

The suggested FEM analysis is focused in the flexural deformation test and pressure test in Chapter 3 and 4, hence two modeling possibilities are approached (Cantilever and simple supported retractor).

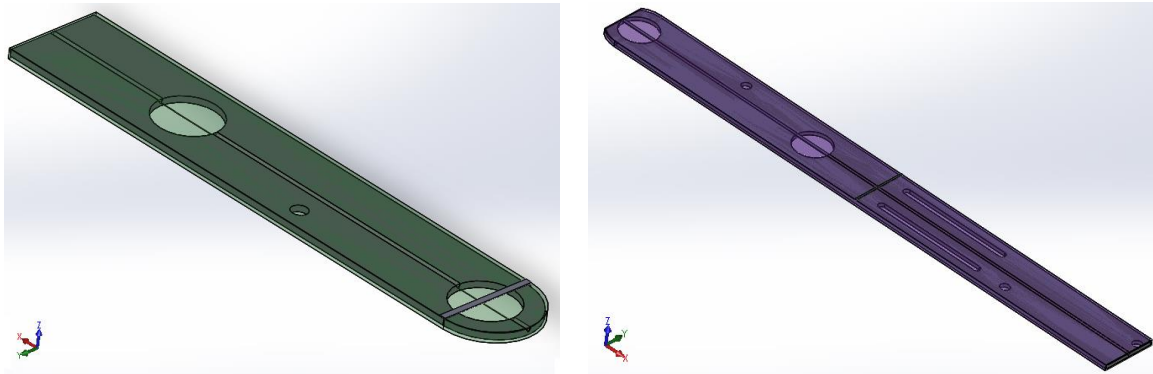


Figure B.3: Cantilever and SS model retractor

The first suggested analysis is a Static Structural analysis, the engineering data is input based on material properties (Appendix A), the geometry is export from the CAD designs without modification. Modeling is executed with fixed supports and force in each respective case.

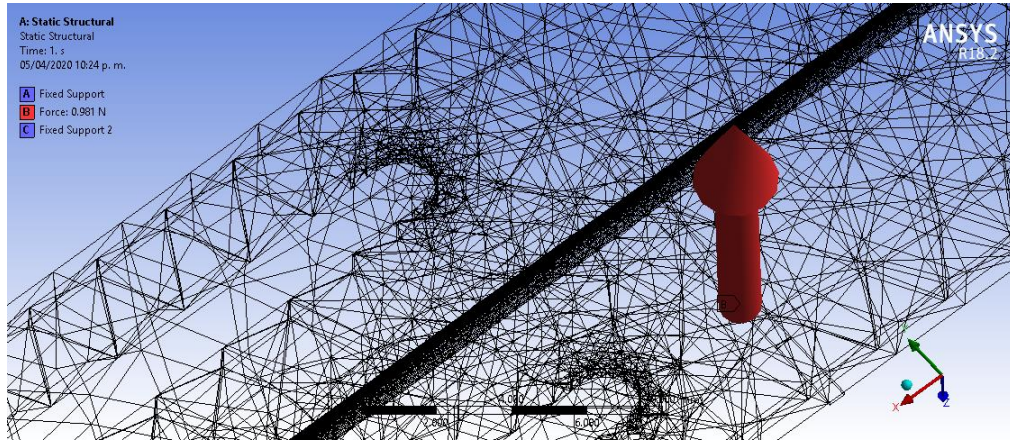


Figure B.4: Retractor self-construct mesh by ANSYS

An important consideration while modeling is the mesh application. Due to the intrinsic low measures of the fiber with respect of the rest of the retractor, the mesh size and geometry is hard to self-construct even if the smoothing, mesh metric and target quality is reduced.

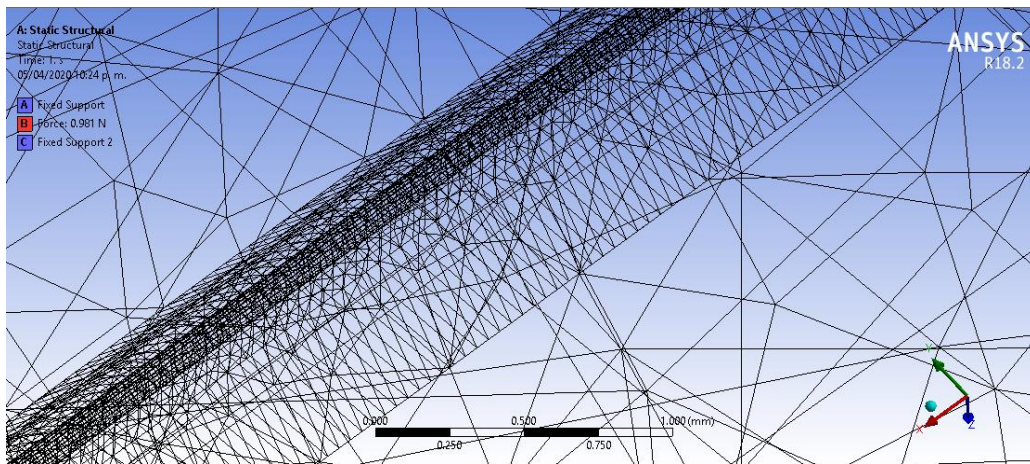


Figure B.5: FO and reticulated adhesive meshing by ANSYS

A final meshing of the total retractor gives 1793238 nodes and 516347 elements which derives to elevated computational demand. Hence further analysis on the retractor must be use symmetry considerations to reduce this demand, and the strategy of 2D analysis might be suitable for preliminary stress studies of the FO. The output of the FEM in consideration provides stress, strain and displacement data, although, the spectrum acquaintance of the wavelength signal gives a small shift due to the lower forces the smart retractor is subjected.

References

- [1] "Medical Instrumentation Application and Design", John G. Webster, 2009.
- [2] "Modelling of Brain Tissue Retraction Using Intraoperative Data", H. Sun, F. Kennedy, E. Carlson, A. Hartov, D. Roberts, K. Paulsen, Springer-Verlag, 2001.
- [3] "Brain mechanics for Neurosurgery: modelling issue", S. Kyriacou, A. Mohamed, K. Miller, S. Neff, Biomechan Model Machanobiol, 2002.
- [4] "Smart Materials", Chapter 14, Fiber Optics Systems, Mel Schwartz, 2013.
- [5] "Design and manufacturing of a fo-based monitoring for load identification on morphing aeronautical Politecnico di Milano, S. Nicoli, 2016.
- [6] "Bend loss measurements on high numerical aperture single-mode fibers as a function of wavelegth and bend radius", Journal of Light LT-4, Harris A. J. and Castle P. F. .LT-4(1), 1999.
- [7] "Advanced materials for neurosurgery", Politecnico di Milano, Veronica Minerva, 2014.
- [8] "Design of a smart instrument for brain surgery", Politecnico di Milano, Claudia Cantarelli 2016.
- [9] "Development of a smart retractor for neurosurgery", Politecnico di Milano, Andres Forero 2017.
- [10] "How to Precision Clean All Fiber Optic Connections", Edward J. Forrest 2014.

- [11] "Structural monitoring with fiber optic technology", Academic, Raymond Measures, 2001.
- [12] "Lifespan of rubber materials and thermoplastic elastomers in air, water and oil, IFP", The Swedish Institute for Fibre and Polymer Research, Andersen C., 1999.
- [13] "Vibrations of Continuous Systems", McGraw-Hill, A. W. Leissa, M.S. Qatu, 2011.
- [14] "Thermal structures for aerospace applications", AIAA Series, E.A. Thornton, 1996.
- [15] "Micro-Computed Technique to Study the quality of FO in composites Materials" Sensors Journal, Gabriele Chiesura, 2015.
- [16] "Tensile Properties of fiber-reinforced metals", A. Kelly and W.r. Tyson, 2011.
- [17] "Fiber Bragg grating signal simulation tool for Finite element method models", G. Pereira, M. McGugan, L.P. Mikkelsen 2016.